Bulk Viscosity of Spin-One Color Superconductors

Dissertation
zur Erlangung des Doktorgrades
der Naturwissenschaften

vorgelegt beim Fachbereich Physik
der Johann-Wolfgang-Goethe-Universität
in Frankfurt am Main

von
Basil A. Sa'd
aus Jordanien

Frankfurt am Main, August 27, 2009

(D 30)

vom Fachbereich Physik der Johann Wolfgang Goethe–Universität
als Dissertation angenommen.

Dekan: Prof. Dr. D. H. Rischke

Gutachter: Prof. Dr. D. H. Rischke

Datum der Disputation: May 26, 2008

Contents

List of Figures

List of Tables

Acknowledgements

First of all, I would like to thank my advisor and boss Dirk Rischke for guiding me through this work, providing me with advice and help throughout my Ph.D.. He did it with enthusiasm and patience that made my work much more exciting and rewarding.

Second, thanks to Igor Shovkovy, without whom this thesis would not have been possible. He closely worked with me throughout the better part of my Ph.D., provided me with insights, and trying to convince him of my results only made my work more concrete, it was simply great working with you, Igor.

Throughout my work, I found discussions with Jürgen Schaffner-Bielich and Igor Mishustin to be very fruitful and insightful.

There are many friends and colleagues who, through their support and fruitful discussions, made this work more pleasant to go through. Of them I mention Veronica Dexheimer, Ben Koch, Irina Sagert, and Hussein Malekzadeh.

I must mention Jorge and Jaki Noronha-Hostler, they were the best of colleagues and friends a person could ask for, they have both supported me and helped me throughout my time in Frankfurt, and sometimes, outside Frankfurt. One of their many ways of helping me was to proof-read this thesis.

The German translation of the summary and the abstract were done by the dear Sophie Nahrwold and checked by Jörg Ruppert, thank you both very much.

Many thanks go to the Frankfurt Institute for Advanced Studies (FIAS) and the Frankfurt International Graduate School for Science (FIGSS) under the wise leadership of Horst Stöcker.

Abstract

The bulk viscosity of several quark matter phases is calculated. It is found that the effect of color superconductivity is not trivial, it may suppress, or enhance the bulk viscosity depending on the critical temperature and the temperature at which the bulk viscosity is calculated. Also, is it found that the effect of neutrino-emitting *Urca* processes cannot be neglected in the consideration of the bulk viscosity of strange quark matter.

The results for the bulk viscosity of strange quark matter are used to calculate the r-mode instability window of quark stars with several possible phases. It is shown that each possible phase has a different structure for the r-mode instability window.

Abstract

Die Volumenviskosität verschiedener Phasen von Quark-Materie wurde berechnet. Es wurde beobachtet, daß der Effekt von Farbsupraleitung nicht trivial beschreibbar ist, da sie die Volumenviskosität, abhängig von der kritischen Temperatur und der Temperatur, vermindern oder vergrößern kann. Außerdem wurde beobachtet, daß der Effekt von Neutrino-emittierenden *Urca*-Prozessen bei der Betrachtung der Volumenviskosität von strange Quark-Materie nicht vernachlässigt werden kann.

Die Ergebnisse für die Volumenviskosität von strange Quark-Materie wurden benutzt, um das r-Moden Instabilitätsfenster von Quarksternen mit einigen möglichen Phasen auszurechnen. Es wurde gezeigt, daß jede mögliche Phase eine individuelle Struktur des r-Moden Instabilitäsfensters aufweist.

Zusammenfassung und Ausblick

Pulsare faszinieren Wissenschaftler seit ihrer Entdeckung vor einigen Jahrzehnten. Es handelt sich bei Ihnen um kompakte stellare Objekte, bis zu zwei Sonnenmassen schwer mit einem Radius von ungefähr zehn Kilometern. Der Name "Pulsar" stammt von der Beobachtung regelmäßiger Strahlungspulse (meistens Radiowellen), die diese Objekte abgeben. Die Frequenz dieser Pulse hängt mit der Rotationsfrequenz der Pulsare zusammen, deren Rotationsperiode von Millisekunden bis zu einigen Sekunden reichen kann.

Die Dichte dieser stellaren Objekte ist bis zu zehnmal größer als die der Materie im Atomkern, so daß es sich hier nicht um konventionelle Materie handeln kann. Stattdessen erwartet man, bei so großen Dichten exotische Materiephasen wie zum Beispiel freie Quark-Materie zu finden. Diese Phase kann auftreten, wenn die starke Wechselwirkung, die die Quarks in Hadronen bindet, schwach genug wird, um sie freizusetzen. In diesem Fall könnte es sein, daß Pulsare die einzigen Orte im Universum sind, an denen freie Quark-Materie in großen Mengen existiert.

Es gibt viele mögliche Strukturen, die Pulsare annehmen können. Die Dichte eines Neutronensterns mit einer Masse von 1.4 $M_\odot$ und einem Radius von 12km wäre $\rho \sim 3.846 \times 10^{14}\text{g cm}^{-3}$. Die einfachste, "am wenigsten exotische" Phase, die man bei solch einer großen Dichte erwartet, besteht aus Neutronen, Protonen und Elektronen in einem neutralen, β-equilibrierten Zustand. Es besteht dabei die Möglichkeit, daß das chemische Potential der Neutronen im Zentrum des Sterns so groß wird, daß schwerere Hadronen, die womöglich auch strange Quarks enthalten, wie Σ, Λ, Ξ, Δ Teilchen gebildet werden können. In diesem Fall nennt man den Stern einen Hyperonstern.

Es ist außerdem möglich, daß bei solch hohen Dichten starke Wechselwirkungen schwach genug werden um eine Phase freier Quark-Materie zu produzieren. Falls diese Phase der wahre Grundzustand von Materie unter den Bedingungen im Innern eines Neutronensterns ist, bestünde der gesamte Stern aus strange Quark-Materie

homogener Dichte. Ein solcher Stern heißt dann Quarkstern oder seltsamer Stern. Im anderen Fall gibt es noch die Möglichkeit, daß Quark-Materie nur im Zentrum des Sterns existiert, ein solcher Stern wird Hybridstern genannt.

Die Temperaturen von Pulsaren sind verglichen mit den chemischen Potentialen und Wechselwirkungsenergien sehr niedrig. Unter diesen Bedingungen und falls Quark-Materie tatsächlich im Innern von Pulsaren existiert, wäre dies höchstwahrscheinlich in Form eines Farbsupraleiters. Es gibt viele bekannte, farbsupraleitende Phasen, die in kalter, dichter Materie existieren könnten, allerdings ist unklar, welche dieser Phasen die freie Quark-Materie in einem Pulsar beschreibt.

Prinzipiell ist es zwar möglich, die Phase der freien Quark-Materie unter den Bedingungen im Innern eines Pulsars zu ermitteln, allerdings sind die theoretischen Unsicherheiten bei der Behandlung der stark gekoppelten, nich perturbativen Dynamik in der QCD (bei den relevanten Baryondichten) so groß, daß es praktisch fast unmöglich ist, die richtige Phase zu bestimmen.

Mit Hilfe astronomischer Daten ist es jedoch möglich, die Menge der erlaubten Phasen zumindest einzugrenzen, wofür eine detailierte Kenntnis der physikalischen Eigenschaften von verschiedenen dieser Phasen, die in Pulsaren existieren könnten, notwendig ist. Dabei sind die Transporteigenschaften am besten geeignet, um ausreichend empfindliche, eindeutige und verifizierbare Vorhersagen für beobachtbare Signale der Sterne zu machen. In dieser Arbeit geht es um die Berechnung der Volumenviskosität von freier Quark-Materie in verschiedenen möglichen Phasen und darum, die Ergebnisse mit beobachteten Pulsarrotationsfrequenzen in Zusammenhang zu bringen, indem der Effekt der Volumenviskosität auf r-Moden Instabilitäten und deren Relation zu Gravitationswellenemmision analysiert wird.

Im Allgemeinen ist die Volumenviskosität ein Maß für die Dissipation der kinetischen Energie während der Ausdehnung und Kompression einer Flüssigkeit. In kompakten Sternen sind die charakteristische Frequenzen der Dichteoszillationen von ähnlicher Größenordnung wie die stellaren Rotationsfrequenzen: $1\ \mathrm{s}^{-1} \lesssim \omega \lesssim 10^3\ \mathrm{s}^{-1}$. Für den am schnellsten rotierenden, bis jetzt bekannten Pulsar, PSR J1748-2446ad, ist $\omega \approx 4.5 \times 10^3\ \mathrm{s}^{-1}$, was einer Frequenz $\nu = 716$ Hz entspricht [6]. Die wichtigsten mikroskopischen Prozesse, die für Energiedissipation innerhalb der zugehörigen Zeitskalen sorgen können, sind schwache Prozesse. Unter den besonderen Bedingungen, die in Sternen gegeben sind, wird die Volumenviskosität der Quark-Materie von den Flavor-ändernden schwachen Prozessen bestimmt, die in Fig. 4.1 diagrammatisch dargestellt sind. Wenn durch Ausdehnung oder Kompres-

sion der Zustand des chemischen Equilibriums verlassen wird, wirken die schwachen Prozesse auf die Wiederherstellung des Gleichgewichts hin und reduzieren dabei die Rotationsenergie.

Das zweite Kapitel gibt einen Überblick über die Herleitung dieser schwachen Wechselwirkungsraten. Uns interessiert hier besonders die Änderung der chemischen Zusammensetzung der oszillierenden Materie, welche durch schwache, Flavor-ändernde Wechselwirkungen bestimmt wird.

Im dritten Kapitel wird die Volumenviskosität für die normale Phase und vier Spin-eins farbsupraleitende Phasen von dichter, zwei-Flavor Quarkmaterie berechnet. Die wichtigsten Beiträge hierzu kommen von den Urca-Prozessen, die in Abb. 3.1 diagrammatisch dargestellt sind. Dabei ist anzumerken, daß die Ergebnisse für die normale Phase auch für die 2SC Phase relevant sind. Wenn berücksichtig wird, daß es zwei (blaue) Gap-lose Moden von Quasiteilchen im Niedrigenergiespektrum der 2SC Phase gibt, ist der Ausdruck für die Volumenviskosität bei niedrigen Temperaturen näherungsweise gleich dem in Kapitel drei, Gl. 3.28, mit den folgenden Neudefinitionen: $\zeta_{max}^{\rm 2SC} = 3\zeta_{max}$ und $\omega_0^{\rm 2SC} = \omega_0/3$. Die äquivalenten Größen der normalen Phase sind in Gleichungen (3.26) and (3.27) gegeben. Die Neudefinitionen tragen der Verminderung der schwachen Wechselwirkungsraten um einen Faktor 3 bei $T \ll \Delta_0$ Rechnung, wobei Δ_0 der Betrag der 2SC Gap ist.

Die mikroskopischen Berechnungen der Volumenviskositäten der Spin-eins farbsupraleitenden Phasen legen nahe, daß Quasiteilchen mit verschiedenen Arten Gaploser Noden (Punkten oder Linien auf der Fermi-Kugel) eine wichtige Rolle spielen könnten. Allerdings ist es im Fall transversaler Phasen so, daß eine einzige, Gap-lose Quasiteilchenmode alle Informationen über Spin-eins Cooper-Paarung auslöscht, siehe Abb. 3.5. Nichtverschwindende Quarkmassen könnten zu einer Gap für solche Moden führen und damit die Situation verändern. In Kapitel drei diskutieren wir diese Möglichkeit in Zusammenhang mit der CSL Phase aus Ref. [7], die Ergebnisse sind in Abb. 3.6 dargestellt.

In Einklang mit allgemeinen Erwartungen beobachten wir, daß die Volumenviskosität oft abnimmt, wenn es zu Cooper-Paarung von Quarks kommt, deren wichtigste Auswirkung darin besteht, die Raten der schwachen Prozesse zu unterdrücken. In manchen Fällen (z. B. bei ausreichend niedrigen Frequenzen und/oder bei Temperaturen nahe der kritischen Temperatur) kann sich dieses Verhalten umkehren, da die Volumenviskosität auf nicht triviale Weise von dem Unterdrückungsfaktor abhängt (siehe Gl. (3.38)). Eine solche Erhöhung der Viskosität

in der farbsupraleitenden CSL Phase wird zum Beispiel in Abbildungen 3.5 und 3.6 bei Temperaturen unterhalb T_c beobachtet, wobei $T_c = 4$ MeV.

Im vierten Kapitel untersuchen wir das subtile Wechselspiel zwischen den semi-leptonischen Urca und den nicht-leptonischen schwachen Prozessen bei der Bestimmung der Volumenviskositaet von neutraler strange-Quark-Materie im β-Equilibrium. In der Regel lassen sich die Beiträge dieser beiden Arten von schwachen Prozesen nicht separieren, wobei der Hochfrequenzgrenzfall, $\omega \gg \omega_{\rm sep}$, siehe auch Gl. (4.22), eine Ausnahme bildet, bei der sich die Beiträge auf natürliche Weise trennen lassen: Wegen der viel größeren Rate von nicht-leptonischen Prozessen dominieren sie in diesem Fall.

Mit abnehmender Frequenz spielen die Urca Prozesse eine immer wichtigere Rolle. Zur maximalen Mischung mit den nicht-leptonischen Prozessen kommt es bei der Frequenz ω_0 (siehe Gl. (4.25) für die Definition), die abhängig von der Wahl der Modellparameter zwischen 1 $\rm s^{-1}$ und 10^3 $\rm s^{-1}$ liegen kann, siehe dazu auch Abb. 4.2 für die dazugehörigen Oszillationsperioden.

Unsere numerischen Ergebnisse für die normalleitende Phase von strange-Quark-Materie zeigen, daß die vielgenutzte Näherung, bei der Urca Prozesse komplett vernachlässigt werden, zu einem viel zu kleinen Wert für die Volumenviskosität führen kann, siehe Abb. 4.2 und 4.3. Beim Untersuchen eines großen Bereichs von Modellparametern stellt sich heraus, daß die Bedeutung der Urca Prozesse bei Temperaturen zwischen 0.1 MeV und 1 MeV am größten ist. Im äußeren Kern eines Quarksterns, also dort, wo die Dichte nicht zu hoch und die Masse des strange Quark nicht zu klein ist und/oder die Oszillationsperioden nicht zu kurz sind, kann die Berücksichtigung von Urca Prozessen zu einem Anstieg der Volumenviskosität um eine Größenordnung führen, siehe Abb. 4.4. Diese Ergebnisse haben möglicher Weise weitreichende Implikationen für die Physik junger Neutronensterne mit strange-Quark-Materie im Innern und/oder für reine seltsame Sterne, die potentiell auch existieren könnten.

Im fünften Kapitel benutzen wir die Ergenisse aus Kapitel vier um r-Moden Instabilitäten von Quarksternen zu untersuchen. Es wird gezeigt, daß das r-Moden Instabilitätsfenster von Quarkmaterie sich stark von dem der Neutronensternmaterie unterscheidet, was eine Möglichkeit bieten könnte, Quarksterne und Neutronensterne voneinander zu unterscheiden. Es wurde gezeigt, daß die Daten für Röntgen-Doppelsterne niedriger Massen das klassische Modell eines Neutronensterns ausschließen, bei dem der Pulsar komplett aus gleichförmiger Neutronen-Protonen-Elektronen Materie besteht. Ein weiterentwickeltes Modell, bei dem der Neutro-

nenstern aus einem flüssigen, rotierenden Zentrum aus Kernmaterie und einer festen, annähernd statischen Kruste besteht, kann jedoch nicht ausgeschlossen werden. Außerdem wurde gezeigt, daß die Tatsache, daß alle jungen Pulsare langsam rotieren, das Quarksternmodell in der ungepaarten oder der 2SC Phase zu stützen scheint.

Jede der unterschiedlichen farbsupraleitenden Phasen weist eine individuelle Struktur des r-Moden Instabilitätsfensters auf. Quarks in der CFL Phase generieren ein schmales Stabilitätsfenster bei Temperaturen, bei denen interessanter Weise junge Pulsare gebildet werden. Das bedeutet, daß ein neuentstandener Stern in der CFL Phase in einer stabilen Region gebildet wird und erst abkühlen muß, um die Instabilitätsregion zu erreichen, die bei $T = 10$ MeV beginnt. Es ist nicht mögliche, weitere Schlußfolgerungen zu ziehen, da für die CFL Phase noch einige weitere Beiträge berücksicht werden müssen.

Das r-Moden Instabilitätsfenster der CSL Phase bietet eine breitere Stabilitätsregion, die bei einer Temperatur $T \sim 0.01$ MeV endet. Die Situation ist für die CSL Phase jedoch nicht völlig geklärt, da es Unsicherheiten bei der Größe der Energie-Gap und der kritischen Temperatur gibt und noch weitere dissipative Phänomene berücksichtigt werden müssen.

Die 2SC Phase ist von der Struktur her der ungepaarten Quark-Materie sehr ähnlich, und die Schlußfolgerungen für die ungepaarte Phase können in ähnlicher Weise auch für die 2SC Phase gezogen werden. Der Grund hierfür ist, daß es in der 2SC Phase immer eine Quar-Farbe ohne Gap gibt, was bedeutet, daß ein Drittel der Quarks sich genau wie in der ungepaarten Quark-Materie-Phase verhält. Darüber hinaus bleibt das strange-Quark immer ohne Gap, was dazu führt, daß die nichtleptonischen schwachen Prozesse um etwa $\frac{2}{9}$, die *Urca* Prozesse des strange-Quark um $\frac{2}{3}$ und die des down-Quark um $\frac{1}{3}$ unterdrückt sind.

Im Anschluss an diese Arbeit könnte man versuchen, andere dissipative Phänomene in freier Quark-Materie zu berechnen, z.B. die Scherviskosität von supraflüssigen Phasen wie der CFL Phase [8] und der CSL Phase oder die Volumenviskosität aufgrund des supraflüssigen Zustands in der CFL [9] und der CSL Phase. Die Kombination dieser Ergebnisse mit denen aus Kap. (5) müßte zu einem präziseren Bild der r-Moden Instabilitätsfenster in den supaleitenden Phasen führen, was uns dann dazu in die Lage versetzen würde, weitreichendere astrophysikalische Konsequenzen zu ziehen.

Es gibt darüber hinaus noch weitere dissipative Phänomene, die berücksichtigt werden müssen, wie z.B. Dissipation aufgrund von Elektron-Elektron-Streuung in-

nerhalb des Systems oder aufgrund von Oberflächenreibung zwischen einem rotierenden Kern und einer annährend statischen Kruste.

Chapter 1

Introduction

Compact (neutron) stars provide a natural laboratory of matter under extreme conditions. In the central regions of such stars the baryon density of matter could reach values up to 10 times the nuclear saturation density (i.e., $10\rho_0$ where $\rho_0 \simeq 0.15$ fm^{-3}). At such high density matter is likely to be in a deconfined state in which quarks rather than hadrons are the natural dynamical degrees of freedom [10, 11, 12, 13, 14].

One can argue that, at sufficiently low temperatures, the ground state of deconfined quark matter is a color superconductor. (For reviews on color superconductivity, see Refs. [15, 16, 17, 18, 19, 20, 21, 22]). Many phases of color superconductivity are known that could possibly be realized in dense matter. It remains unclear, however, which of these describe the ground state of matter under the specific conditions in stars. This is because of theoretical uncertainties in treating the strongly coupled, non-perturbative dynamics in QCD at the baryon densities of relevance.

In order to clarify this one could use observational data from stars to narrow down the range of possibilities. For this program to work, one requires a detailed knowledge of the physical properties of various phases of matter that are likely to exist in stars. The transport properties are most suitable for developing sufficiently sensitive, as well as unique and verifiable predictions regarding observational signals from stars.

In general, the bulk viscosity is a measure of the kinetic energy dissipation during expansion and compression of a fluid. In compact stars, the density oscillations of interest have characteristic frequencies that are of the same order of magnitude as the stellar rotation frequencies. These are bound from below and from above, $1\ \mathrm{s}^{-1} \lesssim \omega \lesssim 10^3\ \mathrm{s}^{-1}$. (For the fastest-spinning pulsar currently known, PSR J1748-2446ad, one has $\omega \approx 4.5 \times 10^3\ \mathrm{s}^{-1}$ corresponding to $\nu = 716$ Hz [6].) The most important microscopic processes that provide the energy dissipation on the corresponding time scales are weak processes. Under conditions in stars, in particular, the bulk viscosity of quark matter is determined by the combined effect of the flavor-changing weak processes diagrammatically shown in Fig. 4.1. When an (instantaneous) departure from chemical equilibrium is induced by expansion/compression of matter, the weak processes try to restore the equilibrium state and, while doing this, reduce the oscillation energy.

The main goal of this thesis is to calculate the bulk viscosity of quark matter and color superconductors and to relate it to the r-mode instabilities of quark stars. Knowledge of the bulk viscosity and other macroscopic properties of quark matter is a very important step if one is to study the behaviour of compact stars containing such phases of matter. The analysis of r-mode instabilities is a good example for the importance of dissipative phenomena in distinguishing between the behaviour of a compact star containing a quark core and the behaviour of a pure hadronic star.

The first chapter of this thesis is a review of the QCD phase diagram, neutron stars' observational properties, and the basic properties of color-superconducting quark matter. The phase diagram of QCD is briefly discussed in the first section where the concepts of quark-gluon plasma and color superconductors are introduced. Properties of neutron stars such as mass, radius, and rotational frequency are briefly reviewed in the second section. From observed masses and radii it becomes clear that the density is too large for conventional matter to exist, and some form of exotic matter should exist. The third section discusses the differences between the several possible color-superconducting phases.

The second chapter is devoted to the calculation of weak interaction rates in quark matter which slightly deviates from β-equilibrium. These flavor-changing interactions regulate the chemical composition of the quark-gluon plasma. As the system oscillates, quark matter deviates from β-equilibrium while weak interactions

try to restore it. Because they lag behind, they cause an energy dissipation from the volume oscillation. Knowledge of weak interaction rates is essential for the study of bulk viscosity of neutron star matter.

In the third chapter we calculate the bulk viscosity of several phases of quark matter. In the third chapter, we calculate the bulk viscosity of the four most popular spin-one color-superconducting phases of two-flavor (non-strange) quark matter: the color-spin-locked (CSL), planar, polar, and the A phase. One of these could be the ground state of dense baryon matter if the spin-zero Cooper pairing of quarks is prevented by the constraints of charge neutrality and β-equilibrium. It turns out that the effect of color superconductivity is not necessarily to suppress the bulk viscosity, it could increase the bulk viscosity under certain conditions.

In the fourth chapter, we study the bulk viscosity of three-flavor (strange) quark matter. One of the key issues that we address here is the interplay between the Urca and the non-leptonic processes. We shall show that, because a resonance-type phenomenon determines the bulk viscosity and because there is a subtle interference of the two weak processes, the simple argument about the dominance of the non-leptonic processes is not always justified.

In the fifth chapter we study the quark contribution to the r-mode instability window of quark stars for different phases of deconfined quark matter. It will be shown that different phases of quark matter have different behaviours of the r-mode instabilities.

The sixth chapter will provide a summary of the results and an outlook to future research.

1.1 QCD Phase Diagram

One of the main features of quantum chromodynamics (QCD) is asymptotic freedom [23, 24, 25], that is, the interactions between quarks and gluons become weaker as the mutual distance decreases or as the exchanged momentum increases. Consequently, at sufficiently large temperatures and/or high densities, the interactions which con-

fine quarks and gluons inside hadrons should become weak enough to release them. The phase where quarks and gluons are deconfined is called the *quark-gluon plasma* (QGP).

At sufficiently low temperatures, fermions with an attractive interaction are expected to go through a superconducting phase transition, for example, the electron gas in metal has a net attractive potential between electrons due to phonon exchange [26]. At low temperatures (4K in mercury) the electrons form Cooper pairs and the metal becomes a superconductor. For quarks, these attractive interactions are the strong interactions. Unlike electrons, which have only spin as an internal degree of freedom, quarks have several internal degrees of freedom, namely color, flavor, and spin, which would lead to the possibility of several pairing schemes, *i.e.*, several possible phases of color superconductivity, see, for instance Refs. [15, 16, 18, 27]. It is *a priori* not clear which of these phases is the true ground state at which temperature and density.

In the conjectured phase diagram of QCD Fig. 1.1, every point represents an infinitely large system of quarks and gluons with a temperature T and a quark chemical potential μ. The phase diagram shows three major phases of QCD, the hadronic "confined" phase, the deconfined quark matter phase, and the color-superconducting phase.

The ground state of (infinite) nuclear matter is at $(T,\ \mu)_0 = (0,\ 308)$ MeV. There is a line of first-order phase transitions emerging from this point and terminating in a critical endpoint at a temperature of order ~ 10 MeV. At this point, the transition is of second order. This phase transition is the nuclear liquid-gas transition. To the left of the line nuclear matter is in the gaseous phase, and to the right in the liquid phase. Above the critical endpoint, there is no distinction between these two phases.

At temperatures below ~ 160 MeV and quark chemical potential below ~ 350 MeV, corresponding to net-baryon densities a few times larger than the ground state density of nuclear matter, strongly interacting matter is in the hadronic phase. There is a line of first-order phase transitions separating the hadronic phase from the QGP, this line terminates at an end point where the transition is of second order. For smaller quark chemical potentials, the transition becomes a crossover, and there is no real distinction between the hadronic phase and the QGP.

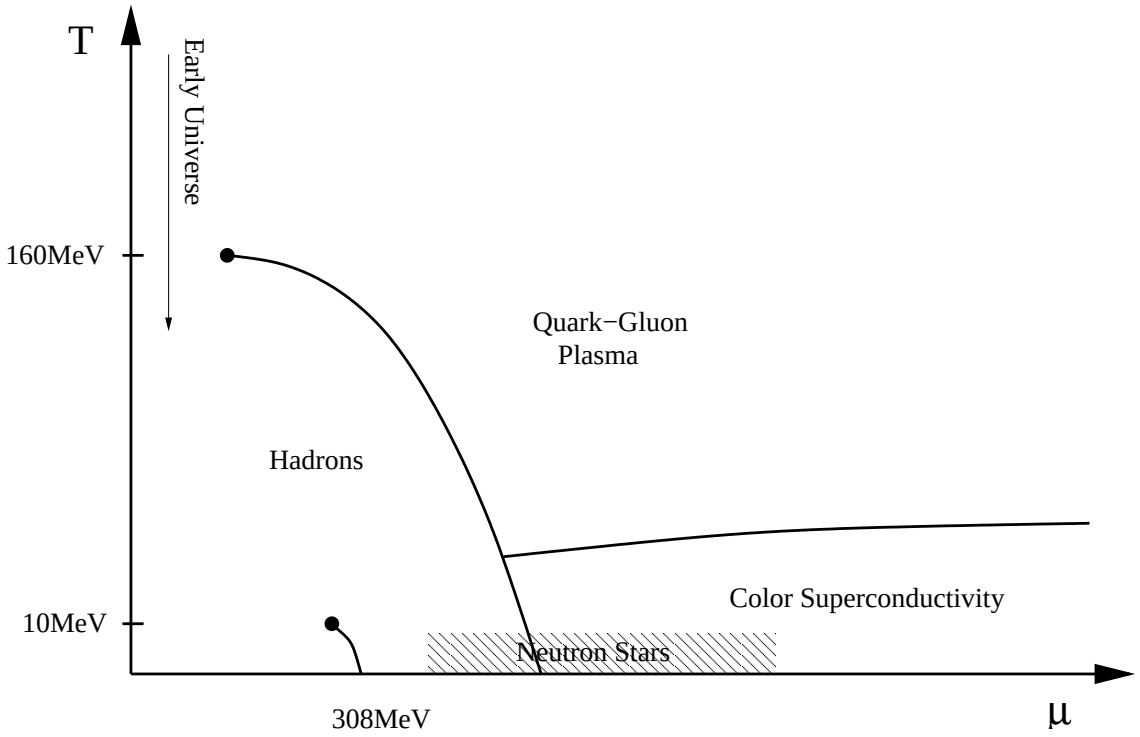

Figure 1.1: A sketch showing the general features of the QCD phase diagram from Ref. [1]

At large quark chemical potentials and small temperatures, the QGP becomes a color superconductor. The dynamics of phase transitions between the QGP and the hadronic phase are yet unclear mainly due to the fact that we don't know which color-superconducting phase exist at a given temperature and quark chemical potential.

The QGP was certainly present during the evolution of the early universe; the early universe evolved close to the T-axis in Fig.1.1, *i.e.*, at high temperature and nearly zero baryon chemical potential. In the present day, deconfined quark matter (QM) may exist in the interior of compact stellar objects such as neutron stars. There the temperature is generally very small compared to the chemical potentials of quarks, thus, neutron stars exist near to the μ- axis of the QCD phase diagram.

1.2 Neutron Stars

Neutron stars provide a rare opportunity to observe matter under extreme conditions. The conditions there are close to the μ-axis in Fig. 1.1, *i.e.*, small temperature and large quark chemical potential. The baryon density in neutron stars may be up to several times the nuclear density, whereas the temperature may be as low as a few tens of keV.

Neutron stars are produced as supernova remnants [28]. Stars originally more massive than around $8M_\odot$ eventually will collapse explosively to produce a supernova. Unless the star had a mass greater than $25M_\odot$ the remains of that star after the supernova explosion become a neutron star. The gravitational energy that is released causes a giant explosion known as "supernova", expelling a large fraction of the star into space. Following the collapse, the core of the star is compressed to a hot proto-neutron star which is, in effect, a neutron star with neutrinos still trapped inside due to the short mean free path because of high temperature. Neutrinos diffuse out of the proto-neutron star rapidly after its creation, leaving a much colder, but still hot neutron star. In a neutron star the neutrino mean free path is larger than the radius of the star, and the star is neutrino-free.

1.2.1 Properties of Neutron Stars

Global properties of neutron stars, such as mass, rotational frequency, and radius are sensitive to the microscopic equation of state. In order to understand the behavior of matter under extreme conditions such as those present in the cores of the stars, a good estimate of these properties is needed. Here we provide a review of a selected set of observational constraints.

Mass

The gravitational mass of neutron stars can be inferred from observations of their gravitational pull on a binary companion star in X-ray binaries and binary pulsars. A recent compilation of the results of pulsar masses was published in Ref. [2], these

results are shown in Fig. 1.2.

In short, Fig. 1.2 suggests that the most common mass of neutron stars is close to $1.4M_{\odot}$ and that the masses of individual neutron stars fall in between $0.8 < M/M_{\odot} < 2.5$.

The major source of uncertainty usually is the inclination of the orbit with respect to the line of sight, and it is only in highly relativistic systems that general relativistic effects allow for a complete characterization of the orbit [29, 30].

Radius

Due to the compactness of neutron stars it is very difficult to observe them directly and measure their radius. However, there is a variety of methods to estimate the radius of a neutron star [31]. Most of these methods depend on the measurements of the surface temperature and the distance.

For example, Ref. [32] provided an estimate of the pulsar **RX J1856.5-3754** as follows. The observed surface temperature is $T \sim 57$ eV and its distance is $d \sim 140$ pc. According to black-body radiation the measured flux should be $F = \sigma_{SB} T^4 R_{\infty}^2/d^2$, where $\sigma_{SB} = 5.6704 \times 10^{-8}\mathrm{Wm}^{-2}\mathrm{K}^{-4}$ is the Stefan-Boltzmann constant. From the measured flux one finds $R_{\infty} \simeq 15$ km, where, R_{∞} is the "radiation" radius using black-body radiation fitting, giving a physical radius of $R \simeq 12$ km.

Rotation Frequencies

The most accurate property that we know about pulsars are their spin frequencies ν and frequency time-derivative $\dot{\nu}$. The characteristic age of the pulsar can be estimated by using $\mathrm{Age} = \frac{\nu}{2\dot{\nu}}$; the observed data for rotation frequencies and ages of pulsars is given in Fig. 1.3.

The fastest rotation frequency measured is 716 Hz for **PSR J1748-244ad** [6]. Rapidly rotating pulsars are believed to be old, recycled pulsars that gained angular

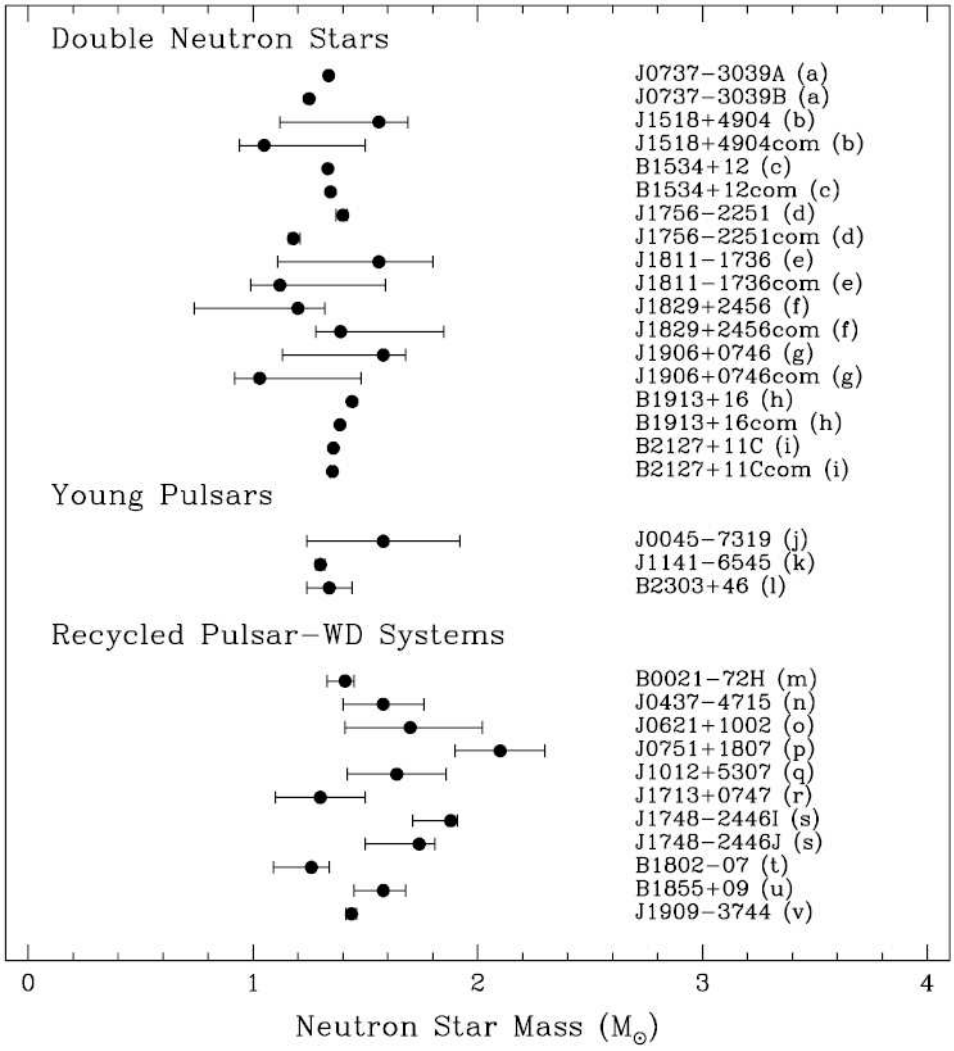

Figure 1.2: Distribution of observed neutron star masses [2].

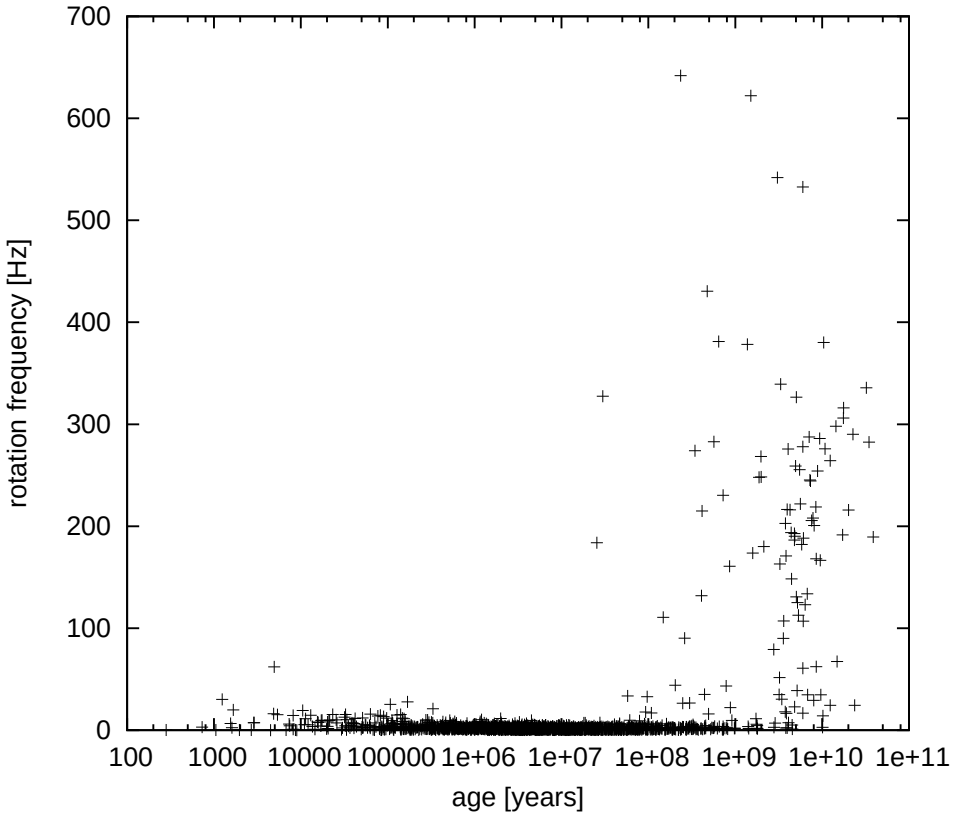

Figure 1.3: The spins of almost all known pulsars vs. their ages [3].

momentum through accretion of matter from a companion star in a binary system.

All young pulsars (younger than 10^7 years) are slowly rotating, $\nu < 80$ Hz, which is interesting since one would expect that a pulsar is generated with a large spin frequency $\nu \sim 1200$Hz in order to conserve the angular momentum of parent star.

The upper limit of rotation frequency of the star is set by the Kepler frequency $\Omega_K \sim 0.78\sqrt{\pi G_N \rho}$ where G_N is Newton's gravitational constant, above this frequency the neutron star would eject matter from the equator.

1.2.2 Structure of Neutron Stars

The density of a neutron star with a mass of $1.4M_\odot$ and a radius of 12km would be $\rho \sim 3.846 \times 10^{14}$g cm^{-3}, which is several times larger than the density of atomic nuclei. At such large densities, one would expect that exotic phases of matter should exist. The simplest "least exotic" phase expected is where the star is composed of a system of neutrons, protons, and electrons in a charge neutral, β-equilibrated state. However, at such high densities, the chemical potentials of neutrons in the core may be large enough to produce other, more massive and/or strangeness carrying hadrons such as Σ, Λ, Ξ, and Δ particles; the star is then called a hyperon star.

It is also possible that at such high densities strong interactions are weak enough to produce a deconfined quark matter phase. If the QGP is the true ground state of matter at the conditions available in neutron stars, then the whole star may be composed of strange quark matter. The star is then called a quark star or a strange star. If that is not the case, quark matter might still be present in the inner core of the star; the star is then called a hybrid star. In this thesis, we will focus on quark stars. A summary of possible structures is shown in Fig. 1.4.

Strange (Quark) Stars

The idea that strange quark matter is the ground state of QCD has been raised by Bodmer [33] and Witten [34]. If the hypothesis is true, then the possibility of the existence of strange quark stars opens up. If so, pulsars are to be interpreted as

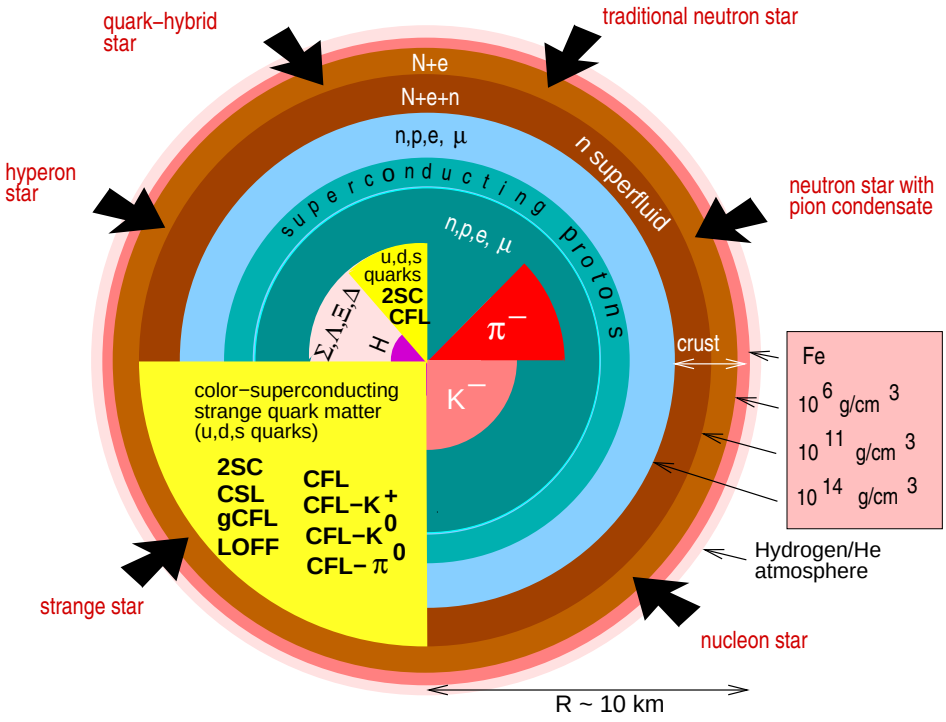

Figure 1.4: Possible phases and structures of a neutron star [4].

rotating strange stars rather than rotating neutron stars.

The structure of quark stars in terms of the mass-radius relationship and density profile has been studied extensively using different models for different phases of quark matter and color superconductivity, see, for instance, Refs. [35, 36, 37, 38, 39]. These calculations show that there is a certain density profile for the quark star. Here, however, we'll follow the widely used approximation that the star has a uniform density.

If strange quark matter is absolutely stable, strange stars may be bare, consisting of quark matter fluid all the way to the surface. In the more likely case, where gas from the supernova explosion or accreted matter reaches the surface, a solid crust is formed which floats on top of a huge electrostatic potential [40]. Thus, the solid crust remains separated from the quark surface, and the star can be treated as being bare.

1.3 Color Superconductivity

One of the main features of superconductivity is that the quasi-particle excitations acquire an energy gap Δ. The quasiparticle excitation energy ϵ then becomes

$$\epsilon = \sqrt{(E-\mu)^2 + \Delta^2}, \tag{1.1}$$

where $E = \sqrt{p^2 + m^2}$ is the relativistic energy of the quasi-particle as it was in vacuum with p being the momentum of the particle and m being the particle mass. Also, μ is the particle chemical potential.

The energy gap is temperature dependent. It reaches a chemical potential-dependent maximum value at zero temperature Δ_0 and becomes zero at a critical temperature T_c,

$$\Delta = \Delta_0 \sqrt{1 - \left(\frac{T}{T_c}\right)^2}. \tag{1.2}$$

In BCS theory [26], the transition between superconducting and normal phase is usually of second order, with a critical temperature T_c^{BCS} proportional to the zero-temperature gap,

$$T_c^{BCS} \simeq 0.567 \Delta_0. \tag{1.3}$$

At least in the mean field approximation, in most color-superconducting phases considered so far, T_c either obeys Eq. (1.3) or differs only by a factor of order one from it [18].

If deconfined quark matter is to exist in the cores of neutron stars, it is most probably color-superconducting. As mentioned in Sec. 1.1 there are many possible pairing schemes. Here we discuss the main possible pairing schemes and phases of color-superconducting quark matter (consult [15, 16, 18, 21, 27] for reviews on color superconductivity).

1.3.1 CFL Phase

With a slight idealization of QCD in which the masses of the u, d, and s quarks are set to zero and those of the c, t, and b quarks are set to infinity, the Cooper pairs *cannot* be flavor singlets and both color and flavor symmetries are necessarily broken [41]; the color symmetry is broken to because the strong interactions that cause Cooper pairing should be attractive, whereas the flavor symmetry is broken to ensure that the total wavefunction of the spin-zero Cooper pair is anti-symmetric.

The condensate in the CFL (Color-Flavor Locked) phase has the form

$$\begin{aligned} \left\langle \psi^a_{Li}(\vec{p})\psi^b_{Lj}(-\vec{p})\right\rangle &= -\left\langle \psi^a_{Ri}(\vec{p})\psi^b_{Rj}(-\vec{p})\right\rangle \\ &= k_1\delta^a_i\delta^b_j + k_2\delta^a_j\delta^b_i, \end{aligned} \tag{1.4}$$

where $i,\ j = 1,\ 2,\ 3$ and $a,\ b = 1,\ 2,\ 3$ are flavor and color indices, $\psi_{L(R)}$ are the left (right) handed quark spinors, $k_1(\equiv \Delta_0^{CFL}) \simeq -k_2$, and $\vec{p}$ is the quark momentum.

All the quark modes are gapped; the nine quasiquarks (three colors times three flavors) fall into $\mathbf{8}\oplus\mathbf{1}$ so there are two gap parameters, the singlet has a larger gap that the octet, twice as large at weak coupling.

The critical temperature might be as large as 50 MeV when the quark chemical potential $\mu_s \sim 400$ MeV [42]. Using Eq. (1.3) we get $\Delta_0^{CFL} \simeq 89$ MeV. When thermal gluon fluctuations are included T_c assumes a larger value and the transition is first order [43].

The CFL phase has many special features. In the CFL phase the baryon symmetry is spontaneously broken, thus, CFL quark matter becomes a superfluid of the same sort as those found in condensed matter systems such as Bose-Einstein condensates. One of the complications of superfluids is that they have more viscosity coefficients than normal fluids. For instance, there are three bulk viscosity coefficients: one associated with the normal fluid hydrodynamic velocity studied in Ref. [9] and two associated with the difference in hydrodynamic velocities between both the normal and superfluid components. Also, the strange quark mass induces a stress on the CFL phase that may lead to neutral kaon condensation, producing a CFL-K^0 phase. The bulk viscosity due to kaons in the CFL-K^0 phase has been studied in Ref. [44].

1.3.2 2SC Phase

The strange quark mass $m_s \sim 100$ MeV is larger than the up and down quark masses $m_{u,\ d} \lesssim 10$ MeV. Therefore, there will be a Fermi surface mismatch between the strange quark and the up and down quarks. In this case the up and down quarks

can pair and form a condensate, the so-called 2-flavor color-superconducting (2SC) phase.

In the 2SC phase the condensate takes the form

$$\begin{aligned} \left\langle \psi^a_{Li}(\vec{p})\psi^b_{Lj}(-\vec{p})\right\rangle &= -\left\langle \psi^a_{Ri}(\vec{p})\psi^b_{Rj}(-\vec{p})\right\rangle \\ &= \epsilon_{ij}\epsilon^{ab3}\Delta^{2SC}, \end{aligned} \tag{1.5}$$

where the flavor indices $i,\ j = 1,\ 2$.

In the 2SC phase, the red and green quarks acquire a gap Δ_{2SC}, whereas there is no gap for the blue quark. The critical temperature is $T_c \sim 30$ MeV. Using Eq. (1.3) we get $\Delta_0^{2SC} \simeq 52.6$ MeV.

Since no global symmetries are broken, the 2SC phase is not a superfluid. And since there are ungapped quarks, they will dominate all interaction rates and the physical properties of the system. They will only be different from normal quark matter by a factor as shown in Sec. 5.4.3 and Refs. [5, 45].

1.3.3 Spin-1 Phases

If the strange quark mass is large enough, the condition of charge neutrality requires that the electron chemical potential to be large. The strange quark mass and the large electron chemical potential will cause a substantial difference in particle species' Fermi momenta and pairing between different quark flavors may not be possible. The remaining option, then, is Cooper pairing of each flavor with itself.

To maintain the fermionic antisymmetry of the Cooper pair wave function, single-flavor pairing phases have to be either symmetric in color, which greatly weakens or even eliminates attractive interactions, or symmetric in spin, which causes particles of the same spin to pair together and, therefore, the Cooper pairs will have a total spin of 1.

Spin-one phases generally break rotational symmetry, only the CSL phase is isotropic. That anisotropy leads the energy gap Δ in Eq. (1.1) to be multiplied

by $\sqrt{\lambda_{\xi,i}}$, where $\lambda_{\xi,i}$ is a function of $\xi = \cos\theta$ where θ is the angle with the spin axis. The values of $\lambda_{\xi,i}$ are shown in Table. 1.1. For details see Refs. [1, 46].

Table 1.1: Functions ω_{ii} and $\lambda_{\xi,i}$ for four spin-one color superconductors.

phase	$\omega_{11}(\xi)$	$\lambda_{\xi,1}$	$\omega_{22}(\xi)$	$\lambda_{\xi,2}$	$\omega_{33}(\xi)$	$\lambda_{\xi,3}$
CSL	2	2	1	0	-	-
planar	2	$1+\xi^2$	1	0	-	-
polar	2	$1-\xi^2$	1	0	-	-
A	1+sgn(ξ)	$(1+\lvert\xi\rvert)^2$	1-sgn(ξ)	$(1-\lvert\xi\rvert)^2$	1	0

The numbers ω_{ii} are given in Ref. [47], they are used to calculate the rate of the d-quark β-decay in spin-1 color superconductors in Ch. 3 in a similar fashion as in Ref. [47]. Since weak interaction do not change the color, *i.e.* a, say, red down-quark decays into a red up-quark, ω_{ii} simply counts the number of colors that have a cirtain gap function $\lambda_{\xi,1}$

Spin-1 color-superconductors may involve pairing of quarks as well as of opposite chiralities. Here we focus on the so-called "transverse" phases, in which exclusively quarks of opposite chiralities pair. Theoretical studies at asympototically large densities suggests that these phases are preferred [47, 46].

Matter in which each flavor pairs with itself, "spin-1 CSC", has been studied using NJL models and weakly-coupled QCD. These calculations agree that the energetically favored state is color-spin-locked (CSL) for each flavor [46, 7, 48]. CSL pairing involves all three colors where the color direction of each Cooper pair is correlated with its spin direction. The phase is isotropic with rotational symmetry surviving as a group of simultaneous spatial and color rotations. Other possible spin-1 CSC phases include the polar, planar, and A phases described in Ref. [46]. These phases do break rotational symmetry and some exhibit a point or line node of the energy gap at the Fermi surface, i.e., the value of the gap vanishes.

The CSL phase is isotropic since $\lambda_{\xi,i}$'s do not depend on ξ. Two color branches of the Cooper pair are gapped, whereas the third remains ungapped $\lambda_{\xi,i} = 0$. It has

been suggested in Ref. [7] that the third "ungapped" mode has a gap dependent on the quark mass, where $\lambda_{\xi,2} = \frac{m_q}{\sqrt{2}\mu_q}$.

The ratios between the gaps at zero temperature and the critical temperatures $\frac{T_c}{\Delta_0}$ were calculated in Ref. [46], 0.8 (CSL), 0.66 (planar), 0.49 (polar), and 0.81 (A phase). Critical temperatures for spin-1 phases are typically smaller than those of cross-flavor-paired phases, perhaps as large as a few MeV, or as small as a few eV.

1.3.4 The Energy Gap

In this section, information about the energy gaps of several color-superconducting phases will be summarized, more details can be found in Ref. [49].

In the 2SC phase, the value of the zero-temperature gap at the Fermi surface is given in terms of the strong interactions' coupling constant $\alpha_s \equiv \frac{g^2}{4\pi}$, the number of flavors contributing to the condensate N_f and the chemical potential μ by [50]

$$\Delta_0^{2SC} = 2\ \tilde{b}\ b_0'\ \mu\ e^{-\frac{\pi}{2\bar{g}}}, \tag{1.6}$$

where

$$\bar{g} \equiv \frac{g}{3\ \sqrt{2}\ \pi}, \tag{1.7}$$

$$\tilde{b} \equiv 256\ \pi^4 \left(\frac{2}{N_f g^2}\right)^{5/2}, \tag{1.8}$$

$$b_0' \equiv e^{-\frac{\pi^2+4}{8}}. \tag{1.9}$$

The critical temperature in the 2SC phase obeys Eq. (1.3).

The excitation energy in Eq. (1.1) can be generalized to take the form,

$$\epsilon_r = \sqrt{(E-\mu)^2 + \lambda_{\xi,r}\Delta^2}. \tag{1.10}$$

The index r labels possible excitation branches in the superconductor, which differ by the value of $\lambda_{\xi,r}$ (the ξ index will be dropped henceforth). The advantage of introducing λ_r is that it allows us to generalize Eq. (1.10) to different color-superconducting systems. For example, in the 2SC phase, quarks with two colors form the Cooper pairs, while the third color remains unpaired. Consequently, there are two different excitation energies, ϵ_1 and ϵ_2, four quasiparticle excitations have $\lambda_1 = 1$, while two have $\lambda_2 = 0$, corresponding to ungapped modes. In the CFL phase, on the other hand, all nine quark colors and flavors form Cooper pairs, but there are still two distinct fermionic excitations. The first with $\lambda_1 = 4$ occurs with degeneracy one, while the other, with $\lambda_2 = 1$, has a degeneracy eight. In spin-one color superconductors, λ_i also defines the angular dependence of the gap, see Table 1.1.

We can write the gap functions of the other phases in terms of the 2SC gap,

$$\frac{\Delta_0^i}{\Delta_0^{2SC}} = \frac{e^{-d}}{\sqrt{\lambda_1^{a_1}\ \lambda_2^{a_2}}}, \tag{1.11}$$

where d is a constant of order one which vanishes for spin-zero color superconductors [49]. The constants a_s are positive numbers, obeying the constraint $\sum_{s=1}^{2} a_s = 1$. The superscript i is just to indicate which phase is in consideration, CFL, 2SC, CSL, and so on. Note that for all the systems we consider there are two excitation branches, and so the indices r and s take the values 1 and 2 only, however, in some spin-0 and spin-1 phases it is possible to have these indices take the values 1,2, and 3, these cases are not of concern to us in this thesis.

The critical temperature T_c is given by

$$\frac{T_c^i}{\Delta_0^i} = 0.567\sqrt{\lambda_1^{a_1}\ \lambda_2^{a_2}}. \tag{1.12}$$

Finally, we provide the values of the constants mentioned in this section for various color-superconducting phases in Table 1.2.

Table 1.2: The values of a_r, λ_r, and d for the 2SC, CFL, and the CSL phases.

phase	λ_1	λ_2	a_1	a_2	d
2SC	1	0	1	0	0
CFL	4	1	1/3	2/3	0
CSL	2	0	1	0	9/2

Chapter 2

Weak Interaction Rates in Quark Matter

This second chapter is devoted to the calculation of weak interaction rates in quark matter which slightly deviates from β-equilibrium. These flavor-changing interactions regulate the chemical composition of the quark-gluon plasma. As the system oscillates, quark matter deviates from β-equilibrium while weak interactions try to restore it. Because they lag behind, they cause an energy dissipation from the volume oscillation. Knowledge of weak interaction rates is essential for the study of bulk viscosity of neutron star matter.

The number densities of particles are controlled by β-equilibrium and electrical charge neutrality. In this chapter we show how to calculate particle number densities using these conditions.

In β-equilibrium, weak interaction rates are such that the forward and backward channels have the same rate. Due to radial oscillations, the chemical potentials will be driven away from their equilibrium values, leading to a difference in interaction rates between the forward and backward channels.

2.1 Quark Matter in β-Equilibrium

In this section we consider three-component (u,d, and s) quark matter in β-equilibrium. The β-equilibrium conditions are

$$\mu_d = \mu_s = \mu_u + \mu_e, \tag{2.1}$$

where the μ_i's are the chemical potentials of the quarks and electrons. We assume that electrons are the only leptons present in the system because the neutrinos and anti-neutrinos leave the system as soon as they are produced in weak interactions due to their large mean free path. Moreover, there are no muons to be considered.

Electric charge neutrality sets an additional constraint on the number densities, n_i, of the quarks and electrons,

$$\frac{2}{3}n_u - \frac{1}{3}n_d - \frac{1}{3}n_s - n_e = 0. \tag{2.2}$$

The relationship between the chemical potentials and the number densities is given by

$$\begin{aligned} n_f &= \frac{\left(\mu_f^2 - m_f^2\right)^{3/2}}{\pi^2} - \frac{2\alpha_s}{\pi^3}\mu_f\left(\mu_f^2 - m_f^2\right) \\ &\times \left(1 - \frac{3m_f^2}{\mu_f\sqrt{\mu_f^2 - m_f^2}}\ln\frac{\mu_f + \sqrt{\mu_f^2 - m_f^2}}{m_f}\right), \quad \text{for} \quad f = u, d, s, \end{aligned} \tag{2.3a}$$

$$n_e = \frac{1}{3\pi^2}\mu_e^3. \tag{2.3b}$$

If the masses of these particle are neglected and the coupling constant is set to zero, we have from Eq(2.1) and 2.3 that $\mu_e = 0$ and all other μ_f are equal such that

$$n_u = n_d = n_s, \qquad n_e = 0. \tag{2.4}$$

Considering quark masses and the coupling constant effects will complicate the situation; in order to find the chemical potentials of quarks and electrons in the system one needs to solve for charge neutrality and chemical equilibrium conditions; the results are shown in Fig. 2.1. The effect of the strange quark mass is to increase the electron chemical potential, this is because of the reduction of the number of strange quarks due to the strange quark mass and, thus, the need for electrons to compensate for the loss of negatively charged particles in order to maintain charge neutrality.

The effect of strong interactions is more subtle, and needs to be studied in detail, but we can see that it lowers the electron chemical potential while keeping the quarks' chemical potentials nearly the same.

It must be noted that at a large value of the coupling constant the electron chemical potential drops to even negative values, we assume that this is impossible and set the electron chemical potential to zero, these results are, however, not very reliable since the effect of the coupling constant is determined perturbatively and the perturbation scheme breaks down at large values of α_s.

The Fermi momentum of the particle p_{Fi} is given by

$$n_i = \frac{N_i \times p_{Fi}^3}{6\pi}, \tag{2.5}$$

where N_i is the degeneracy of the particle species, for electrons it is 2, there are two possible spin orientations. For quarks of a given flavor it is 6, 3 color$\times$ 2 spin.

2.2 Weak Interaction rates

Since the bulk viscosity of matter in compact stars is dominated by the flavor-changing weak interactions, it is necessary to evaluate the rates of these interactions.

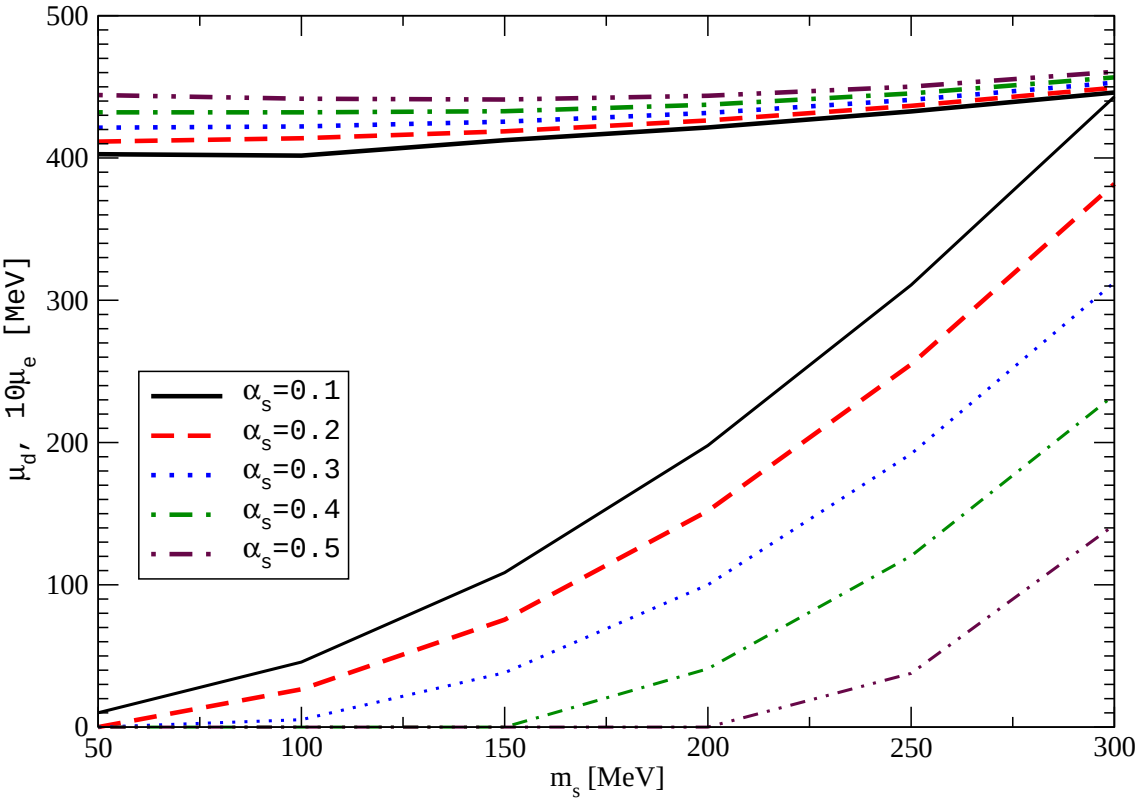

Figure 2.1: The values of $\mu_d = \mu_s$ (thick lines) and $10\mu_e$ (thin lines) vs. the strange quark mass for different values of the coupling constant α_s.

The energy dissipation comes from the fact that the interaction rate difference between the incoming and outgoing channels of each weak interaction oscillates out of phase with the volume oscillations. The interaction rate we calculate is the difference in interaction rates expanded in terms of the deviation $\delta\mu_i$ of chemical potentials from their equilibrium values.

2.2.1 Down-Quark β Decay

In this section we calculate the difference in rates between the d quark β-decay and its inverse interaction which involves electron capture,

$$d \to u + e + \bar{\nu}_e, \tag{2.6}$$
$$u + e \to d + \nu_e \tag{2.7}$$

Assuming that the d and u quarks are massless and non-interacting, *i.e.* , $p_{Fu,d} = \mu_{u,d}$, the d-quark β decay is strongly suppressed [51, 52]. However, including strong interactions, the above mentioned relation becomes

$$\mu_{u,d} = \left(1 + \frac{2}{3\pi}\alpha_s\right) p_{Fu,d}, \tag{2.8}$$

which removes the suppression from the interaction.

We use Fermi's Golden Rule to calculate the interaction rates [51, 52],

$$\begin{aligned}\Gamma_{\bar{\nu}}(\delta\mu) = 6 \prod_{i=d,u,\bar{\nu},e} \left[\int \frac{d^3p_i}{(2\pi)^3 E_i}\right] |M_{du}|^2 (2\pi)^4 \delta^4(P_d - P_u - P_e - P_{\bar{\nu}}) \\ \times f\left(\frac{E_d - \mu_d}{T}\right)\left[1 - f\left(\frac{E_u - \mu_u}{T}\right)\right]\left[1 - f\left(\frac{E_e - \mu_e}{T}\right)\right],\end{aligned} \tag{2.9}$$

where E_i is the energy of the particle and T is the temperature.

The matrix element for the down-quark *Urca* process $|M_{du}|^2$ is given by [51, 52]

$$|M_{du}|^2 = 64G^2 \cos^2\theta_c (P_d \cdot P_{\bar{\nu}})(P_u \cdot P_e), \tag{2.10}$$

where P_i is the 4-momentum of the i^{th} particle, whereas $\vec{p_i}$ is the 3-momentum, and $(P_i \cdot P_j)$ is the scalar product between the four-momenta of the i^{th} and the j^{th} particles. The function f is the Fermi distribution function $f(x) = \frac{1}{1+e^x}$. We can approximate the four products in the matrix element equation by

$$(P_u \cdot P_e) \simeq E_u E_e \left(1 - \frac{|\vec{p}_u|}{E_u}\cos\theta_{ue}\right) \simeq E_u E_e \frac{4\alpha_s}{3\pi}, \tag{2.11a}$$

$$(P_d \cdot P_{\bar{\nu}}) \simeq E_d E_{\bar{\nu}} \left(1 - \frac{|\vec{p}_d|}{E_d}\cos\theta_{d\bar{\nu}}\right) \simeq E_d E_{\bar{\nu}}, \tag{2.11b}$$

where we have assumed that the angle between d and $\bar{\nu}$ is randomised and the integration around it gives zero.

Integrating the electron's 3-momentum with the delta function we get

$$\begin{aligned}
\Gamma_{\bar{\nu}}(\delta\mu) &= \frac{6}{2^4(2\pi)^8} 64G^2 \cos^2\theta_c \frac{4\alpha_s}{3\pi} \\
\times &\int d\Omega_d d\Omega_u d\Omega_{\bar{\nu}} dp_d dp_u dp_{\bar{\nu}} |p_d|^2 |p_u|^2 |p_{\bar{\nu}}|^2 \delta(E_d - E_u - E_e - E_{\bar{\nu}}) \\
\times &\; f\left(\frac{E_d - \mu_d}{T}\right)\left[1 - f\left(\frac{E_u - \mu_u}{T}\right)\right]\left[1 - f\left(\frac{E_e - \mu_e}{T}\right)\right].
\end{aligned} \tag{2.12}$$

The argument in the energy delta function can be written as,

$$\begin{aligned}
\Delta E = E_d - E_u - E_e - E_{\bar{\nu}} &= E_d - E_u - E_{\bar{\nu}} - (|p_d| - |p_u|)\left[1 + \frac{1}{2}\frac{A}{(|p_d| - |p_u|)^2}\right] \\
&= (E_d - |p_d|) - (E_u - |p_u|) - E_{\bar{\nu}} - \frac{1}{2}\frac{A}{|p_d| - |p_u|}
\end{aligned}$$

where A is defined as,

$$A = p_{\bar{\nu}}^2 + 2|p_d||p_u|(1-\cos\theta_{ud}) - 2|p_{\bar{\nu}}|(|p_d|+|p_u|)\cos\theta_{d\bar{\nu}},$$

so that, if we assume that $\theta_{d\bar{\nu}}$ is randomised and the integral over its cosine gives zero,

$$\Delta E \simeq \frac{2\alpha_s}{3\pi}\mu_e - E_{\bar{\nu}} - \frac{|p_{\bar{\nu}}|^2 + 2|p_d||p_u|(1-\cos\theta_{ud})}{2(|p_d|-|p_u|)}. \tag{2.13}$$

Further simplification can be obtained if we assume that $E_{\bar{\nu}} = |p_{\bar{\nu}}| \ll \mu_e$,

$$\Delta E \simeq \frac{2\alpha_s}{3\pi}\mu_e - \frac{|p_d||p_u|(1-\cos\theta_{ud})}{(|p_d|-|p_u|)}, \tag{2.14}$$

which means that the energy conservation becomes

$$1-\cos\theta_{ud} = \frac{(|p_d|-|p_u|)}{|p_d||p_u|}\frac{2\alpha_s}{3\pi}\mu_e. \tag{2.15}$$

Assuming that $(|p_d|-|p_u|) \simeq |p_e| \simeq p_{Fe} \simeq \mu_e$ the previous equation becomes

$$1-\cos\theta_{ud} \simeq \frac{1}{|p_d||p_u|}\frac{2\alpha_s}{3\pi}\mu_e^2, \tag{2.16}$$

which means that the energy delta function becomes

$$\delta(E_d - E_u - E_e - E_{\bar{\nu}}) = \frac{\mu_e}{|p_d||p_u|}\delta\left(\cos\theta_{ud} - 1 + \frac{1}{|p_d||p_u|}\frac{2\alpha_s}{3\pi}\mu_e^2\right). \tag{2.17}$$

After these simplifications we obtain that $\Gamma_{\bar{\nu}}$ is

$$\begin{aligned}
\Gamma_{\bar{\nu}} &= \frac{6}{2^4(2\pi)^8}64G^2\cos^2\theta_c\frac{4\alpha_s}{3\pi}\int d\Omega_d d\Omega_u d\Omega_{\bar{\nu}} dp_d dp_u dp_{\bar{\nu}} \\
&\times |p_d||p_u||p_{\bar{\nu}}|^2\mu_e\delta\left(\cos\theta_{ud} - 1 + \frac{1}{|p_d||p_u|}\frac{2\alpha_s}{3\pi}\mu_e^2\right) \\
&\times f\left(\frac{E_d-\mu_d}{T}\right)\left[1-f\left(\frac{E_u-\mu_u}{T}\right)\right]\left[1-f\left(\frac{E_e-\mu_e}{T}\right)\right].
\end{aligned}$$

Note that the energy delta function restricts only the angular integral $\int d\Omega_d d\Omega_u d\Omega_{\bar{\nu}}$ where the integration over the polar angles of $\bar{\nu}$ and d gives 4π each. Moreover, $\cos\theta_{ud}$ takes one fixed value due to the delta function such that the integration over the u polar angle gives 2π, *i.e.*,

$$\int d\Omega_d d\Omega_u d\Omega_{\bar{\nu}} \delta\left(\cos\theta_{ud} - 1 + \frac{1}{|p_d||p_u|}\frac{2\alpha_s}{3\pi}\mu_e^2\right) = (4\pi)^2 2\pi, \tag{2.18}$$

which means that,

$$\begin{aligned}\Gamma_{\bar{\nu}}(\delta\mu) &= \frac{3}{2(2\pi)^5} 64 G^2 \cos^2\theta_c \frac{4\alpha_s}{3\pi} \int dE_d dE_u dE_{\bar{\nu}} E_d E_u \mu_e E_{\bar{\nu}}^2 \\ &\times f\left(\frac{E_d-\mu_d}{T}\right)\left[1 - f\left(\frac{E_u-\mu_u}{T}\right)\right]\left[1 - f\left(\frac{E_e-\mu_e}{T}\right)\right].\end{aligned}$$

We have assumed that all the particles are relativistic and massless. Making the approximation that $E_d E_u \simeq \mu_d \mu_u$ we have that

$$\begin{aligned}\Gamma_{\bar{\nu}}(\delta\mu) &= \frac{3}{2(2\pi)^5} 64 G^2 \cos^2\theta_c \frac{4\alpha_s}{3\pi} \mu_d\mu_u\mu_e \int dE_d dE_u dE_{\bar{\nu}} E_{\bar{\nu}}^2 \\ &\times f\left(\frac{E_d-\mu_d}{T}\right)\left[1 - f\left(\frac{E_u-\mu_u}{T}\right)\right]\left[1 - f\left(\frac{E_e-\mu_e}{T}\right)\right].\end{aligned}$$

Performing a change of variables, $\frac{E_i-\mu_i}{T} = x_i \Rightarrow dE_i = T dx_i$ (note that $\mu_{\bar{\nu}} = 0$) we get,

$$\begin{aligned}\Gamma_{\bar{\nu}}(\delta\mu) &= \frac{3}{2(2\pi)^5} 64 G^2 \cos^2\theta_c \frac{4\alpha_s}{3\pi} \mu_d\mu_u\mu_e T^5 \\ &\times \int dx_d dx_u dx_{\bar{\nu}} x_{\bar{\nu}}^2 f(x_d)[1-f(x_u)][1-f(x_e)].\end{aligned} \tag{2.19}$$

With the new variables x_i, the conservation condition becomes

$$\begin{aligned} E_d - E_u - E_e - E_{\bar{\nu}} &= T\left(x_d - x_u - x_e - x_{\bar{\nu}} - \frac{\delta\mu_3}{T}\right) \\ &\Rightarrow \quad x_d - x_u - x_e - x_{\bar{\nu}} - \xi = 0, \end{aligned} \tag{2.20}$$

where $\xi = \frac{\delta\mu_3}{T}$ and $\delta\mu_3 = \mu_d - \mu_u - \mu_e$. Then, putting back dx_e and the conservation condition we get

$$\begin{aligned} \Gamma_{\bar{\nu}}(\xi) &= \frac{3}{2(2\pi)^5}\, 64G^2\cos^2\theta_c \frac{4\alpha_s}{3\pi}\, \mu_d\mu_u\mu_e T^5 \\ &\times \int dx_d dx_u dx_e dx_{\bar{\nu}} x_{\bar{\nu}}^2 f(x_d)[1-f(x_u)][1-f(x_e)] \\ &\times \delta(x_d - x_u - x_e - x_{\bar{\nu}} - \xi). \end{aligned} \tag{2.21}$$

Noting that $1 - f(x) = f(-x)$ and changing variables $x_{u,e} \to -x_{u,e}$ we have

$$\begin{aligned} \Gamma_{\bar{\nu}}(\xi) &= \frac{3}{2(2\pi)^5} 64G^2\cos^2\theta_c \frac{4\alpha_s}{3\pi} \mu_d\mu_u\mu_e T^5 \\ &\times \int_0^\infty dx_{\bar{\nu}} x_{\bar{\nu}}^2 \int_{-\infty}^\infty dx_d f(x_d) \int_{-\infty}^\infty dx_u f(x_u) \int_{-\infty}^\infty dx_e f(x_e) \\ &\times \delta(x_d + x_u + x_e - x_{\bar{\nu}} - \xi). \end{aligned} \tag{2.22}$$

Thus, the interaction rate $\Gamma_{\bar{\nu}}$ can be written as

$$\Gamma_{\bar{\nu}}(\xi) = \frac{3}{2(2\pi)^5} 64G^2\cos^2\theta_c \frac{4\alpha_s}{3\pi} \mu_d\mu_u\mu_e T^5 \int_0^\infty dx_{\bar{\nu}} x_{\bar{\nu}}^2 J(x_{\bar{\nu}} - \xi), \tag{2.23}$$

where the integral $J(x)$ is given by

$$J(x) = \left[\prod_{j=1}^{3} \int_{-\infty}^{\infty} dx_j f(x_j)\right] \delta(x_1 + x_2 + x_3 - x) = \frac{\pi^2 + x^2}{2(1+e^x)}. \tag{2.24}$$

The interaction rate $\Gamma_{\bar{\nu}}$ is then given by

$$\Gamma_{\bar{\nu}}(\xi) = \frac{3}{2(2\pi)^5} 64 G^2 \cos^2\theta_c \frac{4\alpha_s}{3\pi} \mu_d \mu_u \mu_e T^5 \int_0^\infty dx_{\bar{\nu}} x_{\bar{\nu}}^2 \frac{\pi^2 + (x_{\bar{\nu}} - \xi)^2}{2(1 + e^{x_{\bar{\nu}} - \xi})}. \tag{2.25}$$

Changing $x_{\bar{\nu}} \to x_{\bar{\nu}} + \xi$ we obtain.

$$\Gamma_{\bar{\nu}}(\xi) = \frac{3}{2(2\pi)^5} 64 G^2 \cos^2\theta_c \frac{4\alpha_s}{3\pi} \mu_d \mu_u \mu_e T^5 \int_\xi^\infty dx_{\bar{\nu}} (x_{\bar{\nu}} + \xi)^2 \frac{\pi^2 + x_{\bar{\nu}}^2}{2(1 + e^{x_{\bar{\nu}}})}. \tag{2.26}$$

Because $\xi \ll 1$ we can approximate the lower limit of the integral by zero, which leads to

$$\Gamma_{\bar{\nu}}(\xi) = \frac{3}{2(2\pi)^5} 64 G^2 \cos^2\theta_c \frac{4\alpha_s}{3\pi} \mu_d \mu_u \mu_e T^5 \int_0^\infty dx_{\bar{\nu}} (x_{\bar{\nu}} + \xi)^2 \frac{\pi^2 + x_{\bar{\nu}}^2}{2(1 + e^{x_{\bar{\nu}}})}. \tag{2.27}$$

Using the fact that $\Gamma_{\bar{\nu}}(\xi) = \Gamma_\nu(-\xi)$ we get the inverse interaction rate Γ_ν,

$$\Gamma_\nu(\xi) = \frac{3}{2(2\pi)^5} 64 G^2 \cos^2\theta_c \frac{4\alpha_s}{3\pi} \mu_d \mu_u \mu_e T^5 \int_0^\infty dx_{\bar{\nu}} (x_{\bar{\nu}} - \xi)^2 \frac{\pi^2 + x_{\bar{\nu}}^2}{2(1 + e^{x_{\bar{\nu}}})}, \tag{2.28}$$

which leads to a difference in interaction rates between the forward and inverse channels given by

$$\Gamma_{\bar{\nu}} - \Gamma_\nu = \frac{3}{2(2\pi)^5} 64 G^2 \cos^2\theta_c \frac{4\alpha_s}{3\pi} \mu_d \mu_u \mu_e T^5 \int_0^\infty dx\ 2\xi x\ \frac{\pi^2 + x^2}{1 + e^x}. \tag{2.29}$$

Using

$$\int_o^\infty \frac{x}{1+e^x}dx = \frac{\pi^2}{12},$$
$$\int_0^\infty \frac{x^3}{1+e^x}dx = \frac{7\pi^4}{120},$$

we finally obtain

$$\Gamma_{\bar{\nu}} - \Gamma_\nu = \frac{17}{15\pi^2}G^2\cos^2\theta_c\alpha_s\mu_d\mu_u\mu_e T^4\delta\mu_3. \tag{2.30}$$

The value of λ_3 defined by $\Gamma_{\bar{\nu}} - \Gamma_\nu = \lambda_3\delta\mu_3$ then becomes

$$\lambda_3 = \frac{17}{15\pi^2}G^2\cos^2\theta_c\alpha_s\mu_d\mu_u\mu_e T^4. \tag{2.31}$$

2.2.2 Strange-Quark β Decay

Here, the two interactions we consider are the β-decay of the s quark and its inverse interaction which includes electron capture,

$$s \to u + e + \bar{\nu_e}, \tag{2.32}$$
$$u + e \to s + \nu_e. \tag{2.33}$$

The matrix element for the s-quark β-decay is given by

$$|M_{su}|^2 = 64G^2\sin^2\theta_c(P_s\cdot P_{\bar{\nu}})(P_u\cdot P_e), \tag{2.34}$$

In the previous section, we used the strong interactions between the quarks to "open" the phase space, cf. Eq. (2.11b). In fact, if we had set the strong interactions coupling constant to zero, the d-quark β-decay is strongly suppressed.

Considering strong interactions, β equilibrium dictates the condition $(1 + \frac{4}{3\pi}\alpha_s)p_{Fd} = (1 + \frac{4}{3\pi}\alpha_s)p_{Fu} + p_{Fe}$. On the other hand, conservation of momenta at the Fermi surface leads to $p_{Fd} = \sqrt{p_{Fu}^2 + p_{Fe}^2 - 2p_{Fu}p_{Fe}\cos\theta_{ue}}$, where θ_{ue} is the angle between the u-quark momentum and the e momentum. From these two conditions one can easily see that if we neglect strong interactions, these two equations can only be solved if $\cos\theta_{ue} = 1$, which blocks the interaction. However, the presence of the α_s terms relaxes the situation allowing for a value of θ_{ue} that is not zero, see Eq.(2.11b).

The situation is different for the strange quark β-decay. The strange quark mass rather than strong interactions is the main way to allow for the interaction to occur.

The calculation of the interaction rate is very similar to the previous section, however, we need to consider a different phase space. It will be very useful to compare the phase space of the previous subsection to the one we need to consider here.

For the s-quark β-decay we consider the strange quark mass as the effect that allows for θ_{ue} to be non-zero. The β-equilibrium condition reads $\mu_s = \sqrt{p_{Fs}^2 + m_s^2} \simeq p_{Fs}(1 + \frac{1}{2}(\frac{m_s}{p_{Fs}})^2) = p_{Fu} + p_{Fe}$. Using this in a similar fashion as discussed for the d-quark β-decay and comparing both results, we find that we only need to make the replacements $\cos\theta_c \to \sin\theta_c$, and $\alpha_s \to \frac{3\pi}{8}\frac{m_s^2}{\mu_u\mu_e}$.

Then we obtain,

$$\lambda_2 = \frac{17}{40\pi}G^2\sin^2\theta_c\mu_s m_s^2 T^4, \tag{2.35}$$

where λ_2 is defined in a similar fashion as λ_3.

2.2.3 Non-Leptonic Weak Interaction

The third interaction we study is the non-leptonic weak interaction, where the s quark is converted into a d quark

$$u_1 + s \leftrightarrow u_2 + d. \tag{2.36}$$

The interaction rate for the non-leptonic weak interactions was studied in Ref. [53]; in here we summarize some details of the calculation.

The rate of the forward channel of interaction (2.36) is given by

$$\begin{aligned}
\Gamma_{su1\to du2} &= \frac{1}{2}\int d^3p_1 d^3p_s d^3p_d d^3p_2 \frac{36}{(2\pi)^5}\frac{1}{2^4 E_s E_1 E_2 E_d} \\
&\times \delta^4(P_s + P_1 - P_2 - P_d)|M_{nl}|^2 f\left(\frac{E_1-\mu_u}{T}\right) f\left(\frac{E_s-\mu_s}{T}\right) \\
&\times \left[1 - f\left(\frac{E_2-\mu_u}{T}\right)\right]\left[1 - f\left(\frac{E_d-\mu_d}{T}\right)\right].
\end{aligned} \tag{2.37}$$

It can be easily shown that the relationship between both the forward and backward directions of the interaction is given by

$$\Gamma_{u2d\to su1} = e^{\frac{\mu_s-\mu_d}{T}}\Gamma_{su1\to du2}, \tag{2.38}$$

which leads to, to first order in $\frac{\mu_s-\mu_d}{T} \equiv \frac{\delta\mu_1}{T}$,

$$\Gamma_{s\to d} = \Gamma_{su1\to du2}\frac{\delta\mu_1}{T}. \tag{2.39}$$

The matrix element summed over final spins and averaged over initial spins reads

$$|M_{nl}|^2 = 64G^2 \sin^2\theta_c \cos^2\theta_c (P_{u1}\cdot P_s)(P_{u2}\cdot P_d). \tag{2.40}$$

The four-momentum products give

$$(P_{u1}\cdot P_s)(P_{u2}\cdot P_d) = E_d E_s E_{u1} E_{u2}\left(1 - \frac{p_s}{E_s}\cos\theta_{u1s}\right)(1 - \cos\theta_{u2d}). \tag{2.41}$$

The effects of strong interactions and strange quark mass do not cause a large effect on the interaction rates, the reason for this difference from the case of the two β-decay (*Urca*) processes is that the *Urca* processes are mainly three-particle interactions, assuming that the neutrino carries only a small momentum and can be neglected from phase space considerations. Here, all particles must be considered in the phase space. We have a four-particle interaction, and the momentum conservation restrictions on the phase space are much more relaxed than those of the *Urca* processes.

Indeed, the strange quark mass will have an effect, however, this effect does not change the interaction rate in a substantial way.

The four-momentum δ function can be written as, labeling $u1$ and $u2$ simply by the numbers 1 and 2,

$$\delta^4(P_s + P_1 - P_2 - P_d) = \delta(E_s + E_1 - E_2 - E_d) \times \delta^3(\vec{p_s} + \vec{p_1} - \vec{p_2} - \vec{p_d}). \quad (2.42)$$

In the spherical coordinate representation,

$$\delta^3(\vec{p_s}+\vec{p_1}-\vec{p_2}-\vec{p_d}) = \frac{1}{|\vec{p_s} + \vec{p_1}|^2}\delta(|\vec{p_s}+\vec{p_1}|-|\vec{p_2}+\vec{p_d}|)\delta(\phi-\phi')\delta(\cos\theta_{2d}-g(\theta_{1s})), \quad (2.43)$$

where

$$g(\theta_{1s}) = \frac{p_1^2 + p_s^2 - p_2^2 - p_d^2 + 2p_2p_d\cos\theta_{1s}}{2p_2p_d}. \quad (2.44)$$

The ϕ delta function fixes the system to azimuthal symmetry, which means that the interaction is solved on a plane, and the ϕ integrals will only lead to multiplying the result by factor of 2π.

The interaction rate is given by [53],

$$\Gamma_{s\to d} = \frac{64}{5\pi^3} G^2 \sin^2\theta_C \cos^2\theta_C \mu_d^5 T^2 \delta\mu_1. \tag{2.45}$$

This should be multiplied by [53]

$$\frac{5}{256}\left[\frac{3}{5}(32+y^5) - (8+y^3)\left(4 + \frac{(\mu_s+\mu_d)^2}{\mu_u^2} + \frac{m_s^2}{\mu_u^2}\right) + (24+12y)\left(\frac{(\mu_s+\mu_d)^2}{\mu_u^2} - \frac{m_s^2}{\mu_u^2}\right)\right],$$

where $y = \frac{\sqrt{\mu_s^2 - m_s^2} - \mu_d}{\mu_u}$, as a correction due to the strange quark mass.

From Eq. (2.45), λ_1 defined by $\Gamma_{s\to d} - \Gamma_{su1\to du2} = \lambda_1 \delta\mu_1$ is given by

$$\lambda_1 = \frac{64}{5\pi^3} G^2 \sin^2\theta_C \cos^2\theta_C \mu_d^5 T^2. \tag{2.46}$$

Chapter 3

Two-Flavor Quark Matter

In this chapter, we calculate the bulk viscosity of the four most popular spin-one color-superconducting phases of two-flavor (non-strange) quark matter: the color-spin-locked (CSL), planar, polar, and the A phase. One of these could be the ground state of dense baryon matter if the spin-zero Cooper pairing of quarks is prevented by the constraints of charge neutrality and β-equilibrium.

The first section introduces the formalism for calculating the bulk viscosity of nonstrange quark matter. We shall see that, since the bulk viscosity is a resonance effect between the interaction rate and the oscillation frequency, the bulk viscosity has a maximum in the limit of zero frequency, and that it falls off as $1/\omega^2$ at high frequency.

In the second section the bulk viscosity of quark matter in the normal phase is calculated, then in the third section the bulk viscosity of spin-one color superconductors is calculated. It turns out that the effect of color superconductivity is not necessarily to suppress the bulk viscosity, it could increase the bulk viscosity under certain conditions.

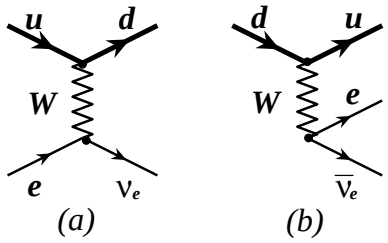

Figure 3.1: Diagrammatic representation of the weak (*Urca*) processes that contribute to the bulk viscosity of non-strange quark matter in stellar cores.

3.1 Bulk Viscosity Formula

As mentioned in the introduction, the bulk viscosity is responsible for the damping of density oscillations in compact stars. The characteristic frequencies of interest (e.g., set by the r-mode instabilities) are comparable to the rotational frequencies of stars, i.e., $\omega \lesssim 10^4 s^{-1}$ [54, 55]. These frequencies are many orders of magnitude smaller than the typical rates of strong interactions, and therefore quark matter cannot be driven substantially out of equilibrium with respect to strong processes. This is the reason why the bulk viscosity is dominated by the much slower, flavor-changing weak processes [56, 57]. In the case of non-strange quark matter studied here, the relevant processes are electron capture by u-quarks and β-decay of d-quarks, see Fig. 3.1.

Let us assume that small oscillations of the quark matter density are described by $\delta n = \delta n_0 \,\mathrm{Re}(e^{i\omega t})$ where δn_0 is the magnitude of the density variations. For such a periodic process, the bulk viscosity ζ is defined as the coefficient in the expression for the energy-density dissipation averaged over one period, $\tau = 2\pi/\omega$,

$$\langle \dot{\mathcal{E}}_{\rm diss} \rangle = -\frac{\zeta}{\tau} \int_0^\tau dt \, (\nabla \cdot \vec{v})^2 \,, \tag{3.1}$$

where $\vec{v}$ is the hydrodynamic velocity associated with the density oscillations. By making use of the continuity equation, $\dot{n} + n \, \nabla \cdot \vec{v} = 0$, we derive

$$\langle \dot{\mathcal{E}}_{\rm diss} \rangle = -\frac{\zeta \omega^2}{2} \left(\frac{\delta n_0}{n} \right)^2 . \tag{3.2}$$

In order to solve for ζ, the dissipated energy on the left-hand side has to be calculated explicitly. This can be done as follows.

The density oscillations drive quark matter slightly out of β-equilibrium, but not out of thermal equilibrium which is restored almost without delay by strong processes. The corresponding instantaneous quasi-equilibrium state can be unambiguously characterized by the total baryon number density n and the lepton fraction X_e,

$$n = \frac{1}{3}\left(n_u + n_d\right), \tag{3.3a}$$

$$X_e = \frac{n_e}{n}, \tag{3.3b}$$

where n_u and n_d are the number densities of up and down quarks, while n_e is the number density of electrons. (In the case of strange quark matter, one should also add the strangeness fraction $X_s = n_s/n$ where n_s is the number density of strange quarks [58], see Chapter 4 for more details.) Charge neutrality requires

$$\frac{2}{3}n_u - \frac{1}{3}n_d - n_e = 0. \tag{3.4}$$

Using this constraint together with the definitions in Eq. (3.3), one can express the number densities and, in fact, all thermodynamic quantities of quark matter in terms of n and X_e. For the number densities, for example, one finds

$$n_e = X_e n, \tag{3.5a}$$

$$n_u = (1 + X_e)n, \tag{3.5b}$$

$$n_d = (2 - X_e)n. \tag{3.5c}$$

These number densities can also be expressed in terms of the corresponding chemical potentials, $n_i = n_i(\mu_i)$. In β-equilibrium, the three chemical potentials are related as follows: $\mu_d = \mu_u + \mu_e$. In pulsating matter, on the other hand, the instantaneous departure from equilibrium is described by the small parameter

$$\delta\mu \equiv \mu_d - \mu_u - \mu_e = \delta\mu_d - \delta\mu_u - \delta\mu_e, \tag{3.6}$$

where $\delta\mu_i$ denotes the deviation of chemical potential μ_i from its value in β-equilibrium. The quantity $\delta\mu$ can be conveniently expressed in terms of the variations of the two independent variables δn and δX_e,

$$\delta\mu = C\frac{\delta n}{n} + B\delta X_e, \tag{3.7}$$

where, as follows from the definition, the coefficient functions C and B are given by

$$C = n_d \frac{\partial \mu_d}{\partial n_d} - n_u \frac{\partial \mu_u}{\partial n_u} - n_e \frac{\partial \mu_e}{\partial n_e}, \tag{3.8a}$$

$$B = -n \left(\frac{\partial \mu_d}{\partial n_d} + \frac{\partial \mu_u}{\partial n_u} + \frac{\partial \mu_e}{\partial n_e} \right). \tag{3.8b}$$

When $\delta\mu$ is non-zero the two Urca processes, shown diagrammatically in Fig. 3.1, have slightly different rates. To leading order in $\delta\mu$, we could write

$$\Gamma_\nu - \Gamma_{\bar{\nu}} = -\lambda \delta\mu. \tag{3.9}$$

(Note that our λ is defined so that it is non-negative.) The net effect of having different rates for the two processes is a change of the electron fraction in the system:

$$n \frac{d(\delta X_e)}{dt} = \lambda \delta\mu. \tag{3.10}$$

This has the tendency to restore the equilibrium value of X_e. Since the rate is finite, however, the weak processes always lag behind the density oscillations. In order to see this explicitly, we substitute $\delta\mu$ from Eq. (3.7) into Eq. (3.10) obtain an equation for δX_e in closed form,

$$n \frac{d(\delta X_e)}{dt} = \lambda \left(C \frac{\delta n}{n} + B \delta X_e \right). \tag{3.11}$$

The periodic solution to this equation can be found most easily by making use of complex variables. Denoting $\delta X_e \equiv \mathrm{Re}\,(\delta X_{e,0}\, e^{i\omega t})$, we derive the following result:

$$\delta X_{e,0} = \frac{\delta n_0}{n} \frac{C}{i\alpha - B}, \tag{3.12}$$

where, by definition, $\alpha \equiv n\omega/\lambda$. In the last equation, the lagging of the weak processes is indicated by a non-vanishing imaginary part of $\delta X_{e,0}$. Such an imaginary part controls the phase shift of the δX_e oscillations with respect to the oscillations of density.

As we show in a moment, the same phase shift also leads to a non-vanishing dissipation of the energy density,

$$\langle \dot{\mathcal{E}}_{\mathrm{diss}} \rangle = \frac{n}{\tau} \int_0^\tau P \dot{V} dt, \tag{3.13}$$

where $V \equiv 1/n$ is the specific volume.

The pressure oscillations around the equilibrium value are driven by the oscillations of its two independent variables, i.e., the quark number density and the lepton fraction,

$$\delta P = \frac{\partial P}{\partial n}\,\delta n - n\,C\,\delta X_e, \tag{3.14}$$

where C is the same as in Eq. (3.8a). In the derivation we took into account that $n_i = \partial P/\partial \mu_i$ and that the total pressure is given by the sum of the partial contributions of the quarks and electrons, $P = \sum_i P_i(\mu_i)$.

After taking into account the relation (3.14) together with the solution for $\delta X_{e,0}$ in Eq. (3.12), the expression (3.13) becomes

$$\begin{aligned} \langle \dot{\mathcal{E}}_{\rm diss} \rangle &= \frac{C}{2}\omega\,\delta n_0\,{\rm Im}\,(\delta X_{e,0}) \\ &= -\frac{1}{2}\left(\frac{\delta n_0}{n}\right)^2 \frac{\lambda\,\omega^2 C^2}{\omega^2 + (\lambda B/n)^2}. \end{aligned} \tag{3.15}$$

By comparing this with the definition in Eq. (3.2), we finally derive an explicit expression for the bulk viscosity,

$$\zeta = \frac{\lambda C^2}{\omega^2 + (\lambda B/n)^2}. \tag{3.16}$$

This expression shows that the viscosity is maximum in the limit of zero frequency, $\zeta_{\rm max} = \zeta_{\omega=0}$, and that it falls off as $1/\omega^2$ at high frequencies, $\omega \gg \omega_0 \equiv \lambda B/n$. It should be also noted that $\omega_0 \sim \lambda$, and that the maximum viscosity is inversely proportional to the rate, i.e., $\zeta_{\rm max} \sim 1/\lambda$. Because the rates of the weak processes in a dense medium usually have a power-law (or even an exponential) dependence on the temperature, the bulk viscosity is a very sensitive function of the temperature, too.

3.2 Bulk Viscosity in the Normal Phase

In order to calculate the bulk viscosity in the normal phase of two-flavor quark matter, we need to determine the corresponding thermodynamic coefficients B and

C [see Eq. (3.8)] and calculate the difference of the rates of the two Urca processes shown in Fig. 3.1 as shown in Sec. 2.2.1.

By making use of the following relations valid for non-interacting quark matter

$$n_{u,d} = \frac{1}{\pi^2}\left(\mu_{u,d}^2 - m_{u,d}^2\right)^{3/2}, \tag{3.17a}$$

$$n_e = \frac{1}{3\pi^2}\mu_e^3, \tag{3.17b}$$

we derive

$$C \simeq \frac{m_u^2}{3\mu_u} - \frac{m_d^2}{3\mu_d}, \tag{3.18a}$$

$$B \simeq \frac{\pi^2}{3} n \left(\frac{1}{\mu_u^2} + \frac{1}{\mu_d^2} + \frac{3}{\mu_e^2}\right). \tag{3.18b}$$

Here we made use of the equilibrium relation satisfied by the chemical potentials, $\mu_d = \mu_u + \mu_e$, and neglected higher-order mass corrections in the expression for B. In the temperature regime of interest, $T \lesssim m_{u,d}$, we also do not need to take into account any corrections due to a non-zero temperature.

It should be noted that the coefficient C, and therefore the bulk viscosity which is proportional to C^2, vanishes in the case of massless quarks. Moreover, this statement remains true even if the following (non-)Fermi liquid correction due to strong forces are taken into account [59, 60, 61, 62],

$$C' = \frac{4\alpha_s}{3\pi}\left[\frac{m_d^2}{\mu_d}\left(\ln\frac{2\mu_d}{m_d} - \frac{2}{3}\right) - \frac{m_u^2}{\mu_u}\left(\ln\frac{2\mu_u}{m_u} - \frac{2}{3}\right)\right]. \tag{3.19}$$

(For a recent discussion of (non-)Fermi liquid corrections see, for example, Ref. [62].) Because of the large logarithms on the right-hand side of Eq. (3.19), this correction can become even larger than the leading-order result for C in Eq. (3.18a). Our estimates show that, in two-flavor quark matter, taking C' into account may increase the value of the viscosity by approximately an order of magnitude. Therefore, in all numerical estimates below we add the contributions from Eqs. (3.18a) and (3.19).

Now let us turn to the calculation of λ defined by Eq. (3.9) "the detailed derivation is shown in Sec. 2.2.1". Following the original approach of Iwamoto [51], we get the rate for β-decay in the following form:

$$\Gamma_{\bar{\nu}}(\delta\mu) = 6 \int \frac{d^3p_d d^3p_u d^3p_{\bar{\nu}} d^3p_e}{(2\pi)^8 E_d E_u E_{\bar{\nu}} E_e} |M|^2 \delta^4 \left(P_d - P_u - P_e - P_{\bar{\nu}}\right) \times f\left(E_d - \mu_d\right)\left[1 - f\left(E_u - \mu_u\right)\right]\left[1 - f\left(E_e - \mu_e\right)\right]. \quad (3.20)$$

Here, P_i and p_i are the 4- and 3-momenta of the ith particle, respectively, and $f(E) \equiv 1/(e^{E/T}+1)$ is the Fermi distribution function. The scattering amplitude squared is given by [51]

$$\begin{aligned} |M|^2 &= 64 G_F^2 \cos^2\theta_C (P_d \cdot P_{\bar{\nu}})(P_u \cdot P_e) \\ &\approx \frac{2^8 \alpha_s}{3\pi} G_F^2 \cos^2\theta_C E_u E_d E_{\bar{\nu}} E_e (1 - \cos\theta_{d\bar{\nu}}). \end{aligned} \quad (3.21)$$

After substituting this approximate form of $|M|^2$, all angular integrals in Eq. (3.20) can be done exactly. Then, using the dimensionless variables $x_i = (E_i - \mu_i)/T$ (note that $\mu_{\bar{\nu}} = 0$), we obtain

$$\Gamma_{\bar{\nu}}(\xi) = \frac{4\alpha_s}{\pi^6} G_F^2 \cos^2\theta_C \mu_d \mu_u \mu_e T^5 \int_0^\infty dx_{\bar{\nu}} x_{\bar{\nu}}^2 J(x_{\bar{\nu}} - \xi), \quad (3.22)$$

where $\xi \equiv \delta\mu/T$, and

$$\begin{aligned} J(x) &= \left[\prod_{j=1}^{3} \int_{-\infty}^{\infty} dx_j f(x_j)\right] \delta(x_1 + x_2 + x_3 - x) \\ &= \frac{\pi^2 + x^2}{2(1+e^x)}. \end{aligned} \quad (3.23)$$

By noting that $\Gamma_{\bar{\nu}}(\xi) = \Gamma_{\nu}(-\xi)$, we finally derive the expression

$$\begin{aligned} \lambda &= \frac{17}{15\pi^2} G_F^2 \cos^2\theta_C \alpha_s \mu_d \mu_u \mu_e T^4 \\ &\simeq \frac{17}{15} G_F^2 \cos^2\theta_C \alpha_s (6X_e)^{1/3} n\, T^4 \left[1 + \mathcal{O}(X_e)\right]. \end{aligned} \quad (3.24)$$

This result, together with the explicit form for the coefficient functions C, C', and B in Eqs. (3.18) and (3.19), is sufficient to calculate the bulk viscosity of the normal phase of dense quark matter. The numerical results are presented in Fig. 3.2. In the calculation, we used the following representative values of the parameters:

$$\mu_d = 500 \text{ MeV}, \quad m_d = 9 \text{ MeV}, \quad (3.25a)$$

$$\mu_u = 400 \text{ MeV}, \quad m_u = 5 \text{ MeV}, \quad (3.25b)$$

$$\mu_e = 100 \text{ MeV}, \quad \alpha_s = 1. \quad (3.25c)$$

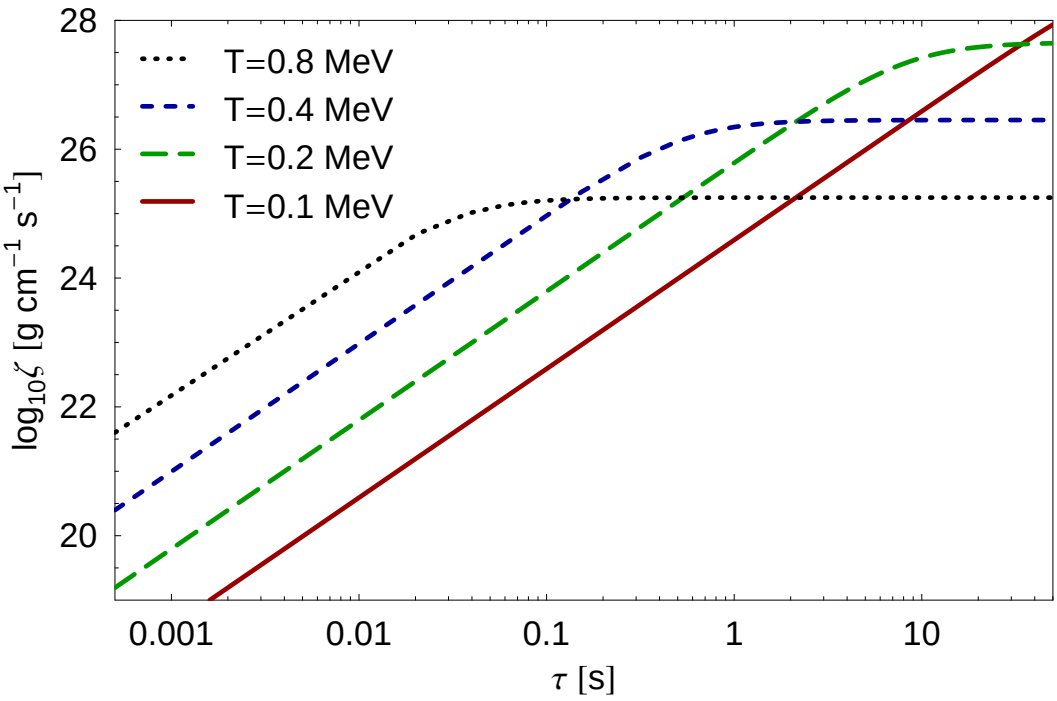

Figure 3.2: The bulk viscosity for the normal phase of two-flavor quark matter as a function of the period of the density oscillations.

In order to understand the numerical results better, we calculate the maximum value of the bulk viscosity, $\zeta_{\max} \equiv \zeta(\omega = 0)$, and the characteristic frequency $\omega_0 = \lambda B/n$, which separates the low- and high-frequency regimes,

$$\zeta_{\max} \approx 7.26 \times 10^{24} \left(\frac{T}{1\ \text{MeV}}\right)^{-4}\ \text{g cm}^{-1}\text{s}^{-1}, \tag{3.26}$$

$$\omega_0 \approx 460 \left(\frac{T}{1\ \text{MeV}}\right)^{4}\ \text{s}^{-1}. \tag{3.27}$$

The knowledge of these two quantities is sufficient for determining the bulk viscosity at all frequencies,

$$\zeta = \frac{\zeta_{\max}}{1 + (\omega/\omega_0)^2}. \tag{3.28}$$

Taking into account the relations in Eqs. (3.26) and (3.27), the temperature dependence of the results in Fig. 3.2 becomes clear. In accordance with the first relation, the maximum value of the viscosity (approached at low frequencies or large τ) becomes larger with decreasing temperature. Also, in agreement with Eq. (3.27), the location of the "shoulder" (occurring at $\tau_0 \equiv 2\pi/\omega_0$) shifts to smaller periods (higher frequencies) when the temperature gets higher.

3.3 Bulk Viscosity in Spin-One Color-Superconducting Phases

In this section, we calculate the bulk viscosity of several spin-one color-superconducting phases that have been proposed and studied in detail in Refs. [46, 63, 64, 65, 66]. Following Ref. [47], we focus on the so-called transverse phases in which only quarks of opposite chiralities pair. Theoretical studies at asymptotically large densities suggest that such phases are preferred [46, 64].

In β-equilibrium, the rates of the Urca processes were calculated in Ref. [47] in four different spin-one phases. Following the same method, here we generalize the calculation to the quasi-equilibrium state, characterized by a small but non-vanishing value of $\delta\mu = \mu_d - \mu_u - \mu_e$.

Starting from equations analogous to Eq. (36) and (37) in Ref. [47], we derive

$$\begin{aligned} \Gamma_\nu - \Gamma_{\bar{\nu}} &= \frac{2}{3\pi^6}\alpha_s G^2 \mu_e \mu_u \mu_d T^5 \sum_r \int_{-1}^{1} d\,\Xi \int x_\nu^2 dx_\nu \\ &\times \left[F^{rr}_{\varphi_u\varphi_d}(\Xi, x_\nu + \xi) - F^{rr}_{\varphi_u\varphi_d}(\Xi, x_\nu - \xi) \right], \end{aligned} \tag{3.29}$$

where $\Xi \equiv \cos\theta_u = \cos\theta_d$ is the angle between the three-momentum of the u/d quark and the z-axis. The functions $F^{rr}_{\varphi_u\varphi_d}(\Xi, x)$ are the same as in Ref. [47]. Their

explicit form is given by

$$F^{rr}_{\varphi_u\varphi_d}(\Xi,x) = \omega_{rr}(\Xi)\sum_{e_1,e_2=\pm}\int_0^\infty\int_0^\infty dx_d dx_u \left(e^{-e_1\sqrt{x_u^2+\lambda_{\Xi,r}\varphi_u^2}}+1\right)^{-1}$$
$$\times \left(e^{e_2\sqrt{x_d^2+\lambda_{\Xi,r}\varphi_d^2}}+1\right)^{-1}\left(e^{x_\nu+e_1\sqrt{x_u^2+\lambda_{\Xi,r}\varphi_u^2}-e_2\sqrt{x_d^2+\lambda_{\Xi,r}\varphi_d^2}}+1\right)^{-1}, \qquad (3.30)$$

where, by definition, $\xi = \delta\mu/T$ and $\varphi_i = \phi_i/T$. For an explicit form of the functions $\lambda_{\Xi,r}$ and ω_{rr}, we refer the reader to Refs. [46, 47] and section 1.3.3.

By expanding the rate difference (3.29) in powers of ξ and extracting the coefficient of the linear term, we derive an expression for λ in the following general form:

$$\lambda(\varphi_d,\varphi_u) = \lambda(0)\left[\frac{1}{3}+\frac{2}{3}H(\varphi_d,\varphi_u)\right], \qquad (3.31)$$

where $\lambda(0)$ is the same as in the normal phase of quark matter, see Eq. (3.24), and $H(\varphi_d,\varphi_u)$ is a reduction factor whose explicit form depends on the choice of a specific spin-one color-superconducting phase. Note that, as in the case of the neutrino-emission rates [47, 67], λ consists of two qualitatively different contributions. The first one is given by the term 1/3 in the square brackets of Eq. (3.31). It originates from the ungapped modes that are present in all considered spin-one phases. The second contribution is given by the term proportional to $H(\varphi_u,\varphi_d)$. This one originates from the gapped modes. An explicit form of the function $H(\varphi_u,\varphi_d)$ in the case of the CSL, planar, and polar phases is given by

$$H(\varphi_d,\varphi_u) = \frac{60}{17\pi^4}\int_{-1}^1 d\,\Xi\int_0^\infty dx_\nu x_\nu F^{11}_{\varphi_u\varphi_d}(\Xi,x_\nu), \qquad (3.32)$$

and, in the case of the A phase, it reads

$$H(\varphi_d,\varphi_u) = \frac{60}{17\pi^4}\int_{-1}^1 d\,\Xi\int_0^\infty dx_\nu x_\nu$$
$$\times \left[F^{11}_{\varphi_u\varphi_d}(\Xi,x_\nu) - F^{22}_{\varphi_u\varphi_d}(\Xi,x_\nu)\right]. \qquad (3.33)$$

In the derivation we integrated by parts so that the results are given in terms of the function $F^{rr}_{\varphi_u\varphi_d}(\Xi,x)$. The reduction factors can be easily calculated numerically for each phase. The results are shown in Fig. 3.3 for the case $\varphi_u = \varphi_d \equiv \varphi$.

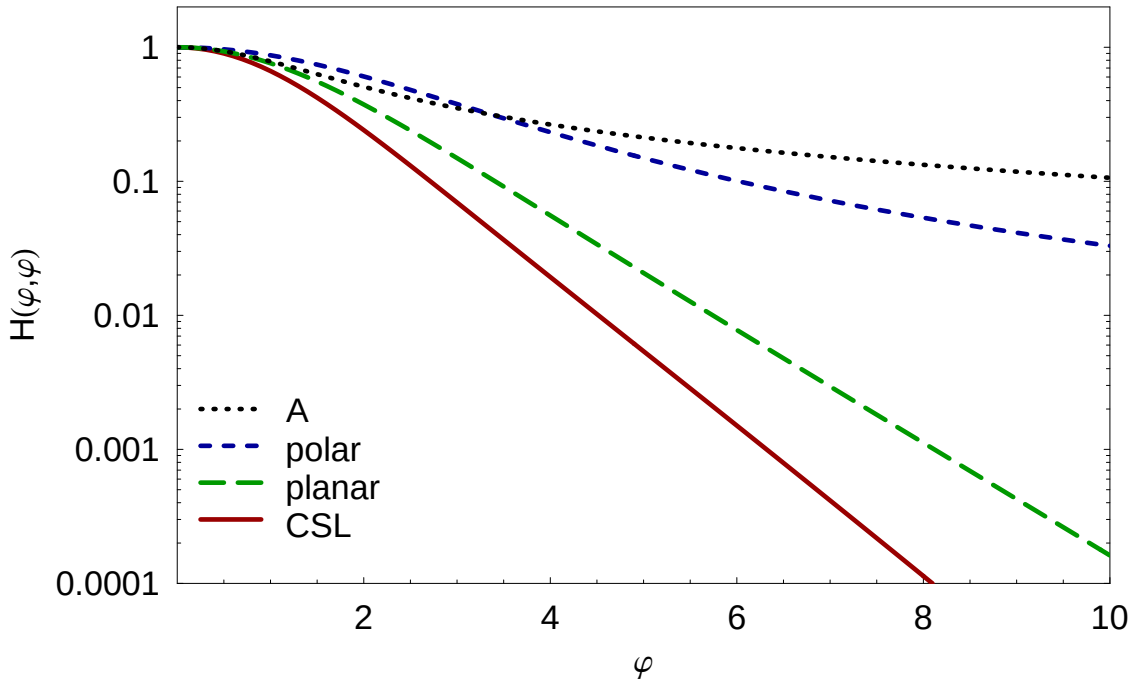

Figure 3.3: The reduction factor as a function of $\varphi \equiv \phi/T$ for the CSL, planar, polar, and A phases.

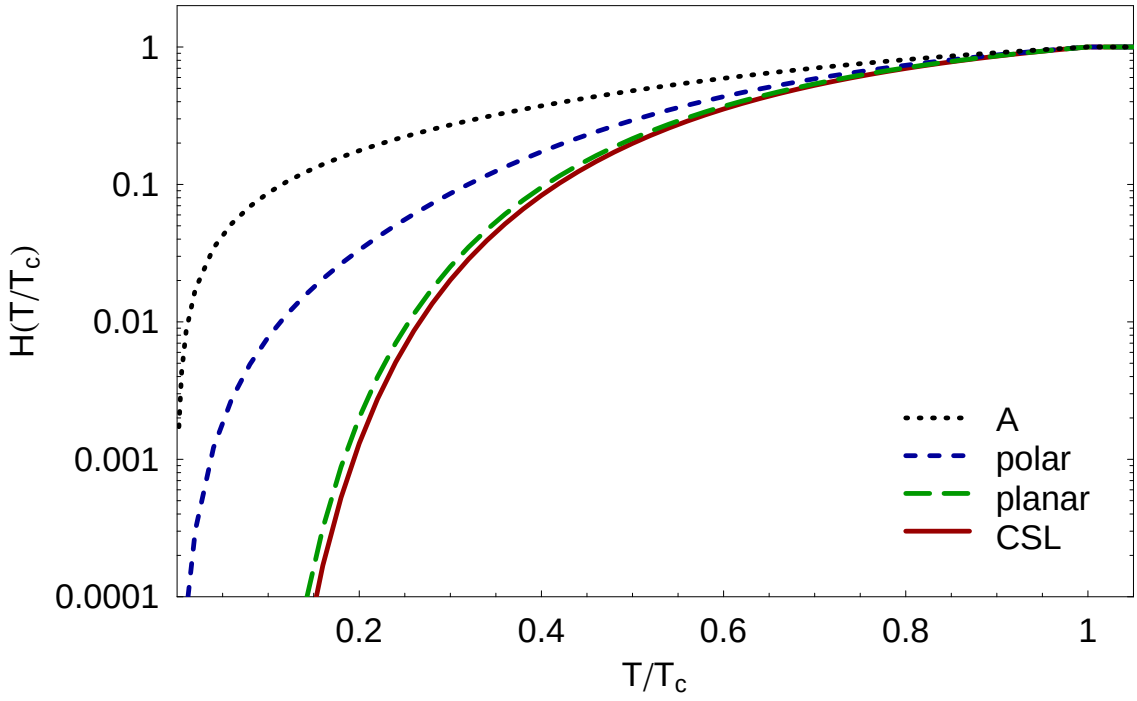

Figure 3.4: The reduction factor as a function of the temperature for the CSL, planar, polar, and A phases.

For many applications, it is of interest to know the temperature dependence of the rates. Therefore, in Fig. 3.4, we also show the temperature dependence of the suppression factor $H(T)$. In the calculation we used the following temperature dependence of the gap parameter,

$$\phi(T) = \phi_0 \sqrt{1 - \left(\frac{T}{T_c}\right)^2}, \tag{3.34}$$

with ϕ_0 being the value of the gap parameter at $T = 0$, and T_c being the value of the critical temperature. Note that the ratio T_c/ϕ_0 depends on the choice of the phase [46]. The approximate values of this ratio are 0.8 (CSL), 0.66 (planar), 0.49 (polar), and 0.81 (A phase).

With the expression for λ at hand, we are now in the position to calculate the bulk viscosity of the spin-one color-superconducting phases. Before we do this, it might be appropriate to mention that the coefficient functions B and C do not change much due to superconductivity. Corrections to B are of order $(\phi_i/\mu_i)^2$ and, thus, are strongly suppressed. The function C, on the other hand, gets corrections of order ϕ_i^2/μ_i which are negligible only if $\phi_i^2 \ll m_i^2$. We assume that this is indeed the case. Notably, the spin-one gap corrections to C should be comparable to the corrections due to a non-zero temperature that we neglected in our calculations.

It should be emphasized that the bulk viscosity in the color-superconducting phases has the same general structure as in the normal phase, see Eq. (3.28), but the quantities $\zeta_{\rm max}$ and ω_0 should be redefined to take into account the rate suppression factors:

$$\zeta_{\rm max}^{\rm sp1} = \frac{\zeta_{\rm max}}{h_{\rm sp1}}, \tag{3.35}$$

$$\omega_0^{\rm sp1} = h_{\rm sp1}\omega_0, \tag{3.36}$$

where ζ_{max} and ω_0 are given in Eqs. (3.26) and (3.27), respectively, and

$$h_{\rm sp1} = \frac{1}{3} + \frac{2}{3}H(T/T_c). \tag{3.37}$$

We see that the effect of the suppression of λ due to Cooper pairing manifests itself in a non-trivial way in the expression for the bulk viscosity, i.e.,

$$\zeta_{\rm sp1} = \frac{\zeta_{\rm max} h_{\rm sp1}}{h_{\rm sp1}^2 + (\omega/\omega_0)^2}. \tag{3.38}$$

From the analysis of this representation, we find that the suppression of the rates tends to decrease the viscosity at high frequencies ($\omega > h_{\rm sp1}\omega_0$) and to increase it at low frequencies ($\omega < h_{\rm sp1}\omega_0$). One should note, though, that the relevant range of low frequencies would shrink a lot if the suppression happened to be strong.

The representation in Eq. (3.38) shows that the effect of color superconductivity cannot be very large. Even if the suppression of the weak rates due to gapped modes is maximal, i.e., $H(T/T_c) = 0$, the results for $\zeta_{\rm max}$ and ω_0 could not change by more than a factor of 3 compared to the normal phase of matter. Of course, this is the consequence of having ungapped quasiparticle modes in the energy spectra.

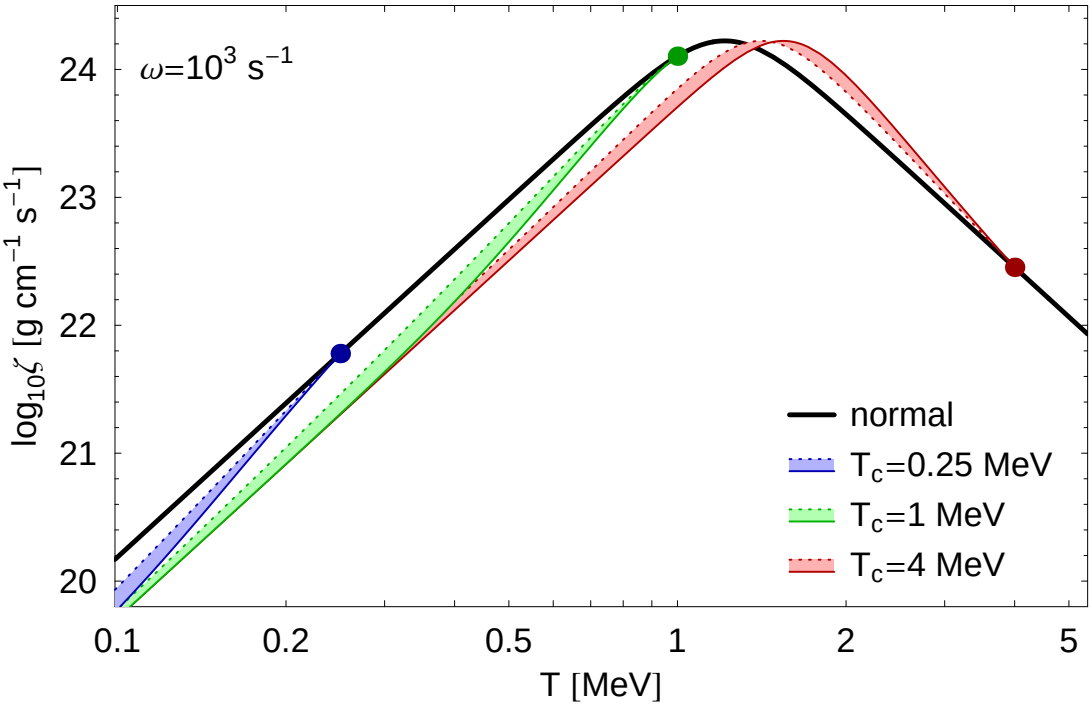

Figure 3.5: The bulk viscosity as a function of the temperature for spin-one color-superconducting quark matter. The oscillation frequency is $\omega = 10^3$ s^{-1}.

The numerical results for the bulk viscosity in the normal phase and spin-one color-superconducting phases with different values of the critical temperature are shown in Fig. 3.5. For each of the three choices of T_c, we show a shaded area (color online: blue, green and red for $T_c = 0.25$, 1, and 4 MeV, respectively), that is bounded by the values of the bulk viscosity in the CSL phase (solid boundary) and in the A phase (dotted boundary). In the calculation, we used the set of parameters given in Eq. (3.25).

For comparison, in Fig. 3.6 we also show the results for the bulk viscosity in a toy model in which all quasiparticles modes are gapped. In this case, the effect is indeed very dramatic. The largest deviations from the result of the normal phase correspond to the CSL phase (thin solid lines), and the smallest to the A phase

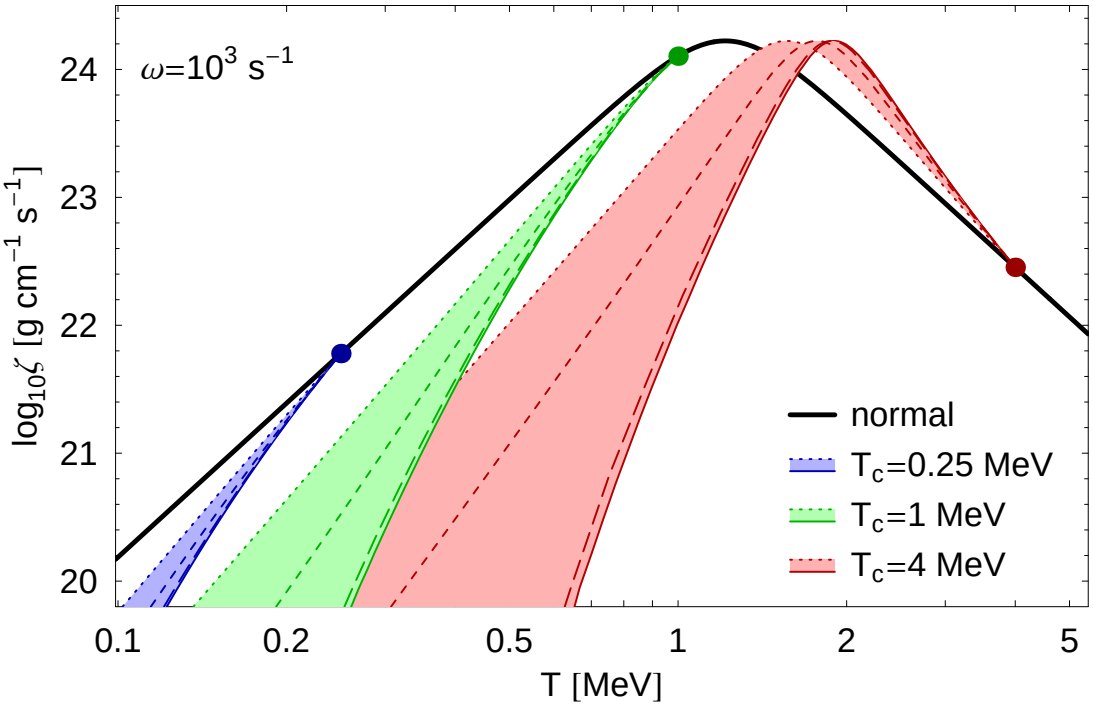

Figure 3.6: The bulk viscosity as a function of the temperature for a toy model of a spin-one color superconductor in which all quasiparticle modes are gapped. The oscillation frequency is $\omega = 10^3$ s^{-1}.

(dotted lines). The viscosity in the planar phase (long-dashed lines) is numerically close to that in the CSL phase, and the viscosity in the polar phase (short-dashed lines) is typically somewhere in between.

At this point it is natural to ask ourselves if there exists the possibility that all quasiparticles in a spin-one color superconductor are gapped. The answer is affirmative. This is the case, e.g., in the version of the CSL phase proposed in Ref. [7], when the quarks are massive. In our notation, the three quasiparticle gaps are given by

$$\phi_{i,1} = \phi_{i,2} \simeq \phi_i, \quad \phi_{i,3} \simeq \frac{m_i \phi_i}{\sqrt{2}\mu_i}, \quad (i = u, d). \tag{3.39}$$

The qualitative change in the low-energy spectrum comes from a different choice of the gap matrix in the CSL phase. (For a discussion of the specific differences, see Sec. VII in Ref. [47].) In fact, it is likely that the ansatz that produces the fully gapped phase is energetically favored [68]. The most important effect of the additional non-zero gap is the appearance of another suppression factor multiplying the first term in the expression for λ, see Eq. (3.31). Therefore, the modified expression for the CSL phase reads

$$\lambda(\varphi_d, \varphi_u) = \lambda(0) \left[\frac{1}{3} H\left(\frac{m_d \varphi_d}{\sqrt{2}\mu_d}, \frac{m_u \varphi_u}{\sqrt{2}\mu_u} \right) + \frac{2}{3} H(\varphi_d, \varphi_u) \right] . \tag{3.40}$$

Note that the additional suppression factor is given in terms of the same function $H(\varphi_d, \varphi_u)$ which was calculated numerically for the transverse CSL phase, see Figs. 3.3 and 3.4. If the up and down quark masses are rather small, the effect from the additional suppression cannot be easily seen before the temperature becomes much lower than the critical value, i.e., $T \ll T_c$. The situation changes dramatically, however, if the relevant constituent values of the quark masses happen to be considerably larger than the current masses of quarks. As suggested by the analysis in Ref. [7], this is indeed possible. Then, the bulk viscosity could be affected almost as much as in the toy model in Fig. 3.6.

Chapter 4

Three-Flavor Quark Matter

In this chapter, we study the bulk viscosity of three-flavor (strange) quark matter. One of the key issues that we address here is the interplay between the Urca and the non-leptonic processes. We shall show that, because a resonance-type phenomenon determines the bulk viscosity and because there is a subtle interference of the two weak processes, the simple argument about the dominance of the non-leptonic processes is not always justified.

This chapter is organized as follows. In the next two sections, we develop the general formalism for calculating the bulk viscosity in three-flavor quark matter, paying special attention to the interplay of several different weak processes. In Sec. 4.3 we calculate the bulk viscosity in the normal phase of strange quark matter. In the same section, we also study the role of the Urca processes on the bulk viscosity.

4.1 Contributing Interactions

It is commonly argued that the bulk viscosity in the normal phase of three-flavor quark matter is dominated by the non-leptonic weak processes $u + d \leftrightarrow u + s$ [5, 56, 57, 69, 70, 71, 72, 73]. These are shown diagrammatically in Figs. 4.1(a) and 4.1(b). As for the Urca (semi-leptonic) processes, see Figs. 4.1(c)–4.1(f), they

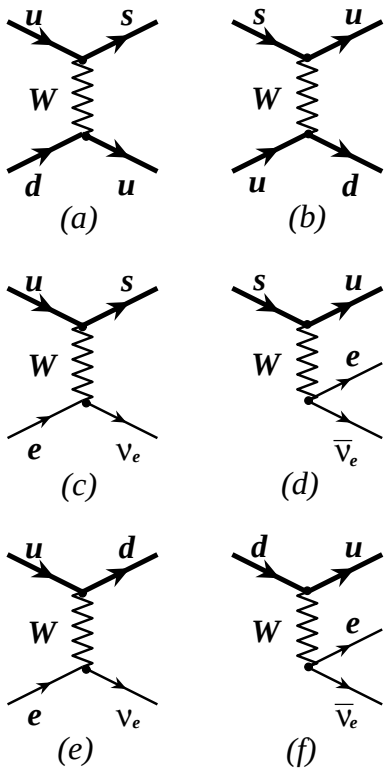

Figure 4.1: Diagrammatic representation of the weak processes that contribute to the bulk viscosity of quark matter in stellar cores.

have considerably lower rates. This is in contrast to two-flavor (non-strange) quark matter, in which case the Urca processes $u + e^- \to d + \nu$ and $d \to u + e^- + \bar{\nu}$ [see Figs. 4.1(e) and 4.1(f)] are the only ones that contribute [58]. (For studies of the viscosity in various phases of dense nuclear matter, see Refs. [74, 75, 76, 77, 78, 79, 80, 81, 82, 83].)

We will, in this chapter, study a more general case in which all the interactions shown in Fig. 4.1 are considered in the bulk viscosity calculations.

4.2 Bulk Viscosity in Strange Quark Matter

In this section, we give a general derivation of the bulk viscosity resulting from the combined effect of all weak processes shown diagrammatically in Fig. 4.1. Following the same method as in Ref. [58] and Sec. 3.1, one can relate the bulk viscosity ζ to the average energy-density dissipation in pulsating matter,

$$\langle \dot{\mathcal{E}}_{\rm diss} \rangle = -\frac{\zeta \omega^2}{2} \left(\frac{\delta n_0}{n} \right)^2 . \tag{4.1}$$

In the derivation of this relation, we assumed that small oscillations of the quark matter density are described by $\delta n = \delta n_0 \, {\rm Re}(e^{i\omega t})$ where δn_0 and ω are the magnitude and the frequency of the oscillations, respectively. The energy dissipation can be also expressed in terms of the induced pressure oscillations,

$$\langle \dot{\mathcal{E}}_{\rm diss} \rangle = \frac{n}{\tau} \int_0^\tau P \dot{V} dt, \tag{4.2}$$

where $V \equiv 1/n$ is the specific volume, and $\tau \equiv 2\pi/\omega$ is the period of the oscillation.

The density oscillations drive strange quark matter out of β-equilibrium. While the weak processes tend to restore equilibrium, they always lag behind. Thermal equilibrium, in contrast, is restored almost without any delay by very fast strong processes. The corresponding instantaneous quasi-equilibrium state is unambiguously characterized by the total baryon density n, the lepton fraction X_e, and the strangeness fraction X_s,

$$n = \frac{1}{3} \left(n_u + n_d + n_s \right), \tag{4.3a}$$

$$X_e = \frac{n_e}{n}, \tag{4.3b}$$

$$X_s = \frac{n_s}{n}, \tag{4.3c}$$

where n_u, n_d, and n_s are the number densities of up, down, and strange quarks, while n_e is the number density of electrons. Because of the charge neutrality constraint, the number densities satisfy the following relation:

$$\frac{2}{3} n_u - \frac{1}{3} n_d - \frac{1}{3} n_s - n_e = 0. \tag{4.4}$$

(Note that there are no microscopic processes that would lead to deviations from this charge neutrality constraint.) Using this constraint together with the definitions in Eq. (4.3), one can express the separate densities and, in fact, any thermodynamic quantity of quasi-equilibrium quark matter in terms of n, X_e, and X_s. For the number densities, for example, one finds

$$\begin{aligned} n_e &= X_e n, && \text{(4.5a)} \\ n_u &= (1 + X_e)\, n, && \text{(4.5b)} \\ n_d &= (2 - X_e - X_s)\, n. && \text{(4.5c)} \\ n_s &= X_s n. && \text{(4.5d)} \end{aligned}$$

The number densities can also be expressed in terms of the corresponding chemical potentials, $n_i = n_i(\mu_i)$. In β-equilibrium, the chemical potentials are related as follows: $\mu_s = \mu_d = \mu_u + \mu_e$. In pulsating matter, on the other hand, the instantaneous departure from equilibrium is described by the following two independent parameters:

$$\begin{aligned} \delta\mu_1 &\equiv \mu_s - \mu_d = \delta\mu_s - \delta\mu_d, && \text{(4.6a)} \\ \delta\mu_2 &\equiv \mu_s - \mu_u - \mu_e = \delta\mu_s - \delta\mu_u - \delta\mu_e, && \text{(4.6b)} \end{aligned}$$

where $\delta\mu_i$ denotes the deviation of the chemical potential μ_i from its value in β equilibrium. Note that the third possible combination of the chemical potentials, i.e., $\delta\mu_3 \equiv \mu_d - \mu_u - \mu_e = \delta\mu_2 - \delta\mu_1$, is not independent.

In quasi-equilibrium, both quantities $\delta\mu_1$ and $\delta\mu_2$ can be expressed in terms of the variations of the three independent variables, δn, δX_e, and δX_s,

$$\delta\mu_i = C_i \frac{\delta n}{n} + B_i \delta X_e + A_i \delta X_s\,, \quad (i = 1, 2) \qquad \text{(4.7)}$$

where, as follows from the definition, the coefficient functions are given by

$$A_1 = n\left(\frac{\partial\mu_d}{\partial n_d}+\frac{\partial\mu_s}{\partial n_s}\right), \tag{4.8a}$$

$$B_1 = n\frac{\partial\mu_d}{\partial n_d}, \tag{4.8b}$$

$$C_1 = n_s\frac{\partial\mu_s}{\partial n_s}-n_d\frac{\partial\mu_d}{\partial n_d}, \tag{4.8c}$$

$$A_2 = n\frac{\partial\mu_s}{\partial n_s}, \tag{4.8d}$$

$$B_2 = -n\left(\frac{\partial\mu_u}{\partial n_u}+\frac{\partial\mu_e}{\partial n_e}\right), \tag{4.8e}$$

$$C_2 = n_s\frac{\partial\mu_s}{\partial n_s}-n_u\frac{\partial\mu_u}{\partial n_u}-n_e\frac{\partial\mu_e}{\partial n_e}. \tag{4.8f}$$

When the quantity $\delta\mu_i$ is non-zero, the two weak processes in the ith row of Fig. 4.1 have slightly different rates. To leading order in $\delta\mu_i$, we could write

$$\Gamma_{(a)}-\Gamma_{(b)} = -\lambda_1\delta\mu_1, \tag{4.9a}$$

$$\Gamma_{(c)}-\Gamma_{(d)} = -\lambda_2\delta\mu_2, \tag{4.9b}$$

$$\Gamma_{(e)}-\Gamma_{(f)} = -\lambda_3\left(\delta\mu_2-\delta\mu_1\right), \tag{4.9c}$$

(Note that our conventions are such that the quantities λ_i are non-negative.) The net effect of having different rates for each pair of the weak processes in Fig. 4.1 is a change of the electron and strangeness fractions in the system, i.e.,

$$n\frac{d(\delta X_e)}{dt} = \lambda_2\delta\mu_2+\lambda_3\left(\delta\mu_2-\delta\mu_1\right), \tag{4.10a}$$

$$n\frac{d(\delta X_s)}{dt} = -\lambda_1\delta\mu_1-\lambda_2\delta\mu_2. \tag{4.10b}$$

According to these equations, the instantaneous values of the electron and strangeness fractions, i.e., $X_e \equiv X_e^{(0)}+\delta X_e$ and $X_s \equiv X_s^{(0)}+\delta X_s$, tend to approach their equilibrium values, $X_e^{(0)}$ and $X_s^{(0)}$, respectively. For example, a deficit of electrons (indicated by either $\delta\mu_2>0$ or $\delta\mu_2-\delta\mu_1>0$, or both) causes their production, see Eq. (4.10a). Similarly, a surplus of strange quarks (indicated by either $\delta\mu_1>0$ or $\delta\mu_2>0$, or both) is to be removed through the weak processes, see Eq. (4.10b). Because of finite rates for the weak processes, however, the oscillations of δX_e and δX_s always lag behind the density oscillations. In order to see this

explicitly, we substitute $\delta\mu_i$ from Eq. (4.7) into Eq. (4.10), and get the following set of equation for δX_e and δX_s:

$$\begin{aligned} n\frac{d(\delta X_e)}{dt} &= \left[(\lambda_2+\lambda_3)\,C_2-\lambda_3 C_1\right]\frac{\delta n}{n} \\ &+ \left[(\lambda_2+\lambda_3)\,B_2-\lambda_3 B_1\right]\delta X_e+\left[(\lambda_2+\lambda_3)\,A_2-\lambda_3 A_1\right]\delta X_s, \quad (4.11a) \\ n\frac{d(\delta X_e)}{dt} &= -\left[\lambda_1 C_1+\lambda_2 C_2\right]\frac{\delta n}{n} \\ &- \left[\lambda_1 B_1+\lambda_2 B_2\right]\delta X_e-\left[\lambda_1 A_1+\lambda_2 A_2\right]\delta X_s. \quad (4.11b) \end{aligned}$$

The periodic solution to this equation can be found most easily by making use of complex variables. Thus, by defining

$$\begin{aligned} \delta X_e &= \mathrm{Re}\left(\delta X_{e,0}\, e^{i\omega t}\right), \quad (4.12a) \\ \delta X_s &= \mathrm{Re}\left(\delta X_{s,0}\, e^{i\omega t}\right), \quad (4.12b) \end{aligned}$$

we derive the following results for the complex magnitudes:

$$\begin{aligned} \delta X_{e,0} &= \frac{\delta n_0}{n}\frac{d_1+id_2}{g_1+ig_2}, \quad (4.13a) \\ \delta X_{s,0} &= \frac{\delta n_0}{n}\frac{f_1+if_2}{g_1+ig_2}, \quad (4.13b) \end{aligned}$$

where

$$\begin{aligned} d_1 &= (\alpha_1+\alpha_2+\alpha_3)\,(A_1C_2-A_2C_1)\,, \quad (4.14a) \\ d_2 &= \alpha_1\alpha_2\,(C_2-C_1)+\alpha_1\alpha_3 C_2, \quad (4.14b) \\ f_1 &= (\alpha_1+\alpha_2+\alpha_3)\,(C_1B_2-C_2B_1)\,, \quad (4.14c) \\ f_2 &= -\alpha_1\alpha_3 C_2-\alpha_2\alpha_3 C_1, \quad (4.14d) \\ g_1 &= -\alpha_1\alpha_2\alpha_3+(\alpha_1+\alpha_2+\alpha_3)\,(B_1A_2-A_1B_2)\,, \quad (4.14e) \\ g_2 &= \alpha_1\alpha_2\,(B_1-B_2)+\alpha_1\alpha_3\,(A_2-B_2)+\alpha_2\alpha_3 A_1, \quad (4.14f) \end{aligned}$$

with $\alpha_i \equiv n\omega/\lambda_i$ $(i=1,2)$. The pressure oscillations can be given in terms of the instantaneous values of δn, δX_e, and δX_s,

$$\delta P = \frac{\partial P}{\partial n}\,\delta n + n\,(C_1-C_2)\,\delta X_e + nC_1\delta X_s, \quad (4.15)$$

where the C_i are the same as in Eq. (4.8). In the derivation we took into account that $n_i = \partial P/\partial \mu_i$ and that the total pressure is given by the sum of the partial contributions of the quarks and electrons, $P = \sum_i P_i(\mu_i)$.

After taking into account the relation (4.15) together with the solution for $\delta X_{e,0}$ and $\delta X_{s,0}$, see Eq. (4.13), the expression (4.2) becomes

$$\langle \dot{\mathcal{E}}_{\rm diss} \rangle = -\frac{\omega}{2} \delta n_0 \left[(C_1 - C_2)\, {\rm Im}\left(\delta X_{e,0}\right) + C_1 {\rm Im}\left(\delta X_{s,0}\right) \right]. \tag{4.16}$$

This shows that the imaginary parts of $\delta X_{e,0}$ and $\delta X_{s,0}$ are directly related to the dissipation of the energy density. From the physical point of view, these imaginary parts are related to the phase shifts (i.e., lagging) in the oscillations of the electron and strangeness fractions with respect to the oscillations of the density of quark matter.

Now, by comparing Eq. (4.16) with the definition in Eq. (4.1), we derive an explicit expression for the bulk viscosity,

$$\zeta = \frac{n^2}{\omega \delta n_0} \left[(C_1 - C_2)\, {\rm Im}\left(\delta X_{e,0}\right) + C_1 {\rm Im}\left(\delta X_{s,0}\right) \right]. \tag{4.17}$$

A similar derivation of the bulk viscosity in strange quark matter was also presented in Appendix A of Ref. [5]. Finally, after making use of the expressions for $\delta X_{e,0}$ and $\delta X_{s,0}$, see Eq. (4.13), this result can be rewritten as follows:

$$\zeta = \zeta_1 + \zeta_2 + \zeta_3, \tag{4.18}$$

where

$$\begin{aligned}
\zeta_1 &= \frac{n}{\omega}\frac{\alpha_2\alpha_3}{g_1^2+g_2^2} \\
&\times \left[\alpha_1\alpha_2\alpha_3 C_1^2 + (\alpha_1+\alpha_2+\alpha_3)\right. \\
&\times \left.(A_1C_2 - A_2C_1)\,(A_1C_2 - (A_1-B_1)C_1)\right], \qquad (4.19a)\\
\zeta_2 &= \frac{n}{\omega}\frac{\alpha_1\alpha_3}{g_1^2+g_2^2} \\
&\times \left[\alpha_1\alpha_2\alpha_3 C_2^2 + (\alpha_1+\alpha_2+\alpha_3)\right. \\
&\times \left.[(A_2-B_2)\,C_1 - (A_1-B_1)C_2]\,[(A_2-B_2)\,C_1 - A_2C_2]\right], \qquad (4.19b)\\
\zeta_3 &= \frac{n}{\omega}\frac{\alpha_1\alpha_2}{g_1^2+g_2^2} \\
&\times \left[\alpha_1\alpha_2\alpha_3\,(C_1-C_2)^2 + (\alpha_1+\alpha_2+\alpha_3)\right. \\
&\times \left.(B_1C_2 - B_2C_1)\,[(A_1-A_2)C_2 - (B_2-B_1+A_1-A_2)C_1]\right]. \qquad (4.19c)
\end{aligned}$$

This can be simplified using the relation $A_1 - A_2 \equiv B_1$, which follows from the definitions in Eq. (4.8). Therefore, we obtain

$$\begin{aligned}
\zeta_1 &= \frac{n}{\omega}\frac{\alpha_2\alpha_3}{g_1^2+g_2^2}\left[\alpha_1\alpha_2\alpha_3 C_1^2 + (\alpha_1+\alpha_2+\alpha_3)\,(A_1C_2 - A_2C_1)^2\right], \qquad (4.20a)\\
\zeta_2 &= \frac{n}{\omega}\frac{\alpha_1\alpha_3}{g_1^2+g_2^2}\left[\alpha_1\alpha_2\alpha_3 C_2^2 + (\alpha_1+\alpha_2+\alpha_3)\,[(A_2-B_2)\,C_1 - A_2C_2]^2\right], \qquad (4.20b)\\
\zeta_3 &= \frac{n}{\omega}\frac{\alpha_1\alpha_2}{g_1^2+g_2^2}\left[\alpha_1\alpha_2\alpha_3\,(C_1-C_2)^2 + (\alpha_1+\alpha_2+\alpha_3)\,(B_1C_2 - B_2C_1)^2\right]. \qquad (4.20c)
\end{aligned}$$

Let us emphasize that the ζ_i, $i = 1, 2, 3$, are **not** directly associated with the separate contributions of the three types of weak processes in Fig. 4.1. Because of an interference of the weak processes, each of these contributions depends on all three rates λ_i, $i = 1, 2, 3$. The separation occurs **only** in the high-frequency limit, i.e., $\alpha_i \equiv n\omega/\lambda_i \to \infty$. Indeed, in this case

$$\zeta_i \simeq \frac{\lambda_i}{\omega^2}C_i^2, \quad \text{(no sum over } i\text{)}, \qquad (4.21)$$

where $C_3 \equiv C_2 - C_1$. Note that the formal criterion for this separation reads $\omega \gg \omega_{\rm sep}$. An estimate for $\omega_{\rm sep}$ is derived from the parametric dependence of the coefficient functions A_i and B_i on densities,

$$\omega_{\rm sep} \simeq \frac{\sqrt{\lambda_1\,(\lambda_2+\lambda_3)}}{n_e^{2/3}}. \qquad (4.22)$$

In order to understand the general features of the result in Eq. (4.20), let us consider the interplay of the non-leptonic and semi-leptonic contributions to the bulk viscosity. In the limit of vanishing rates for the semi-leptonic processes, i.e., $\lambda_2, \lambda_3 \to 0$, the bulk viscosity reduces to the following well-known result for strange quark matter [56, 57]:

$$\zeta_{\rm non} \simeq \frac{\lambda_1 C_1^2}{\omega^2 + (\lambda_1 A_1/n)^2}. \tag{4.23}$$

In this limit, there are only non-leptonic processes left, and they induce the dissipation of the oscillation energy.

In order to better understand the interplay of different types of processes, it is instructive to consider also the limit of an infinitely large non-leptonic rate, $\lambda_1 \to \infty$, keeping the semi-leptonic rates λ_2 and λ_3 finite. In this case, the expression for the bulk viscosity is given by

$$\zeta_{\rm lep} \simeq \frac{(\lambda_2 + \lambda_3)\,(C_2 - C_1 A_2/A_1)^2}{\omega^2 + [(\lambda_2 + \lambda_3)\,(B_2 - B_1 A_2/A_1)\,/n]^2}. \tag{4.24}$$

It may appear puzzling that the two seemingly equivalent limits, namely $\lambda_1 \gg \lambda_2, \lambda_3$, lead to such very different results. The problem can be resolved by noting that the result in Eq. (4.23) is reliable only if the following additional constraint is satisfied: $(\lambda_2 + \lambda_3) \ll n^{4/3}\omega^2/\lambda_1$. [In deriving this constraint, we assumed that the coefficient functions A_i and B_i scale with the density as $n^{1/3}$, which will turn out to be a reasonable approximation, see Eq. (4.27) below.] In contrast, the result in Eq. (4.24) is reliable only if $\lambda_1 \gg n^{4/3}\omega^2/\,(\lambda_2 + \lambda_3)$. It is convenient, therefore, to introduce the following characteristic frequency:

$$\omega_0 = \frac{\sqrt{\lambda_1\,(\lambda_2 + \lambda_3)}}{n^{2/3}}, \tag{4.25}$$

which separates the two qualitatively different regimes. The result in Eq. (4.23) is to be used when the frequency of the density pulsations is sufficiently high, $\omega \gg \omega_0$, so that only the fast non-leptonic processes have a chance to dampen the kinetic energy efficiently. The result in Eq. (4.24), on the other hand, should be used at sufficiently low frequencies, $\omega \ll \omega_0$, when only the much slower semi-leptonic processes provide a substantial damping of the oscillations. At intermediate frequencies, $\omega \simeq \omega_0$, neither Eq. (4.23) nor Eq. (4.24) provides a good approximation to the bulk viscosity because of a strong interference of the non-leptonic and semi-leptonic processes. Below we study this interference in some more detail.

4.3 Bulk Viscosity in Normal Phase

In order to calculate the bulk viscosity in the normal phase of three-flavor quark matter, we need to determine the corresponding thermodynamic coefficients A_i, B_i and C_i [see Eq. (4.8)] and calculate the difference of the rates of the three pairs of weak processes in Fig. 4.1.

Let us start from the derivation of the coefficients A_i, B_i and C_i. For this purpose, we use of the following zero-temperature expressions for the number densities of quarks and electrons given in eq. 2.3:

$$\begin{aligned} n_f &= \frac{\left(\mu_f^2 - m_f^2\right)^{3/2}}{\pi^2} - \frac{2\alpha_s}{\pi^3}\mu_f\left(\mu_f^2 - m_f^2\right) \\ &\times \left(1 - \frac{3m_f^2}{\mu_f\sqrt{\mu_f^2 - m_f^2}}\ln\frac{\mu_f + \sqrt{\mu_f^2 - m_f^2}}{m_f}\right), \text{ for } f = u, d, s, \\ n_e &= \frac{1}{3\pi^2}\mu_e^3. \end{aligned}$$

Note that the expressions for quarks include the leading-order corrections due to strong interactions [59, 60, 61, 62]. By making use of these relations together with the definitions in Eq. (4.8), we derive the following approximate expressions for the coefficient functions:

$$A_1 \simeq \frac{2\pi^2 n}{3\mu_d^2}, \tag{4.27a}$$

$$B_1 \simeq \frac{\pi^2 n}{3\mu_d^2}, \tag{4.27b}$$

$$C_1 \simeq -\frac{m_s^2 - m_d^2}{3\mu_d} - C_s' + C_d', \tag{4.27c}$$

$$A_2 \simeq \frac{\pi^2 n}{3\mu_d^2}, \tag{4.27d}$$

$$B_2 \simeq -\frac{\pi^2 n}{3}\left(\frac{3}{\mu_e^2} + \frac{1}{\mu_u^2}\right), \tag{4.27e}$$

$$C_2 \simeq -\frac{m_s^2}{3\mu_s} + \frac{m_u^2}{3\mu_u} - C_s' + C_u'. \tag{4.27f}$$

On the right-hand side of these expressions, we made use of the equilibrium relations

satisfied by the chemical potentials, $\mu_s = \mu_d = \mu_u + \mu_e$, and neglected higher-order mass corrections in the expressions for A_i and B_i. In the expressions for C_i, on the other hand, we kept the leading-order mass corrections, which also include the contributions linear in the strong coupling constant α_s,

$$C_f' = -\frac{4\alpha_s m_f^2}{3\pi\mu_f}\left(\ln\frac{2\mu_f}{m_f} - \frac{2}{3}\right). \tag{4.28}$$

The reason for keeping the mass corrections is that the functions C_i vanish in the massless limit. In that limit, all ζ_i's are zero as appropriate for scale invariant theories [84].

In order to further proceed with the calculation of the bulk viscosity in the normal phase of three-flavor quark matter, we also need to know the rate difference of the three pairs of weak processes in Fig. 4.1. The rates of both the non-leptonic and semi-leptonic processes have been calculated in the literature, see Refs. [53, 56, 69, 85] and Refs. [51, 52], respectively. In the limit of three massless quarks, for example, the rates are (see Chapter 2 for derivations)

$$\lambda_1 \simeq \frac{64}{5\pi^3} G_F^2 \cos^2\theta_C \sin^2\theta_C \mu_d^5 T^2, \tag{4.29a}$$

$$\lambda_2 \simeq \frac{17}{40\pi} G_F^2 \sin^2\theta_C \mu_s m_s^2 T^4, \tag{4.29b}$$

$$\lambda_3 \simeq \frac{17}{15\pi^2} G_F^2 \cos^2\theta_C \alpha_s \mu_d \mu_u \mu_e T^4. \tag{4.29c}$$

When the value of the strange quark mass is not small, the expressions for the rates are more complicated [53, 85] and can only be calculated numerically. For the purposes of this thesis it suffices to use the approximate expressions in Eq. (4.29). These provide a reasonable approximation for the range of strange quark masses considered below.

Now, by making use of the results for the rates (4.29) as well as for the coefficient functions in Eq. (4.27), we can straightforwardly calculate the bulk viscosity. In the calculation, we use the following two representative sets of model parameters:

set A	set B
$n = 5\rho_0$	$n = 10\rho_0$
$m_s = 300$ MeV	$m_s = 140$ MeV
$\alpha_s = 0.2$	$\alpha_s = 0.1$

set	μ_e	μ_u	$\mu_d = \mu_s$	A_1	A_2	B_1	B_2	C_1	C_2
A	39.139	402.463	441.602	239.432	127.937	111.386	-3.726×10^4	-60.463	-60.460
B	7.396	495.275	502.671	324.118	164.288	160.268	-2.080×10^6	-10.692	-10.709

Table 4.1: Values of the chemical potentials and the coefficient functions for the parameter sets A, and B. All numbers are in MeV.

In both cases the light quark masses are $m_u = 5$ MeV and $m_d = 9$ MeV. Regarding the choice of parameters for sets A and B, several comments are in order. Set B is supposed to be characteristic for the conditions in the inner core of a quark star. The strong coupling constant α_s is small due to asymptotic freedom and the in-medium constituent strange quark mass m_s assumes a value close to its current value on account of chiral symmetry restoration at large baryon densities. Set A applies to intermediate densities, such as occur in the outer core of a quark star. Here, the strong coupling constant α_s and the in-medium constituent strange quark mass m_s assume larger values.

It can be shown that the electron chemical potential is determined by both the strange quark mass and the leading-order corrections due to strong interactions, see Eq. (2.3) and Fig. 2.1. Without α_s-corrections, the electron chemical potential would be 9.9 and 50.5 MeV for strange quark masses of 140 MeV ($n = 10\rho_0$) and 300 MeV ($n = 5\rho_0$), respectively. The leading-order corrections due to strong interactions tend to reduce the values of μ_e. A simple analysis shows that, in fact, the electron chemical potential could even formally change the sign when the value of α_s is sufficiently large (e.g., $\alpha_s \gtrsim 0.5$). This would mean that strange quark matter requires the presence of the positrons rather than electrons to stay neutral. While not forbidden, such a possibility should be accepted with great caution. Indeed, the leading-order α_s-corrections may be unreliable in this regime.

The general algorithm for calculating the bulk viscosity is as follows. First, by assuming a fixed value of the baryon density of neutral quark matter n (i.e., $n = 5\rho_0 \approx 0.75$ fm^{-3} or $n = 10\rho_0 \approx 1.5$ fm^{-3} for the two cases considered), we determine the chemical potentials of the quarks and electrons in β-equilibrium. For the two representative sets, the values of the chemical potentials as well as the coefficient functions A_i, B_i and C_i are given in Table 4.1. These are used in the calculation of the rates of the weak processes. Putting everything together, the result for the bulk

viscosity follows from Eq. (4.18).

The numerical results for the bulk viscosity as a function of the period of density oscillations τ are presented in Fig. 4.2 for the two cases: (i) $n = 10\rho_0$ and $m_s = 140$ MeV (upper panel), and (ii) $n = 5\rho_0$ and $m_s = 300$ MeV (lower panel). Different line types correspond to different values of the temperature: $T = 0.1$ MeV (solid lines), $T = 0.2$ MeV (dashed lines), $T = 0.4$ MeV (dotted lines), and $T = 0.8$ MeV (dashed-dotted lines). The thin lines show the high- and low-frequency approximations, defined in Eqs. (4.23) and (4.24), for each value of the temperature.

Note the double-step structure of the bulk viscosity as a function of τ. The first step at small τ is the usual one. It corresponds to the low-frequency saturation (with $\zeta_{\rm non}^{(\rm max)} \sim 1/\lambda_1$) of the non-leptonic contribution to the bulk viscosity, see Eq. (4.23). The second step at about $\tau = 2\pi/\omega_0$ (marked by dots in the figures) is a qualitatively new feature. As should be clear from our discussion in the preceding section, its appearance is the consequence of the interplay between the non-leptonic and the semi-leptonic weak processes contributing to the bulk viscosity of strange quark matter. At sufficiently large τ (i.e., low frequencies) the contribution of the semi-leptonic processes also saturates.

Recently, a qualitatively similar double-step structure of the bulk viscosity was also pointed out in Ref. [86]. However, a quantitative comparison of the two results is not very easy. This is because of the use of two different sets of model parameters. We also note that the results of the present study should be compared only to the physically relevant case described by eq. (6) in Ref. [86]. We consider the other case discussed in Ref. [86], where strange quarks do not flow, unlikely to occur due to the strong and electromagnetic interactions of quarks.

The increase of the bulk viscosity at low frequencies due to the contributions of the slower semi-leptonic processes is not unexpected. (For the same reason, weak processes are much more important for compact stars than strong processes, operating on typical QCD time scales of order 1 fm/c). However, the main observation here is that the increase of the bulk viscosity due to the interplay between the non-leptonic and semi-leptonic weak processes could already be visible at frequencies relevant for the physics of compact stars. Moreover, by comparing the results in the two panels of Fig. 4.2, we find that for the conditions corresponding to lower den-

sities, the range of frequencies where the semi-leptonic processes contribute widens significantly.

The bulk viscosity as a function of the temperature is given in Fig. 4.3 for set B (upper panel) and for set A (lower panel). The additional increase of the bulk viscosity due to the semi-leptonic processes is seen as a "bump" at intermediate values of the temperature. The results in the two panels demonstrate once again that the relative role of the semi-leptonic processes increases with increasing period of density oscillations, provided the baryon density is sufficiently small (set A).

From Fig. 4.3, we find that the substantial modification of the bulk viscosity due to the Urca processes occurs at temperatures between about 0.1 MeV and 1 MeV. This temperature range is of relevance to young neutron stars and, therefore, should be studied in more detail.

Perhaps the best way to appreciate the relative role of the Urca processes is to study the ratio between the complete expression for the bulk viscosity (4.18) and the commonly used approximate form (4.23) that takes only the non-leptonic interactions into account. In the more interesting case of parameter set A, this ratio is shown in Fig. 4.4 as a function of temperature for four different values of the period of density oscillations: $\frac{1}{\tau} = 1$ Hz (solid line), $\frac{1}{\tau} = 10$ Hz (dashed line), $\frac{1}{\tau} = 100$ Hz (dotted line), $\frac{1}{\tau} = 1000$ Hz (dashed-dotted line). The plot shows how the ratio $\zeta/\zeta_{\rm non}$ changes when the period of oscillations τ varies in the whole range from 1 ms to 1 s.

The results presented in Fig. 4.4 are the main results of this chapter. They show that neglecting the Urca processes can result in underestimating the value of the bulk viscosity by an order of magnitude, at intermediate densities and sufficiently large in-medium strange quark masses. We believe this finding might be of relevance for strange quark matter under conditions realized inside young neutron stars.

Before concluding this chapter, it is appropriate to note that the role of the semi-leptonic processes is negligible in the case of the smaller strange quark mass, $m_s = 140$ MeV. This is seen from Fig. 4.3 (upper panel), and this can also be

confirmed by studying the ratio $\zeta/\zeta_{\rm non}$. Its value deviates from 1 by at most 28%. This is in qualitative agreement with earlier studies [5, 56, 57, 69, 70, 71, 72, 73], neglecting the semi-leptonic processes.

The bulk viscosity of color-superconducting strange quark matter is calculated in a similar fashion as in Sec. 3.3 *i.e.* neglecting the effect of color superconductivity on the thermodynamic factors A_i, B_i and C_i, and finding the reduction to the interaction rates. This will be discussed in the following chapter.

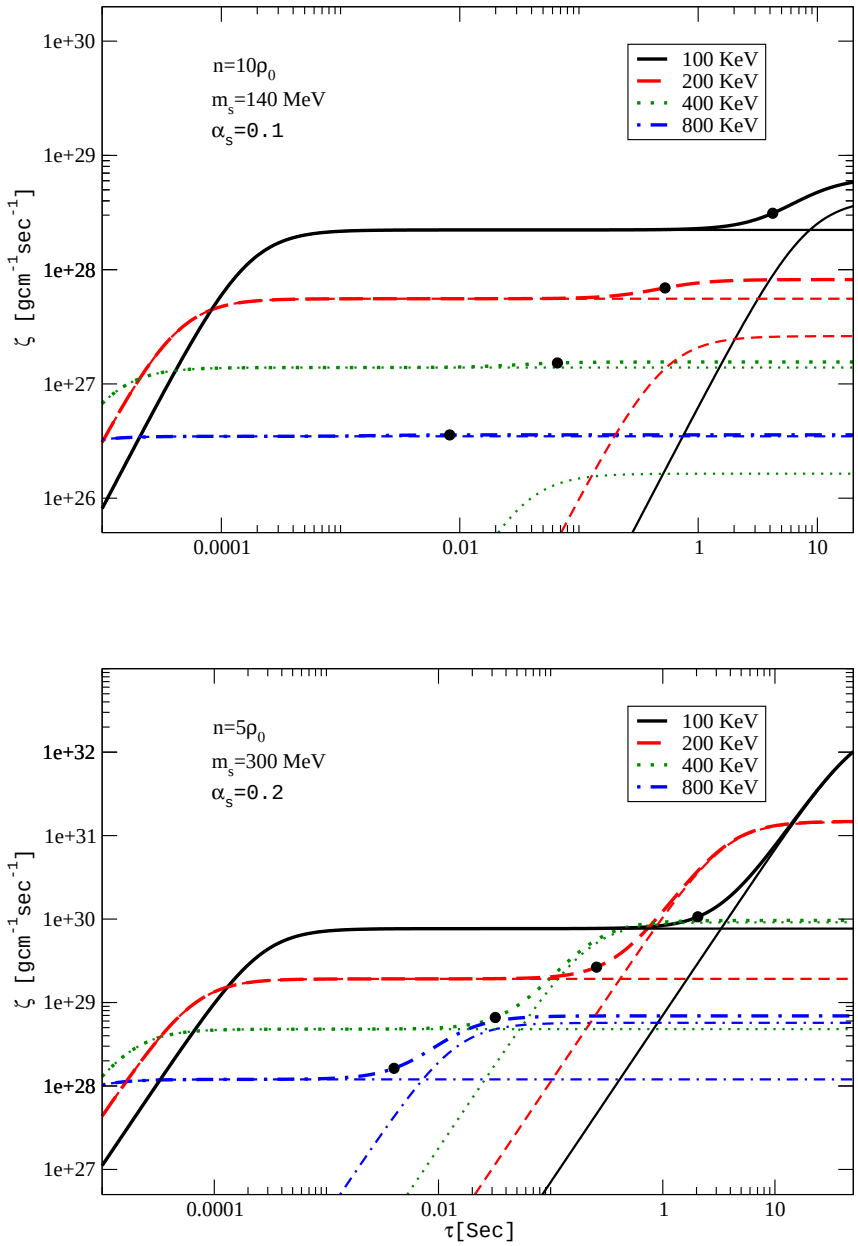

Figure 4.2: (Color online) The bulk viscosity for the normal phase of three-flavor quark matter as a function of the period of density oscillations. Results for set B are shown in the upper panel and those for set A in the lower panel. For each temperature, the dots on the lines correspond to the values of the frequency defined in Eq. (4.25).

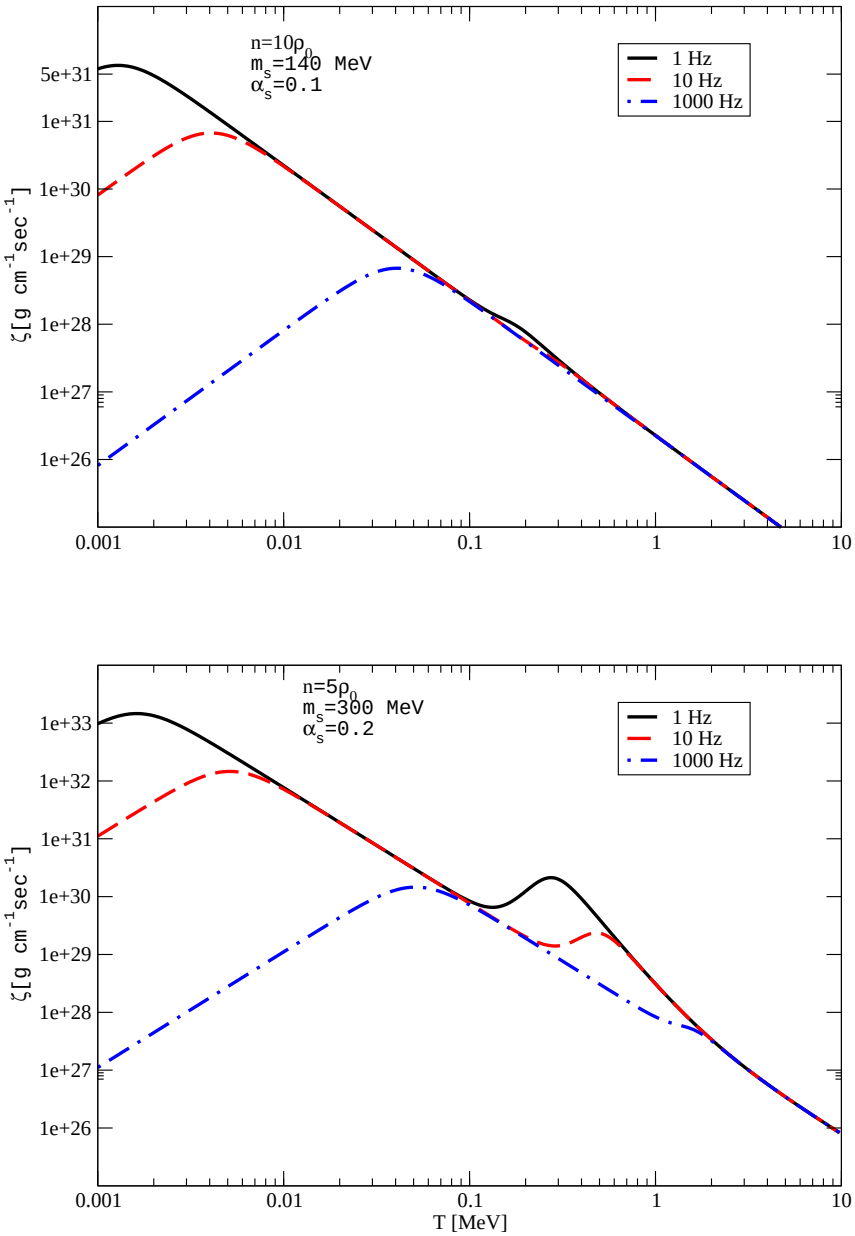

Figure 4.3: (Color online) The bulk viscosity for the normal phase of three-flavor quark matter as a function of the temperature for several fixed values of the frequency of density oscillations. Results for set B are shown in the upper panel and those for set A in the lower panel.

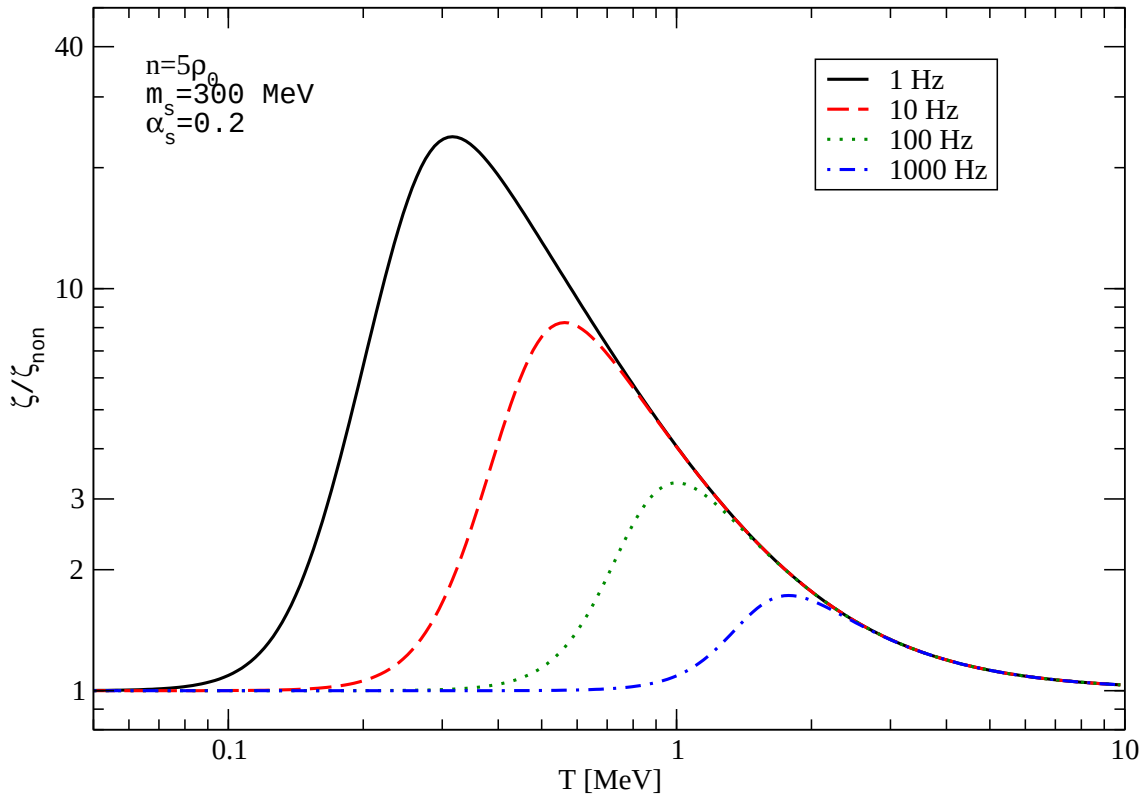

Figure 4.4: (Color online) The ratio $\zeta/\zeta_{\rm non}$ as a function of temperature for set A. The results for three fixed values of the density oscillation frequencies are shown: $\frac{1}{\tau} = 1$ Hz (solid line), $\frac{1}{\tau} = 10$ Hz (dashed line), $\frac{1}{\tau} = 100$ Hz (dotted line), and $\frac{1}{\tau} = 1000$ Hz (dashed-dotted line).

Chapter 5

R-mode Instabilities

There are many instabilities that can be operative in a neutron star. The most familiar instability is due to the existence of a maximum mass, beyond which the star must collapse into a black hole. Furthermore, if the star rotates with frequencies above a critical value, known as the Kepler frequency, mass shedding sets in from the star's equator. This frequency is $\nu_K \sim 1200$Hz in a typical neutron star.

Of concern to us are the r-mode instabilities. R-modes are fluid waves in rotating stars with the Coriolis force acting as the restoring force. These waves couple to gravitational radiation emission causing the star to lose angular momentum. Only when dissipative phenomena dampen these r-modes the star can rotate without losing any angular momentum. This sets a limit on the maximum rotation frequency of the star at any given temperature. This might also be used to study the rotation frequency evolution of the star.

In this chapter we study the quark contribution to the r-mode instability window of quark stars for different phases of deconfined quark matter. In the first section the main features of the analysis of r-mode instabilities and the r-mode instability window will be reviewed. Then we focus on the connection between dissipative phenomena and the stability window (for reviews on the subject see Refs. [54, 55]).

In order to study the effect of dissipative phenomena on r-mode instabilities, it is necessary to calculate the timescales of these dissipative phenomena. The second

section is devoted to such calculations.

Combining these timescales, one can find a window of instability where gravitational radiation emission is the dominant effect and the star must slow down. The method and an example for a normal neutron star are discussed in the third section of this chapter.

The fourth section presents the results of our work on the effect of quarks on the r-mode instabilities for quark stars. Several phases are considered, namely, the normal "unpaired" phase, and also the CFL, 2SC, and CSL phases.

5.1 R-modes

Non-radial pulsations of the star couple to gravitational radiation (GR) emission and the GR emitted carries away energy and angular momentum from the star. In a non-rotating star, the effect of emitted GR is to dampen these oscillations. In a rotating star, however, the situation is rather different. The emission of GR causes the modes to grow, the reason being that modes which propagate in the direction opposite to the star's rotation have *negative* angular momentum as seen in the co-rotating frame. Therefore, GR lowers the already negative angular momentum, *i.e.*, the mode accelerates in the opposite direction of the star's rotation and the energy of the mode grows, *i.e.*, the amplitude of the mode grows.

R-modes are fluid waves on rotating stars with the Coriolis force acting as the restoring force. The r-modes are primarily velocity perturbations, which are solutions to the perturbed fluid equations. For a slowly rotating star they have the form

$$\delta\vec{v} = \alpha R\Omega \left(\frac{r}{R}\right)^{l} \vec{Y}^{B}_{lm} e^{i\omega t}, \tag{5.1}$$

where R and Ω are the radius and angular velocity of the unperturbed star, α is an arbitrary dimensionless amplitude of the mode, and $\vec{Y}^{B}_{lm}$ is the magnetic-type spherical harmonic defined by

$$\vec{Y}^B_{lm} \equiv \frac{r\vec{\nabla} \times (r\vec{\nabla} Y_{lm})}{\sqrt{l(l+1)}}. \tag{5.2}$$

Because the Coriolis force dominates, the frequencies of the r-modes are independent of the equation of state and are proportional to the angular velocity of the star

$$\omega = -\frac{(m-1)(m+2)}{m+1}\Omega. \tag{5.3}$$

The expressions for $\delta\vec{v}$ and ω are the lowest-order terms in Ω.

The lowest-order expression for the (Eulerian) density perturbation $\delta\rho$ can be deduced from the perturbed fluid equation [87, 88, 89]

$$\frac{\delta\rho}{\rho} = \alpha R^2\Omega^2 \frac{d\rho}{dp}\left[\frac{2l}{2l+1}\sqrt{\frac{l}{l+1}}\left(\frac{r}{R}\right)^{l+1} + \delta\Psi(r)\right] Y_{l+1l} e^{i\omega t}, \tag{5.4}$$

where $\delta\Psi(r)$ is proportional to the gravitational potential $\delta\Phi$ and satisfies

$$\frac{d^2\delta\Psi}{dr^2} + \frac{2}{r}\frac{d\delta\Psi}{dr} + \left[4\pi G_N \rho \frac{d\rho}{dp} - \frac{(l+1)(l+2)}{r^2}\right]\delta\Psi = -\frac{8\pi G_N l}{2l+1}\rho\frac{d\rho}{dp}\left(\frac{r}{R}\right)^{l+1}, \tag{5.5}$$

where $G_N = 6.6742 \times 10^{-11}\mathrm{m}^3\mathrm{Kg}^{-1}\mathrm{s}^{-2}$ is the gravitational constant.

Since r-modes are generally velocity perturbations, the energy of the mode has both kinetic and gravitational potential energy terms. We follow the Cowling approximation, in which the perturbation of the gravitational potential can be neglected. This has been shown to be a very good approximation, see, for instance, Refs. [54, 55, 88, 89]. The energy of the mode (measured in the co-rotating frame) is

$$\tilde{E} = \frac{1}{2}\int \rho(\delta\vec{v}^* \cdot \delta\vec{v}) d^3x. \tag{5.6}$$

This energy is conserved in the absence of dissipation. Including dissipation it satisfies [54, 55, 88]

$$\begin{aligned}\frac{d\tilde{E}}{dt} = & - \omega(\omega+m\Omega)\sum_{l\geq m} N_l\omega^{2l}\left[|\delta D_{lm}|^2 + \frac{4l|\delta J_{lm}|^2}{c^2(l+1)}\right] \\ & - \int \left[2\eta(\delta\sigma^*_{ab}\delta\sigma^{ab}) + \zeta(\delta\sigma^*\delta\sigma)\right] d^3x. \end{aligned} \tag{5.7}$$

The second term in Eq. (5.7) represents the dissipation due to viscosities of the fluid. It can be seen from the *negative* sign in front of the term that the effect is always to reduce the energy of the mode converting it to heat. The thermodynamic functions η and ζ are the shear and bulk viscosities of the fluid. The viscous forces are driven by the shear $\delta\sigma_{ab}$ and the expansion scalar $\delta\sigma$ of the perturbation defined by

$$\delta\sigma_{ab} \equiv \frac{1}{2}(\nabla_a\delta v_b + \nabla_b\delta v_a - \frac{2}{3}\delta_{ab}\nabla_c\delta v^c), \tag{5.8}$$

$$\delta\sigma \equiv \nabla_a\delta v^a. \tag{5.9}$$

The first term in Eq. (5.7) represents the effect of GR; δD_{lm} and δJ_{lm} are the mass and current multipole moments of the perturbation,

$$\delta D_{lm} = \int \delta\rho r^l Y^*_{lm} d^3x, \tag{5.10}$$

$$\delta J_{lm} = \int r^l(\rho\delta\vec{v} + \delta\rho\vec{v})\cdot\vec{Y}^{B*}_{lm} d^3x. \tag{5.11}$$

The constants $N_l = \frac{4\pi G_n}{c^{2l+1}}\frac{(l+1)(l+2)}{(l(l-1))[(2l+1)!!]^2}$ are positive and the sum is also positive definite. Thus, the effect of GR is determined by the sign of $\omega(\omega+m\Omega)$, which is the product of the frequencies of r-modes in the inertial and the rotating frame,

$$\omega(\omega+m\Omega) = -\frac{2(m-1)(m+2)}{(m+1)^2}\Omega^2 < 0, \tag{5.12}$$

which implies that the total sign of the first term in Eq (5.7) is always positive. GR always increases the energy of the mode.

It has been shown [54, 88, 89, 90] that only modes with $l = m$ can exist and that the most unstable mode is the one with $l = m = 2$, which will be the one considered in our calculations.

5.2 Dissipative Timescales

In order to compare the relative strengths of dissipative phenomena and GR emission it is convenient to calculate the dissipative timescales associated with these effects defined as

$$\tau_i \equiv -\frac{2\tilde{E}}{(d\tilde{E}/dt)_i}, \tag{5.13}$$

where the index i can stand for any dissipative phenomenon such as bulk viscosity (bv), shear viscosity (sv), or GR emission (GR).

The energy of the mode can be found using Eqs. (5.1) and (5.6). Assuming spherical symmetry,

$$\tilde{E} = \frac{1}{2}\alpha^2\Omega^2 R^{-2l+2}\int^R \rho r^{2l+2} dr. \tag{5.14}$$

5.2.1 Gravitational Radiation Timescale

The lowest-order contribution to the GR terms in Eq. (5.7) comes entirely from the current multipole moment δJ_{ll}. This can be evaluated using Eqs. (5.1) and (5.11), to lowest order in Ω

$$\delta J_{ll} = \frac{2\alpha\Omega}{cR^{l-1}}\sqrt{\frac{l}{l+1}}\int^R \rho r^{2l+2} dr. \tag{5.15}$$

This leads to a dissipative timescale [54, 88, 89, 90]

$$\frac{1}{\tau_{GR}} = -\frac{32\pi G\Omega^{2l+2}}{c^{2l+3}}\frac{(l-1)^2 l}{[(2l+1)!!]^2}\left(\frac{l+2}{l+1}\right)^{2l+2}\int^R \rho r^{2l+2} dr. \tag{5.16}$$

Note that we are only interested in the case where $l = m = 2$. Assuming a uniform density star, which is not a bad approximation for both neutron stars and quark stars, the dissipative "growth" time for GR emission becomes

$$\frac{1}{\tau_{GR}} = -\frac{1}{3.26}\left(\frac{\Omega^2}{\pi G\rho}\right)^2. \tag{5.17}$$

5.2.2 Shear Viscosity Timescale

The time derivative of the mode energy due to the shear viscosity coefficient can be calculated from Eqs. (5.1), (5.7), and (5.9), which leads to [54, 88, 89, 90]

$$\frac{1}{\tau_{sv}} = (l-1)(2l+1)\frac{\int^R \eta r^{2l} dr}{\int^R \rho r^{2l+2} dr}. \tag{5.18}$$

Using $l = 2$ and constant density, we get,

$$\frac{1}{\tau_{sv}} = \frac{28\pi}{3}\frac{\eta R}{M}, \tag{5.19}$$

where M is the mass of the star.

5.2.3 Bulk Viscosity Timescale

The time derivative of the co-rotating frame energy $\tilde{E}$ due to the effect of bulk viscosity is

$$\left(\frac{d\tilde{E}}{dt}\right)_{bv} = -\int \zeta |\vec{\nabla}\cdot\delta\vec{v}|^2 d^3x. \tag{5.20}$$

The reduction of $d\tilde{E}/dt$ to a one-dimensional integral is not straightforward; the expansion scalar of the mode $\vec{\nabla}\cdot\delta\vec{v}$ is a complicated function radius and angle. However, since the bulk viscosity generally has no angular dependence, we may convert Eq. (5.20) to a one-dimensional integral by defining an angle-averaged expansion scalar squared $\left\langle|\vec{\nabla}\cdot\delta\vec{v}|^2\right\rangle$,

$$\left(\frac{d\tilde{E}}{dt}\right)_{bv} = -4\pi\int_0^R \zeta\left\langle|\vec{\nabla}\cdot\delta\vec{v}|^2\right\rangle r^2 dr. \tag{5.21}$$

The angle-averaged scalar expansion is in general a complicated function, it has only been determined numerically in Ref. [91], however, the simple analytical expression

$$\left\langle|\vec{\nabla}\cdot\delta\vec{v}|^2\right\rangle = \frac{\alpha^2\Omega^2}{690}\left(\frac{r}{R}\right)^6\left[1+0.86\left(\frac{r}{R}\right)^2\right]\left(\frac{\Omega^2}{\pi G_N\rho}\right)^2 \tag{5.22}$$

is an excellent fit to those numerical solutions [78].

Using Eqs. (5.14), (5.21), and (5.22) we get

$$\frac{1}{\tau_{bv}} \equiv \frac{(d\tilde{E}/dt)_{bv}}{-\tilde{E}} \simeq 4.828\times10^{-2}\left(\frac{\Omega^2}{\pi G_N\rho}\right)^2\frac{\zeta}{\rho R^2}. \tag{5.23}$$

5.3 R-mode Instability Window for *npe* Stars

The critical angular velocity above which GR has the shortest timescale is found by solving

$$\frac{1}{\tilde{E}}\frac{d\tilde{E}}{dt} = \frac{1}{\tau_{GR}} + \sum\frac{1}{\tau_{diss}} = 0. \tag{5.24}$$

Above the critical frequency the growth of the r-modes due to GR emission is the most dominant effect and the star emits GR and loses angular momentum until the effect of viscosities is the dominant one.

For a neutron star [55],

$$\sum \frac{1}{\tau_{diss}} = \frac{1}{3 \times 10^8 s} \left(\frac{10^9 K}{T} \right)^2 + \frac{1}{2 \times 10^{11} s} \left(\frac{T}{10^9 K} \right)^6 \left(\frac{\Omega^2}{\pi G \rho} \right). \tag{5.25}$$

The first term comes from the shear viscosity and is responsible for stabilizing the region at low temperatures $T < 0.5$MeV. The second term comes from the bulk viscosity and is responsible for the stability above 0.5MeV. The result for the r-mode instability window is shown in Fig 5.1.

5.4 The R-mode Instability Window for Quark Stars

We are now ready to tackle the problem of the r-mode instability window for quark stars. The dominant dissipative phenomena in a quark star are the quark bulk and shear viscosities. There are other dissipative phenomena that can play a role in determining the r-mode instability window, for example, the shear viscosity due to electron-electron scattering, or, in the case of a superfluid phase, the friction between the normal and the superfluid component that adds other viscosity coefficients [92]. We are concerned with the contribution of quarks to the r-mode instability window.

Our results are also of relevance to hybrid stars. However, to get a complete picture, the effect of hadrons need to be considered as well, and friction between the quark core and the hadronic mantle will also play a decisive role in finding the r-mode instability window.

The bulk viscosity of strange quark matter SQM was discussed in detail in Chapter 4. The shear viscosity is given by [93]

$$\eta = 5 \times 10^{15} \left(\frac{0.1}{\alpha_s} \right) \left(\frac{n}{\rho_0} \right)^{14/9} \left(\frac{T}{10^9 K} \right)^{-5/3} \quad g c m^{-1} s^{-1}. \tag{5.26}$$

For the following results we choose $\alpha_s = 0.1$, $n = 5\rho_0$.

5.4.1 R-mode Instability Window for the Normal Phase

The bulk viscosity for unpaired SQM was studied in Chapter 4. Using Eqs. (4.20) and (5.26) alongside with Eqs. (5.17), (5.19), and (5.23) one can calculate the r-mode instability window from Eq. (5.24). The results for the critical frequencies are shown in Fig. 5.1, the region above the curve is the unstable region towards the emission of GR from r-modes.

At low temperatures $T < 0.1$keV the shear viscosity of quark matter starts to be significant. Above that temperature the bulk viscosity is responsible for the stability of the star. At temperatures above $1 - 10$MeV, where the bulk viscosity starts dropping, the region is unstable towards GR emission from r-modes. This implies that a newly born quark star that has a temperature above 1MeV and a rotation frequency of $\nu \sim 1200$ Hz would be in an unstable region and should immediately start losing angular momentum via GR emission. This is not the case for a newly born neutron star which would be stable towards GR emission in the same region. Thus, if one assumes that the dominant mechanism for slowing down the newly born pulsars is GR emission from r-modes as opposed to, say, magnetic breaking, then the observation that all young pulsars are slowly rotating, see Fig. 1.3, would seem to indicate that most pulsars are quark stars. However, this should be investigated further.

The observed distribution of Low Mass X-ray Binaries (LMXB's), presumed to be old pulsars spun up by accretion of matter from the binary companion to become rapid millisecond pulsars, is indicated in the plot by a shaded box. It can easily be seen that ordinary neutron star models place these pulsars within an unstable region, leading us to exclude the *classical* model of neutron stars. On the other hand, the quark matter model places them within a stable region. One *cannot*, however, exclude the possibility of *npe* matter in these stars if one considers a more sophisticated neutron star model with a liquid core surrounded by a nearly static crust. This configuration leads to damping due to viscosity in the boundary layer between the oscillating fluid and the crust, which is about 10^5 times bigger than the damping from the shear viscosity in the interior. This would place the LMXB's in a stable region, see, for instance, Ref. [45].

Before we proceed, it is instructive to discuss the effect of color superconductivity

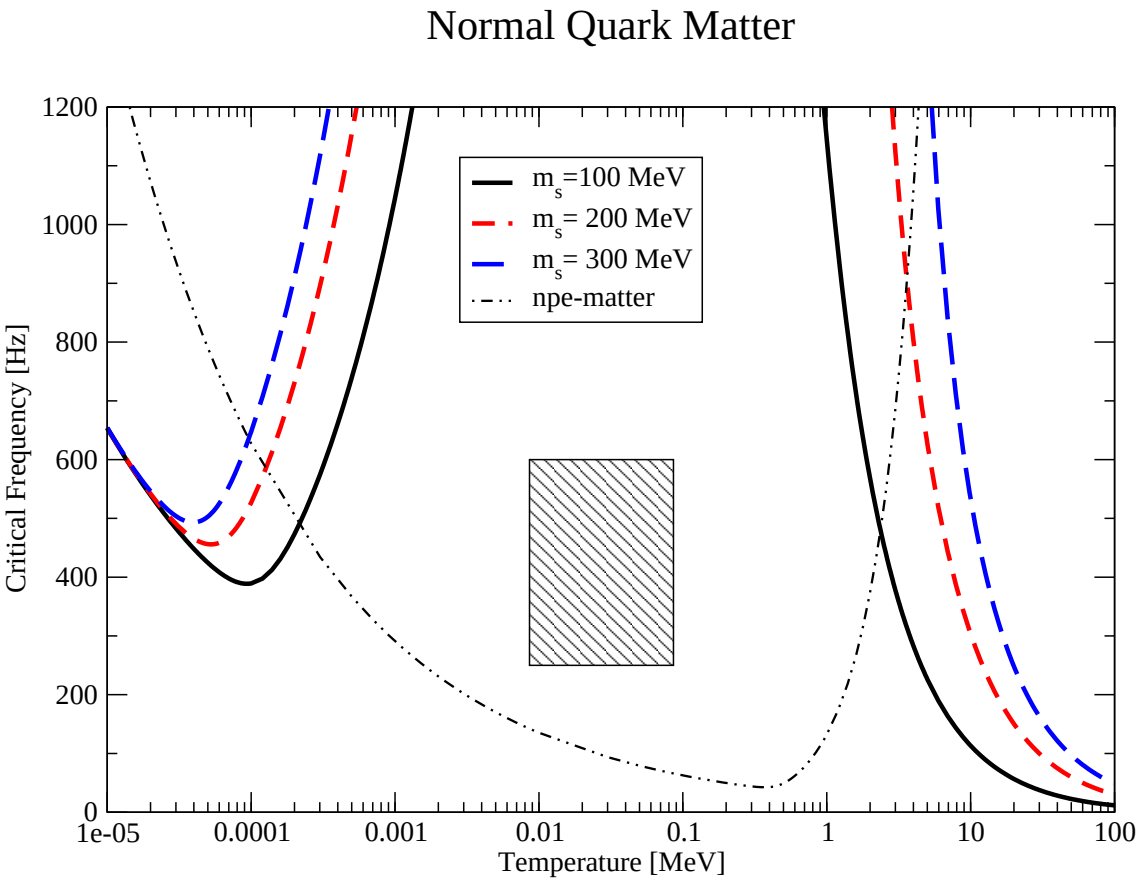

Figure 5.1: The r-mode instability window for normal quark stars (thick lines) for strange quark masses of 100, 200, and 300 MeV, and neutron stars (thin line). the shaded box represents the region in which most LMXB's are observed.

on the λ_i's calculated in chapter 2. Recall that $\Gamma_i(\delta\mu_i,\ \Delta) - \bar{\Gamma}_i(\delta\mu_i,\ \Delta) = \lambda_i(\Delta)\delta\mu_i$, see Eqs. (4.9) and that $\Gamma_i(\delta\mu_i,\ 0) = \bar{\Gamma}_i(-\delta\mu_i,\ 0)$ where $\Gamma_i(\delta\mu_i, \Delta)$ is the forward interaction rate as a function of both $\delta\mu_i$ and Δ. $\bar{\Gamma}_i(\delta\mu_i,\ \Delta)$ is the inverse interaction (backwards channel). For instance, if we choose $\Gamma_{(a)}$ in Fig. 4.1 and Eqs. (4.9) as the forward channel $\Gamma_1(\delta\mu_1,\ \Delta)$, $\bar{\Gamma}_1$ would be $\Gamma_{(b)}$ in Fig. 4.1 and so forth. From the two equations mentioned above it is easy to show that $\Gamma_i(\delta\mu_i, 0) = -\bar{\Gamma}_i(\delta\mu_i, 0) = \frac{1}{2}\lambda_i(0)\delta\mu_i$.

Color superconductivity introduces a reduction factor $H_i(\Delta)$ to the interaction rate Γ_i and another suppression factor $\bar{H}_i(\Delta)$ to the inverse interaction,

$$\Gamma_i(\delta\mu_i, \Delta) = \Gamma_i(\delta\mu_i, 0)H_i(\Delta), \tag{5.27}$$

$$\bar{\Gamma}_i(\delta\mu_i, \Delta) = \bar{\Gamma}_i(\delta\mu_i, 0)\bar{H}_i(\Delta). \tag{5.28}$$

The relation between the gapped $\lambda_i(\Delta)$ and the ungapped $\lambda_i(0)$ calculated in chapter 2 becomes,

$$\begin{aligned}
\lambda_i(\Delta)\delta\mu &= \Gamma_i(\delta\mu_i,\ 0)H_i(\Delta) - \bar{\Gamma}_i(\delta\mu_i,\ 0)\bar{H}_i(\Delta) \\
&= \Gamma_i(\delta\mu_i,\ 0)H_i(\Delta) - \Gamma_i(-\delta\mu_i,\ 0)\bar{H}_i(\Delta) \\
&= \lambda_i(0)\frac{H_i(\Delta) + \bar{H}_i(\Delta)}{2}\delta\mu.
\end{aligned} \tag{5.29}$$

Then the reduction to $\lambda_i(0)$ would be a function of the suppressions to both the forward and the inverse interactions.

$$\lambda_i(\Delta) = \lambda_i(0)\frac{H_i(\Delta) + \bar{H}_i(\Delta)}{2}. \tag{5.30}$$

In the following, we will approximate the reduction $H(\Delta)$ to be of an exponential form for each incoming gapped quark branch in the interaction.

5.4.2 R-mode Instability Window for the CFL Phase

Color superconductivity changes the situation from that of unpaired quark matter. The severity of this change depends on the type of pairing and the value of the gap. The CFL phase discussed in Chapter 1 gaps all quark modes equally. Here we consider the contribution of quarks on the bulk viscosity and r-mode instabilities of the CFL phase.

As in Chapter 3 we neglect the effect of color superconductivity on the thermodynamic coefficients A_i, B_i, and C_i. Therefore, the effects of the CFL phase are simply to reduce the λ_i's as in Eq. (5.30). Non-leptonic weak interactions have two quarks on both the forward and backward channels, each of which will be suppressed exponentially, leading to $H_1(\Delta_{CFL}) = \bar{H}_1(\Delta_{CFL}) \simeq e^{-\frac{2\Delta_{CFL}}{T}}$. Thus,

$$\lambda_1(\Delta_{CFL})/\lambda_1(0) = e^{-\frac{2\Delta_{CFL}}{T}}. \tag{5.31}$$

The two other neutrino-emitting interactions both have one quark flavor in both channels. Hence, we expect the reduction to the interaction rates to take the form $H_{2,\,3}(\Delta_{CFL}) = \bar{H}_{2,\,3}(\Delta_{CFL}) \simeq e^{-\frac{\Delta_{CFL}}{T}}$. Then the reduction of $\lambda_{2,\,3}$ is

$$\lambda_{2,3}(\Delta_{CFL})/\lambda_{2,3}(0) = e^{-\frac{\Delta_{CFL}}{T}}. \tag{5.32}$$

We follow the same procedure as for normal quark matter to calculate the bulk viscosity and r-mode instability window. Since the shear viscosity only participates in the r-mode instability at low temperature and all quark flavors are strongly suppressed, we can safely neglect the quark shear viscosity. The results for a critical temperature $T_c = 50$ MeV are shown in Fig. 5.2

Quarks allow for a narrow stability window at high temperatures $T > 5$ MeV. This is due to the fact that color superconductivity may actually increase the bulk viscosity as can be seen in Fig. 5.2.

It is clear from Fig. 5.2 that considering the quarks' contribution to the stability window places all LMXB in an unstable region. However, one cannot yet draw any significant astrophysical conclusions; there are other dissipative phenomena besides

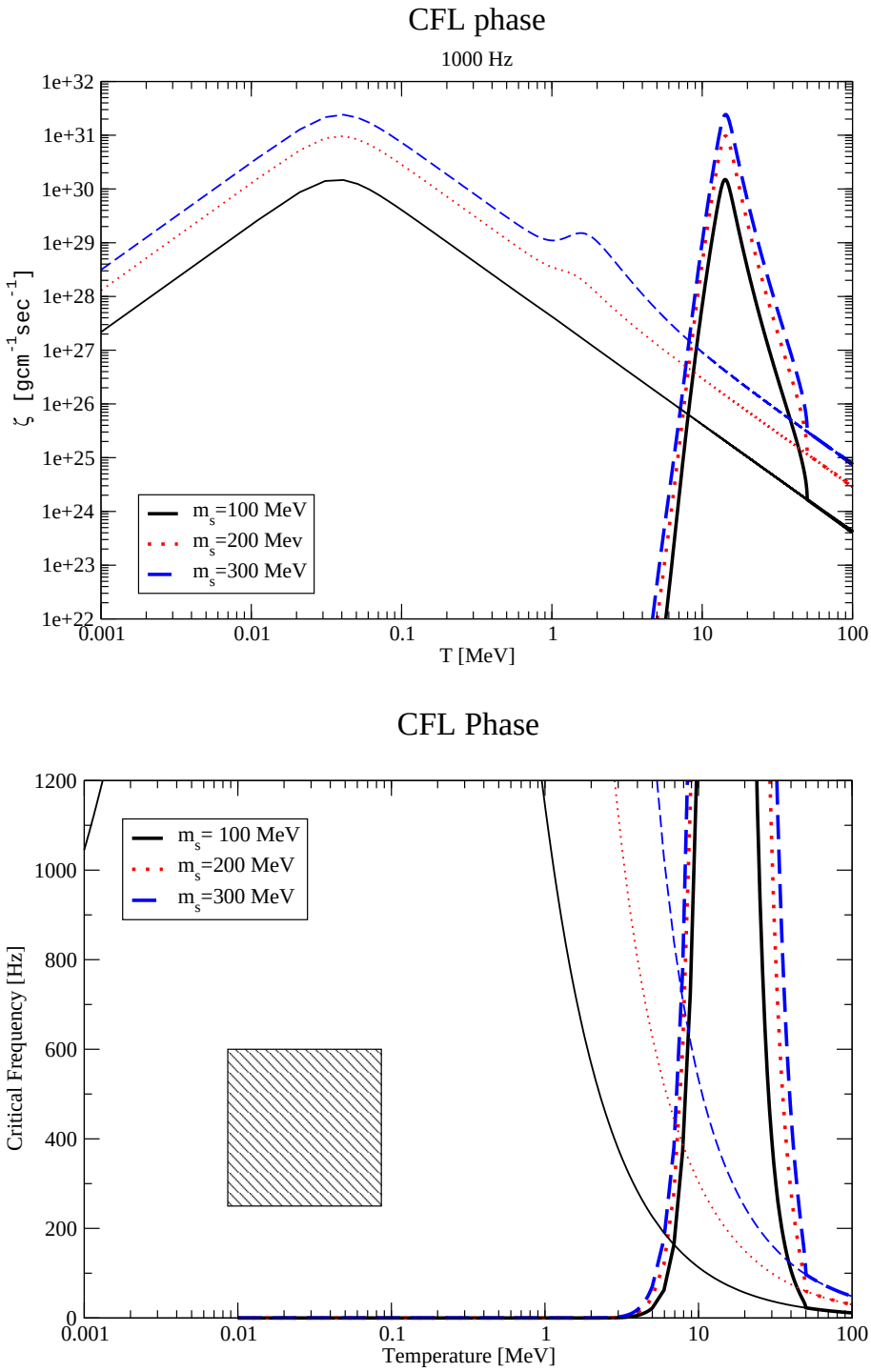

Figure 5.2: The quark contribution to the bulk viscosity as a function of temperature at constant frequency "1000 Hz" and r-mode instabilities of the CFL phase for different values of the strange quark mass. The thin lines show the results for unpaired quark matter.

just the bulk and shear viscosities due to quarks in the CFL phase, such as the bulk and shear viscosities due to superfluid phonons [9, 8], and the bulk viscosity due to kaons [44]. Without a complete analysis of all these phenomena, no significant conclusions can be drawn. However, we do notice that at large temperatures there is a narrow stability region. Incidentally, this is the region where young pulsars are born, which means that young quark stars in the CFL phase are produced in a stable region and then have to cool down before entering the instability region and slowing down.

The result for the r-mode instability window differs significantly from that in Ref. [45], which arises from the fact that the bulk viscosity may be enhanced rather than suppressed due to the suppression of the interaction rates. This enhancement was not considered in Ref. [45].

5.4.3 R-mode Instability Window for the 2SC Phase

The effect of the gap in the 2SC phase on the bulk viscosity is less severe than in the CFL phase. The reason is that there is an ungapped color for the up and down quarks and that the strange quarks remain unpaired as discussed in Sec. 1.3.

Since weak interactions do not change the quark colors at the vertices, we can decompose the non-leptonic weak interaction (the first interaction in Fig 4.1) into four different interactions according to the quark colors conserving the color at each vertex. This translates to a decomposition according to the gapped and ungapped modes of the quarks playing a role in the interaction as in Ref. [5], see Fig. 5.3.

This leads to a reduction of the interaction rates Γ_1 and $\bar{\Gamma}_1$,

$$H_1(\Delta_{2SC}) = \frac{4}{9}e^{-\frac{2\Delta_{2SC}}{T}} + \frac{4}{9}e^{-\frac{\Delta_{2SC}}{T}} + \frac{1}{9}, \tag{5.33}$$

$$\bar{H}_1(\Delta_{2SC}) = \frac{6}{9}e^{-\frac{\Delta_{2SC}}{T}} + \frac{3}{9}, \tag{5.34}$$

which gives

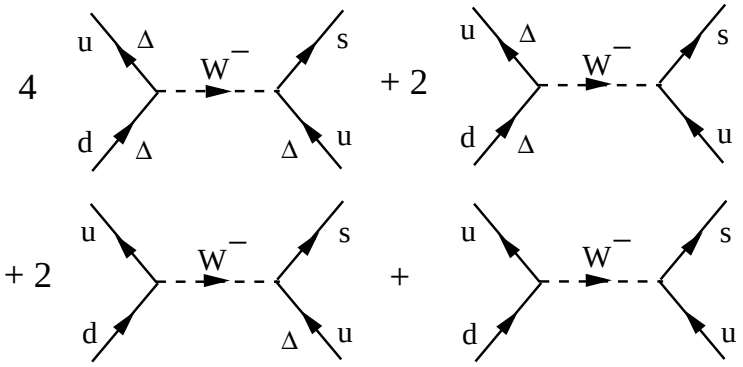

Figure 5.3: Contributions to the process $u+s \leftrightarrow u+d$ in the 2SC phase. A gapped fermion is marked with the gap Δ_{2SC} at the respective line [5].

$$\lambda_1(\Delta_{2SC})/\lambda_1(0) = \frac{2}{9}e^{-\frac{2\Delta_{2SC}}{T}} + \frac{5}{9}e^{-\frac{\Delta_{2SC}}{T}} + \frac{2}{9}. \tag{5.35}$$

This gives a different fraction for the ungapped mode compared to that in Ref. [5]. This is due to their "erroneous" assumption that $\delta\mu_1 > 0$. Assuming that $\delta\mu_i$ is positive neglects the effect of one direction of the interaction.

The same thing can be said about the other two weak interactions. However, since there is only one quark participating in the interaction in each channel, we decompose each interaction into two. The terms $\lambda_{2,\,3}$ then take the form

$$\lambda_2(\Delta_{2SC})/\lambda_2(0) = \frac{2}{3} + \frac{1}{3}e^{-\frac{\Delta_{2SC}}{T}} \tag{5.36}$$

$$\lambda_3(\Delta_{2SC})/\lambda_3(0) = \frac{1}{3} + \frac{2}{3}e^{-\frac{\Delta_{2SC}}{T}}. \tag{5.37}$$

Choosing the critical temperature to be $T_c = 30$ MeV, the bulk viscosity and r-mode instability window can both be calculated. The results are shown in Fig. 5.4.

The results for the r-modes are also different from those in Ref. [45]. This is due to the assumption that the ungapped mode leads to a 1/9 reduction of the interaction rate whereas we have shown that it should be 2/9, and due to the fact that the

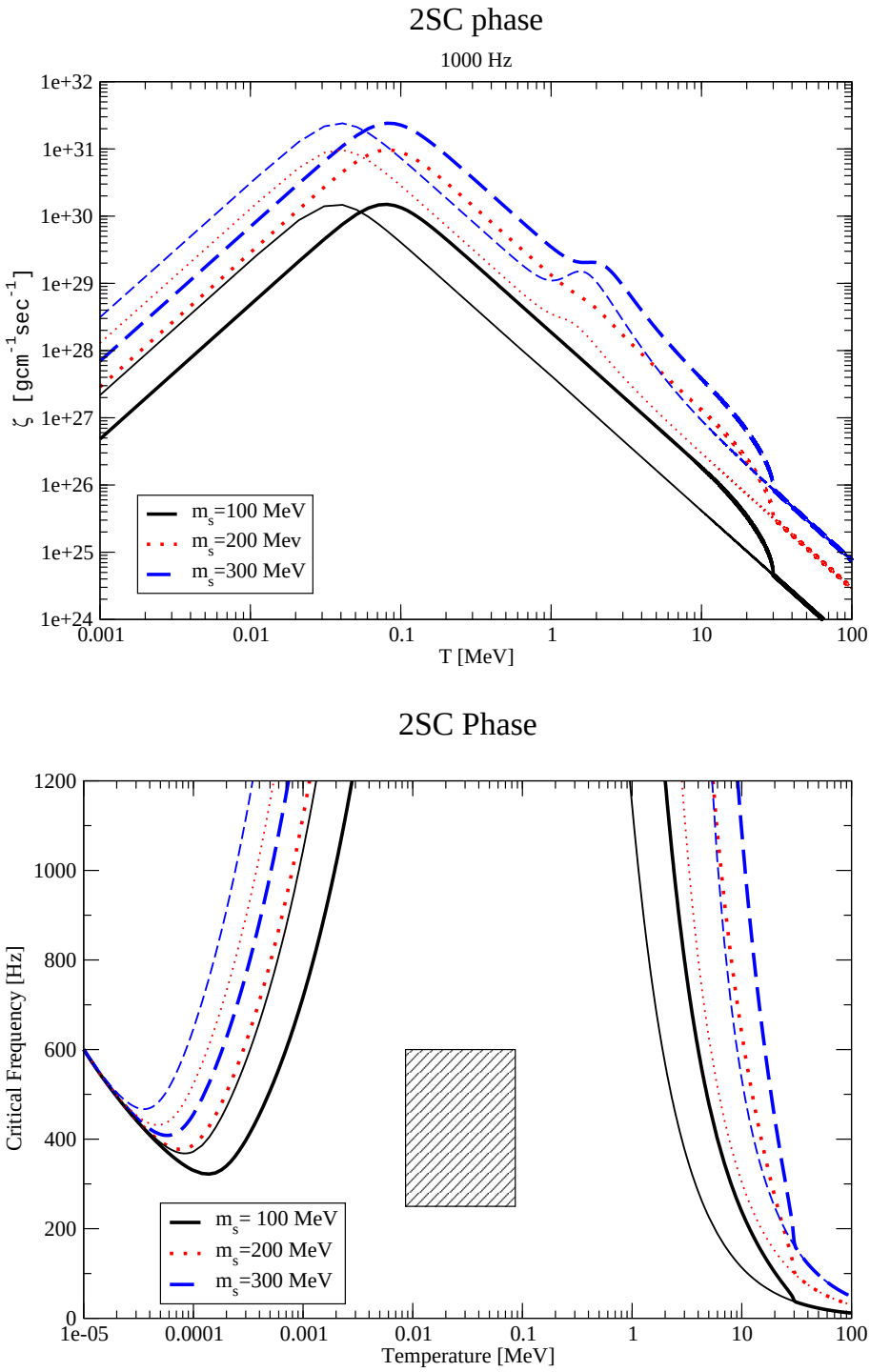

Figure 5.4: Same as Fig. 5.2, but for the 2SC phase.

reduction of the interaction rate has an effect on the bulk viscosity that is not as trivial as only suppressing it.

It can be seen from Fig. 5.4 that the effect of the 2SC phase is mainly to shift the bulk viscosity and r-mode instability window sideways by a multiplicative factor. LMXB data do not exclude the possibility of having a 2SC phase in pulsars.

5.4.4 R-mode Instability Window for the CSL Phase

For spin-1 color-superconducting phases which are discussed in Refs. [1, 46, 47], the situation is very similar to the 2SC phase since there are ungapped modes. However, it has been suggested [7] that for a particular spin-1 phase, the CSL phase, all modes are gapped. There are two modes gapped with an energy gap Δ_{CSL} and the "ungapped" mode is now gapped with $X_i\Delta_{CSL} = \frac{m_i}{\mu_i}\Delta_{CSL}$ where m_i and μ_i are the mass, and chemical potential of the quark flavor.

Following the same procedure as for the 2SC phase, the weak interaction rates λ_i take the form

$$\begin{aligned}
\lambda_1(\Delta_{CSL})/\lambda_1(0) &= \frac{4}{9}e^{-\frac{2\Delta_{CSL}}{T}} + \frac{2}{9}e^{-\frac{(1+X_u)\Delta_{CSL}}{T}} + \frac{1}{9}\left(e^{-\frac{(1+X_d)\Delta_{CSL}}{T}} + e^{-\frac{(1+X_s)\Delta_{CSL}}{T}}\right) \\
&+ \frac{1}{18}\left(e^{-\frac{(X_u+X_s)\Delta_{CSL}}{T}} + e^{-\frac{(X_u+X_d)\Delta_{CSL}}{T}}\right), \qquad (5.38)\\
\lambda_2(\Delta_{CSL})/\lambda_2(0) &= \frac{1}{6}\left(e^{-\frac{X_s\Delta_{CSL}}{T}} + e^{-\frac{X_u\Delta_{CSL}}{T}}\right) + \frac{2}{3}e^{-\frac{\Delta_{CSL}}{T}}, \qquad (5.39)\\
\lambda_3(\Delta_{CSL})/\lambda_3(0) &= \frac{1}{6}\left(e^{-\frac{X_d\Delta_{CSL}}{T}} + e^{-\frac{X_u\Delta_{CSL}}{T}}\right) + \frac{2}{3}e^{-\frac{\Delta_{CSL}}{T}}. \qquad (5.40)
\end{aligned}$$

Choosing a critical temperature of 5 MeV, we calculate the bulk viscosity and the critical frequencies of the CSL phases. The results are shown in Fig. 5.5. The effect of the quark shear viscosity has again been neglected since it only acts at low temperature and is then strongly suppressed.

In Fig. 5.5 we see that the quark contribution places LMXB's partially within the window of stability. The situation will change, however, if we consider a smaller

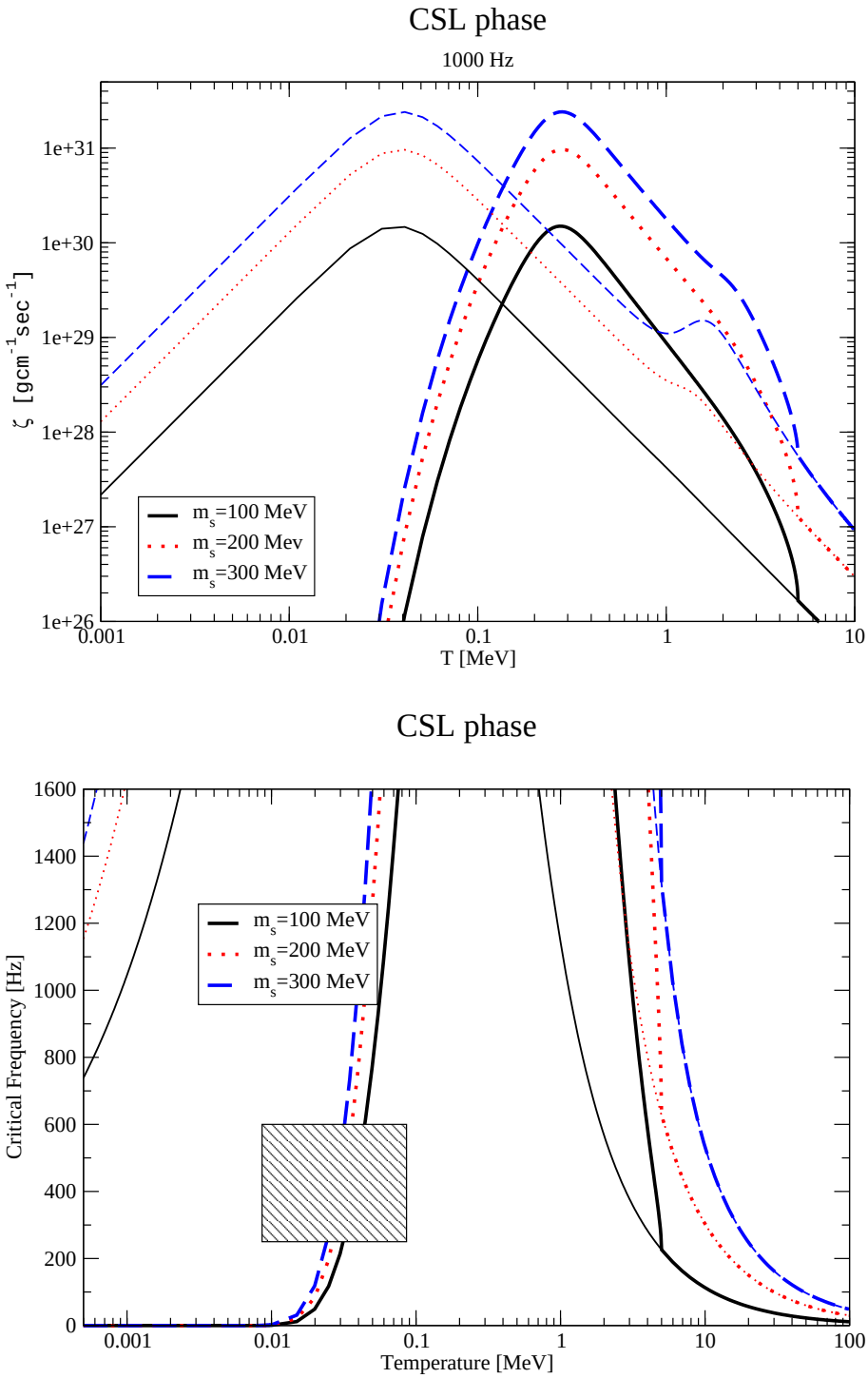

Figure 5.5: Same as Fig. 5.2, but for the CSL phase.

critical temperature than 5MeV. At a small enough T_c LMXB's would be completely placed in a stable region.

It must be noted that the CSL phase is a superfluid, and so, much like in the CFL phase, there are many other dissipative phenomena that need to be considered, such as the bulk and shear viscosities due to superfluid phonons, bulk viscosity due to Goldstone bosons, and friction between both superfluid and normal fluid components [94].

Chapter 6

Summary and Outlook

Pulsars have been puzzling researchers for decades since their discovery. They are compact stellar objects with masses that could reach up to twice the solar mass and a radius of about 10 km. The term "pulsar" stems from the observation of regular pulses of radiation, commonly radio waves, emanating from these objects. These pulses are linked to the rotation frequency of the pulsar. Pulsars have rotation periods ranging from milliseconds to a few seconds.

These stellar objects have densities too large for conventional matter to exist. The density of matter could reach up to ten times the density inside an atomic nucleus. At such large densities exotic phases of matter are expected. One of the possible phases is the deconfined quark matter phase. This phase occurs if the strong interactions which bind the quarks inside hadrons become weak enough to release them. If that is the case, pulsars might be the only place in the universe where deconfined quark matter exists in bulk.

There are many possible structures that pulsars can assume. The density of a neutron star with a mass of $1.4M_{\odot}$ and a radius of 12km would be $\rho \sim 3.846 \times 10^{14}\text{g cm}^{-3}$. At such large densities, one expects exotic phases of matter to exist. The most simple "least exotic" phase expected is where neutrons, protons and electrons exist in a charge neutral, β-equilibrated state. However, at such high densities, the chemical potentials of neutrons in the core may be large enough

to produce other, more massive and/or strangeness carrying hadrons such as the Σ, Λ, Ξ, Δ particles. The star is then called a hyperon star.

It is also possible that at such high densities strong interactions would become weak enough to produce a deconfined quark matter phase. If the deconfined quark matter phase is the true ground state of matter at the conditions available in neutron stars, then the whole star should be composed of a uniform density strange quark matter. The star is then called a quark star or a strange star. If that is not the case, quark matter might still be present in the core of the star, the star is then called a hybrid star.

The temperatures of pulsars are very low compared to the chemical potentials and interactions energy scales. At such conditions, if quark matter is to exist in the interiors of pulsars, it is most likely a color superconductor. There are many known color-superconducting phases that could be realized in cold dense matter. It remains unclear, however, which of these phases describe the possible deconfined quark matter inside pulsars.

It is, in principle, possible to determine the phase of deconfined quark matter under the conditions present in pulsars. However, theoretical uncertainties in treating the strongly coupled, non-perturbative dynamics in QCD at the baryon densities of relevance make it nearly impossible to make that determination.

It is possible, though, to narrow down the range possibilities using observational data. For this to work, a detailed knowledge of the physical properties of various phases that are likely to exist in pulsars is needed. Transport properties are most suitable for developing sufficiently sensitive, as well as unique and verifiable predictions regarding observational signals from stars. This work is devoted to the calculation of the bulk viscosity of deconfined quark matter in various possible phases, and relating the results to the observations of pulsar spin frequencies through the analysis of the effect of the bulk viscosity on r-mode instabilities and their relation to gravitational radiation emission.

In general, the bulk viscosity is a measure of the kinetic energy dissipation during expansion and compression of a fluid. In compact stars, the density oscillations of interest have characteristic frequencies that are of the same order of magnitude as the

stellar rotation frequencies. These are bound from below and from above, $1\ \mathrm{s}^{-1} \lesssim \omega \lesssim 10^3\ \mathrm{s}^{-1}$. (For the fastest-spinning pulsar currently known, PSR J1748-2446ad, one has $\omega \approx 4.5 \times 10^3\ \mathrm{s}^{-1}$, corresponding to $\nu = 716$ Hz [6].) The most important microscopic processes that provide the energy dissipation on the corresponding time scales are weak processes. Under conditions in stars, in particular, the bulk viscosity of quark matter is determined by the combined effect of the flavor-changing weak processes diagrammatically shown in Fig. 4.1. When an instantaneous departure from chemical equilibrium is induced by expansion/compression of matter, the weak processes try to restore the equilibrium state and, while doing this, reduce the oscillation energy.

The second chapter provides a review on the derivation of these weak interaction rates. Of interest to us is the change in the chemical composition of matter subject to oscillations. This is regulated through weak flavor-changing interactions.

In the third chapter we have calculated the bulk viscosity for the normal phase as well as for four spin-one color-superconducting phases of two-flavor dense quark matter. The main contributions come from the Urca processes shown diagrammatically in Fig. 3.1. Note that the results for the normal phase are also relevant for the 2SC phase. Indeed, after taking into account that there are two (blue) ungapped modes of quasiparticles in the low-energy spectrum of the 2SC phase, the low-temperature bulk viscosity is approximately given by the same expression (3.28), provided the following redefinitions are made: $\zeta_{max}^{\mathrm{2SC}} = 3\zeta_{max}$ and $\omega_0^{\mathrm{2SC}} = \omega_0/3$, where the normal-phase quantities are given in Eqs. (3.26) and (3.27), respectively. The redefinitions account for the decrease of the weak rates by a factor of 3 at $T \ll \Delta_0$ where Δ_0 is the value of the 2SC gap.

The microscopic calculations of the bulk viscosity in the spin-one color-superconducting phases suggests that quasiparticles with different types of gapless nodes (e.g., points or lines at the Fermi sphere) could potentially play a very important role. In the case of the transverse phases, however, the presence of a single ungapped quasiparticle mode washes out essentially all information about spin-one Cooper pairing, see Fig. 3.5. The presence of non-zero quark masses may provide a gap for such a mode and the situation changes. In this paper, we briefly discussed such a possibility in connection with the CSL phase of Ref. [7]. The results are shown in Fig. 3.6.

In agreement with the general expectation, we find that the bulk viscosity often tends to decrease when there is Cooper pairing of quarks whose main effect is to suppress the rates of the weak processes. In some cases (e.g., at sufficiently low frequencies and/or at temperatures close to the critical value) the behavior may reverse because of the non-trivial dependence of the bulk viscosity on the suppression factor, see Eq. (3.38). Such an increase of the viscosity in the color-superconducting CSL phase is seen, for example, in a range of temperatures below T_c in Figs. 3.5 and 3.6 in the case when $T_c = 4$ MeV.

In the fourth chapter we have studied the subtle interplay between the Urca (semi-leptonic) and the non-leptonic weak processes in determining the bulk viscosity of neutral, β-equilibrated strange quark matter. In general, the contributions of the two types of weak processes are not separable. The exception is the high-frequency limit, $\omega \gg \omega_{\rm sep}$, see Eq. (4.22), in which case the contributions naturally separate. Because of a much higher rate of the non-leptonic processes, they dominate in this high-frequency limit.

With decreasing frequency the role of the Urca processes gradually increases. The maximal mixing with the non-leptonic processes occurs at about the frequency ω_0, see Eq. (4.25) for the definition. Depending on the specific choice of model parameters, typical values of ω_0 are in the range from about 1 s^{-1} to 10^3 s^{-1}, see also Fig. 4.2 for the corresponding values of the period of oscillations.

Our numerical results for the normal-conducting phase of strange quark matter demonstrate that the commonly used approximation, in which the Urca processes are completely neglected, could substantially underestimate the value of the bulk viscosity, see Figs. 4.2 and 4.3. By sweeping over a wide range of model parameters, we find that the role of the Urca processes is most important in the range of temperatures between about 0.1 MeV and 1 MeV. In the outer core of a quark star, i.e., when the density is not too large, the strange quark mass not too small, and/or the period of oscillations not too short, the inclusion of the Urca processes could lead to an increase of the viscosity by an order of magnitude, see Fig. 4.4. These findings could have important implications for the physics of young neutron stars with strange quark matter interiors and/or for pure strange stars that could potentially exist, too.

In the fifth chapter, we used the results of the fourth chapter to study the r-mode instabilities for quark stars. It is shown that the r-mode instability window is very different for quark matter than for neutron star matter. This might provide us with an opportunity to distinguish between quark stars and neutron stars. It was shown that the data for low-mass X-ray binaries exclude the possibility of the classical model of neutron stars in which the pulsar is formed entirely of uniform neutron-proton-electron matter. However, a more sophisticated model in which the neutron star has a liquid rotating core of nuclear matter and a solid, nearly static crust is not ruled out. It was also shown that the fact that all young pulsars are slowly rotating seems to favor the quark star model in the unpaired phase or the 2SC phase.

Each different color-superconducting phase has a different structure for the r-mode instability window. Quarks in the CFL phase generate a narrow window of stability at temperatures which are, incidentally, the temperatures at which a young pulsar is formed. This implies that a newly born quark star in the CFL phase is generated in a stable region, and has to cool down first to reach the instability region which starts at $T = 10\text{MeV}$. One cannot draw more conclusions because the CFL phase has several other contributions to be considered.

The r-mode instability window for the CSL phase provides a wider stability region which ends at a temperature $T \sim 0.01\text{MeV}$. The situation is not fully resolved in the case of the CSL phase due to the uncertainties in the values of the energy gap and the critical temperature, and the fact that there are other dissipative phenomena to be considered.

The 2SC phase has a structure very similar to unpaired quark matter, and the conclusions for the unpaired phase can be similarly drawn for the 2SC phase. This is because in the 2SC phase there is always an ungapped quark color. This means that $\frac{1}{3}$ of the quarks behave exactly as the unpaired quark matter phase. Moreover, the strange quark always remains gapless. This leads to a suppression for the non-leptonic weak interaction close to $\frac{2}{9}$, for the strange quark *Urca* processes it is $\frac{2}{3}$, and for the down quark *Urca* processes it is $\frac{1}{3}$.

As a follow up to this work, one could attempt to calculate other dissipative phenomena in deconfined quark matter, such as the shear viscosity in superfluid

phases like the CFL [8] and the CSL phase, or the bulk viscosity due to superfluidity in the CFL [9] and the CSL phase. Supplementing these results with the ones in Chapter (5) should provide us with more accurate figures for the r-mode instability window in the superfluid phases, which would then allow us to draw more firm astrophysical conclusions.

There are other dissipative phenomena that need to be considered, such as the dissipation due to electron-electron scattering in the system, or due to surface friction between a rotating core and a nearly static crust in the case of hybrid stars.

Bibliography

[1] Andreas Schmitt. Spin-one color superconductivity in cold and dense quark matter. *nucl-th/0405076*, 2004.

[2] I. H. Stairs. Masses of radio pulsars. *J. Phys.*, G32:S259–S265, 2006.

[3] R N Manchester, G B Hobbs, A Teoh, and M Hobbs. The ATNF pulsar catalogue. *astro-ph/0412641*, 2004.

[4] Fridolin Weber. Strange quark matter and compact stars. *Prog. Part. Nucl. Phys.*, 54:193–288, 2005.

[5] Mark G. Alford and Andreas Schmitt. Bulk viscosity in 2SC quark matter. *J. Phys.*, G34:67–102, 2007.

[6] Jason W. T. Hessels, Scott M. Ransom, Ingrid H. Stairs, Paulo C. C. Freire, Victoria M. Kaspi, and Fernando Camilo. A radio pulsar spinning at 716 Hz. *Science*, 311:1901–1904, 2006.

[7] D. N. Aguilera, D. Blaschke, M. Buballa, and V. L. Yudichev. Color-spin locking phase in two-flavor quark matter for compact star phenomenology. *Phys. Rev.*, D72:034008, 2005.

[8] Cristina Manuel, Antonio Dobado, and Felipe J. Llanes-Estrada. Shear viscosity in a CFL quark star. *JHEP*, 09:076, 2005.

[9] Cristina Manuel and Felipe Llanes-Estrada. Bulk viscosity in a cold CFL superfluid. *arXiv:0705.3909 [hep-ph]*, 2007.

[10] D. Ivanenko and D. F. Kurdgelaidze. Hypothesis of quark stars. *Astrofiz.*, 1:479, 1965.

[11] D. Ivanenko and D. F. Kurdgelaidze. Remarks on quark stars. *Lett. Nuovo Cim.*, 2:13, 1969.

[12] N. Itoh. Hydrostatic equilibrium of hypothetical quark stars. *Prog. Theor. Phys.*, 44:291, 1970.

[13] F. Iachello, W. D. Langer, and A. Lande. A quark-like model of high-density matter. *Nucl. Phys. A*, 219:612, 1974.

[14] J. C. Collins and M. J. Perry. Superdense matter: Neutrons or asymptotically free quarks. *Phys. Rev. Lett.*, 34:1353, 1975.

[15] Krishna Rajagopal and Frank Wilczek. The condensed matter physics of QCD. *hep-ph/0011333*, 2000.

[16] Mark G. Alford. Color superconducting quark matter. *Ann. Rev. Nucl. Part. Sci.*, 51:131–160, 2001.

[17] Sanjay Reddy. Novel phases at high density and their roles in the structure and evolution of neutron stars. *Acta Phys. Polon.*, B33:4101–4140, 2002.

[18] Dirk H. Rischke. The quark-gluon plasma in equilibrium. *Prog. Part. Nucl. Phys.*, 52:197–296, 2004.

[19] Michael Buballa. NJL model analysis of quark matter at large density. *Phys. Rept.*, 407:205–376, 2005.

[20] Mei Huang. Understanding magnetic instability in gapless superconductors. *Int. J. Mod. Phys.*, A21:910–913, 2006.

[21] Igor A. Shovkovy. Two lectures on color superconductivity. *Found. Phys.*, 35:1309–1358, 2005.

[22] Mark Alford and Krishna Rajagopal. Color superconductivity in dense, but not asymptotically dense, quark matter. *hep-ph/0606157*, 2006.

[23] D. J. Gross and Frank Wilczek. Asymptotically free gauge theories. 2. *Phys. Rev.*, D9:980–993, 1974.

[24] D. J. Gross and Frank Wilczek. Asymptotically free gauge theories. 1. *Phys. Rev.*, D8:3633–3652, 1973.

[25] H. David Politzer. Asymptotic freedom: An approach to strong interactions. *Phys. Rept.*, 14:129–180, 1974.

[26] John Bardeen, L. N. Cooper, and J. R. Schrieffer. Microscopic theory of superconductivity. *Phys. Rev.*, 106:162, 1957.

[27] Mark G. Alford, Andreas Schmitt, Krishna Rajagopal, and Thomas Schäfer. Color superconductivity in dense quark matter. *arXiv:0709.4635 [hep-ph]*, 2007.

[28] John D. Fix. *Astronomy.* McGraw-Hill, 1999.

[29] Dany Page and Sanjay Reddy. Dense matter in compact stars: Theoretical developments and observational constraints. *Ann. Rev. Nucl. Part. Sci.*, 56:327–374, 2006.

[30] S. E. Thorsett and Deepto Chakrabarty. Neutron star mass measurements. i. radio pulsars. *Astrophys. J.*, 512:288, 1999.

[31] Henning Heiselberg. Neutron star masses, radii and equation of state. *astro-ph/0201465*, 2002.

[32] D. L. Kaplan, M. H. van Kerkwijk, and J. Anderson. The parallax and proper motion of RX J1856.5-3754 revisited. *astro-ph/0111174*, 2001.

[33] A. R. Bodmer. Collapsed nuclei. *Phys. Rev.*, D4:1601–1606, 1971.

[34] Edward Witten. Cosmic separation of phases. *Phys. Rev.*, D30:272–285, 1984.

[35] M. Hanauske, L. M. Satarov, I. N. Mishustin, Horst Stoecker, and W. Greiner. Strange quark stars within the nambu-jona-lasinio model. *Phys. Rev.*, D64:043005, 2001.

[36] I. N. Mishustin et al. Catastrophic rearrangement of a compact star due to the quark core formation. *Phys. Lett.*, B552:1–8, 2003.

[37] D. Blaschke, S. Fredriksson, H. Grigorian, A. M. Oztas, and F. Sandin. The phase diagram of three-flavor quark matter under compact star constraints. *Phys. Rev.*, D72:065020, 2005.

[38] David Blaschke, S. Fredriksson, H. Grigorian, and A. M. Oztas. Diquark condensation effects on hot quark star configurations. *Nucl. Phys.*, A736:203–219, 2004.

[39] Stefan B. Ruester and Dirk H. Rischke. Effect of color superconductivity on the mass and radius of a quark star. *Phys. Rev.*, D69:045011, 2004.

[40] C. Kettner, F. Weber, M. K. Weigel, and N. K. Glendenning. Structure and stability of strange and charm stars at finite temperatures. *Phys. Rev.*, D51:1440–1457, 1995.

[41] Nick J. Evans, Stephen D. H. Hsu, and Myckola Schwetz. Non-perturbative couplings and color superconductivity. *Phys. Lett.*, B449:281–287, 1999.

[42] R. Rapp, Thomas Schäfer, Edward V. Shuryak, and M. Velkovsky. Diquark bose condensates in high density matter and instantons. *Phys. Rev. Lett.*, 81:53–56, 1998.

[43] Jorge L. Noronha, Hai-cang Ren, Ioannis Giannakis, Defu Hou, and Dirk H. Rischke. Absence of the london limit for the first-order phase transition to a color superconductor. *Phys. Rev.*, D73:094009, 2006.

[44] Mark G. Alford, Matt Braby, Sanjay Reddy, and Thomas Schäfer. Bulk viscosity due to kaons in color-flavor-locked quark matter. *Phys. Rev.*, C75:055209, 2007.

[45] Jes Madsen. Probing strange stars and color superconductivity by r-mode instabilities in millisecond pulsars. *Phys. Rev. Lett.*, 85:10–13, 2000.

[46] Andreas Schmitt. The ground state in a spin-one color superconductor. *Phys. Rev.*, D71:054016, 2005.

[47] Andreas Schmitt, Igor A. Shovkovy, and Qun Wang. Neutrino emission and cooling rates of spin-one color superconductors. *Phys. Rev.*, D73:034012, 2006.

[48] Florian Marhauser, Dominik Nickel, Michael Buballa, and Jochen Wambach. Color-spin locking in a selfconsistent Dyson-Schwinger approach. *Phys. Rev.*, D75:054022, 2007.

[49] Andreas Schmitt, Qun Wang, and Dirk H. Rischke. When the transition temperature in color superconductors is not like in bcs theory. *Phys. Rev.*, D66:114010, 2002.

[50] Dirk H. Rischke. (gluon self-energy in a two-flavor color superconductor). *Phys. Rev.*, D64:094003, 2001.

[51] N. Iwamoto. Quark beta decay and the cooling of neutron stars. *Phys. Rev. Lett.*, 44:1637–1640, 1980.

[52] N. Iwamoto. Neutrino emissivities and mean free paths of degenerate quark matter. *Annals Phys.*, 141:1–49, 1982.

[53] J. Madsen. Rate of the weak reaction s + u $\rightarrow$ u + d in quark matter. *Phys. Rev.*, D47:325–330, 1993.

[54] Nils Andersson and Kostas D. Kokkotas. The r-mode instability in rotating neutron stars. *Int. J. Mod. Phys.*, D10:381–442, 2001.

[55] Lee Lindblom. Neutron star pulsations and instabilities. *astro-ph/0101136*, 2000.

[56] R. F. Sawyer. Damping of vibrations and of the secular instability in quark stars. *Phys. Lett.*, B233:412–416, 1989.

[57] J. Madsen. Bulk viscosity of strange dark matter, damping of quark star vibration, and the maximum rotation rate of pulsars. *Phys. Rev.*, D46:3290–3295, 1992.

[58] Basil A. Sa'd, Igor A. Shovkovy, and Dirk H. Rischke. Bulk viscosity of spin-one color superconductors with two quark flavors. *Phys. Rev.*, D75:065016, 2007.

[59] Barry A. Freedman and Larry D. McLerran. Fermions and gauge vector mesons at finite temperature and density. 3. The ground state energy of a relativistic quark gas. *Phys. Rev.*, D16:1169, 1977.

[60] Varouzhan Baluni. Nonabelian gauge theories of Fermi systems: Chromotheory of highly condensed matter. *Phys. Rev.*, D17:2092, 1978.

[61] Eduardo S. Fraga and Paul Romatschke. The role of quark mass in cold and dense perturbative QCD. *Phys. Rev.*, D71:105014, 2005.

[62] Thomas Schäfer. The CFL phase and m(s): An effective field theory approach. *nucl-th/0602067*, 2006.

[63] Robert D. Pisarski and Dirk H. Rischke. Color superconductivity in weak coupling. *Phys. Rev.*, D61:074017, 2000.

[64] Thomas Schäfer. Quark hadron continuity in QCD with one flavor. *Phys. Rev.*, D62:094007, 2000.

[65] Michael Buballa, Jiri Hosek, and Micaela Oertel. Anisotropic admixture in color-superconducting quark matter. *Phys. Rev. Lett.*, 90:182002, 2003.

[66] Mark G. Alford, Jeffrey A. Bowers, Jack M. Cheyne, and Greig A. Cowan. Single color and single flavor color superconductivity. *Phys. Rev.*, D67:054018, 2003.

[67] Qun Wang, Zhi-gang Wang, and Jian Wu. Phase space and quark mass effects in neutrino emissions in a color superconductor. *Phys. Rev.*, D74:014021, 2006.

[68] Michael Buballa. Private communication. 2006.

[69] Q. D. Wang and T. Lu. The damping effects of the vibrations in the core of a neutron star. *Phys. Lett.*, B148:211, 1984.

[70] Zheng Xiaoping, Kang Miao, Liu Xuewen, and Yang Shuhua. Running coupling constant from lattice data and bulk viscosity of strange quark matter. *Phys. Rev.*, C72:025809, 2005.

[71] Zheng Xiaoping, Liu Xuewen, Kang Miao, and Yang Shuhua. Bulk viscosity of strange quark matter in a density- dependent quark mass model and dissipation of the r mode in strange stars. *Phys. Rev.*, C70:015803, 2004.

[72] Xiao-ping Zheng, Shu-hua Yang, and Jia-rong Li. Bulk viscosity of interacting strange quark matter. *Phys. Lett.*, B548:29–34, 2002.

[73] Zi-Gao Dai and Tan Lu. The u + d ¡—¿ u + s reaction rate and bulk viscosity of strange matter. *Z. Phys.*, A355:415–420, 1996.

[74] E. Flowers and N. Itoh. Transport properties of dense matter. *Astrophys. J.*, 206:218–242, 1976.

[75] E. Flowers and N. Itoh. *Astrophys. J.*, 230:847–, 1979.

[76] R. F. Sawyer. Bulk viscosity of hot neutron–star matter and the maximum rotation rates of neutron stars. *Phys. Rev.*, D39:3804–3806, 1989.

[77] P. B. Jones. Bulk viscosity of neutron-star matter. *Phys. Rev.*, D64:084003, 2001.

[78] Lee Lindblom and Benjamin J. Owen. Effect of hyperon bulk viscosity on neutron-star r-modes. *Phys. Rev.*, D65:063006, 2002.

[79] Lee Lindblom and Benjamin J. Owen. Effect of hyperon bulk viscosity on neutron-star r-modes. *Phys. Rev.*, D65:063006, 2002.

[80] Alessandro Drago, A. Lavagno, and G. Pagliara. Bulk viscosity in hybrid stars. *Phys. Rev.*, D71:103004, 2005.

[81] P. Haensel, K. P. Levenfish, and D. G. Yakovlev. Bulk viscosity in superfluid neutron star cores. i. direct urca processes in npeμ matter. *Astron. Astrophys.*, 357:1157–1169, 2000.

[82] P. Haensel, K. P. Levenfish, and D. G. Yakovlev. Bulk viscosity in superfluid neutron star cores. ii. modified urca processes in *npe*μ matter. *Astron. Astrophys.*, 372:130–137, 2001.

[83] Debarati Chatterjee and Debades Bandyopadhyay. Effect of hyperon hyperon interaction on bulk viscosity and r-mode instability in neutron stars. *Phys. Rev.*, D74:023003, 2006.

[84] D. T. Son. Vanishing bulk viscosities and conformal invariance of unitary fermi gas. *Phys. Rev. Lett.*, 98:020604, 2007.

[85] J. D. Anand, A. Goyal, V. K. Gupta, and S. Singh. Burning of two-flavor quark matter into strange matter in neutron stars and in supernova cores. *Astrophys. J.*, 481:954–962, 1997.

[86] Hui Dong, Nan Su, and Qun Wang. Baryon number conservation and enforced electric charge neutrality for bulk viscosity in quark matter. *astro-ph/0702104*, 2007.

[87] Lee Lindblom and James R. Ipser. The r-modes of the maclaurin spheroids. *Phys. Rev.*, D59:044009, 1999.

[88] Lee Lindblom, Benjamin J. Owen, and Sharon M. Morsink. Gravitational radiation instability in hot young neutron stars. *Phys. Rev. Lett.*, 80:4843–4846, 1998.

[89] Benjamin J. Owen et al. Gravitational waves from hot young rapidly rotating neutron stars. *Phys. Rev.*, D58:084020, 1998.

[90] K. D. Kokkotas and N. Stergioulas. Analytic description of the r-mode instability in uniform density stars. *Astron. Astrophys.*, 341:110, 1999.

[91] Lee Lindblom, Gregory Mendell, and Benjamin J. Owen. Second-order rotational effects on the r-modes of neutron stars. *Phys. Rev.*, D60:064006, 1999.

[92] E. M. Lifshitz L. D. Landau. *Fluid Mechanics*. Pergamon Press, 1987.

[93] Dorota Gondek-Rosinska, Eric Gourgoulhon, and Pawel Haensel. Are rotating strange quark stars good sources of gravitational waves? *Astron. Astrophys.*, 412:777–790, 2003.

[94] M. E. Gusakov. Bulk viscosity of superfluid neutron stars. *Phys. Rev.*, D76:083001, 2007.